

**MAGNETISATION AND MAGNETOCRYSTALLINE ANISOTROPY  
MEASUREMENTS OF Ni-Mo AND Fe<sub>2</sub>P ALLOYS**

**BY**

**MD.FEROZ ALAM KHAN**

**A THESIS SUBMITTED TO THE DEPARTMENT OF PHYSICS,  
BANGLADESH UNIVERSITY OF ENGINEERING AND TECHNOLOGY IN  
PARTIAL FULFILLMENT OF THE REQUIREMENT FOR THE DEGREE  
OF  
DOCTOR OF PHILOSOPHY**



**DEPARTMENT OF PHYSICS  
BANGLADESH UNIVERSITY OF ENGINEERING AND TECHNOLOGY  
DHAKA, BANGLADESH  
OCTOBER 1995**

**Bangladesh University of Engineering and Technology**  
**Department of Physics**

**Certification of thesis work**

A thesis on  
"Magnetisation and Magnetocrystalline Anisotropy Measurements of Ni-Mo  
and Fe<sub>2</sub>P Alloys"

by

**Md. Feroz Alam Khan**

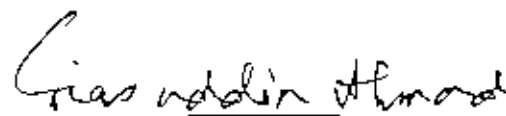
has been accepted as satisfactory in partial fulfilment of the requirement for the degree of Doctor of Philosophy in Physics and certify that the student demonstrated a satisfactory knowledge of the field covered by this thesis in an oral examination held on 28 October, 1995.

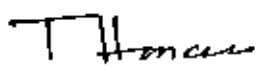
**Board of Examiners**

1. **Prof. Dr. M. Ali Asgar**  
Dept. of Physics  
B.U.E.T, Dhaka
2. **Dr. Per Nordblad**  
Assoc. Professor  
Dept. of Solid State Physics  
Institute of Technology  
Uppsala University  
Sweden.
3. **Prof. Dr. Gias Uddin Ahmad**  
Head, Dept. of Physics,  
B.U.E.T, Dhaka.
4. **Prof. Dr. Tafazzal Hossain**  
Dept. of Physics,  
B.U.E.T, Dhaka

  
\_\_\_\_\_  
Supervisor and Chairman


  
\_\_\_\_\_  
Co-Supervisor

  
\_\_\_\_\_  
Member


  
\_\_\_\_\_  
Member

.....Contd.

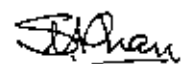
5. **Prof. Dr. Ajoy Kumar Roy**  
**Dept. of Physics**  
**University of Dhaka, Dhaka**

  
Member

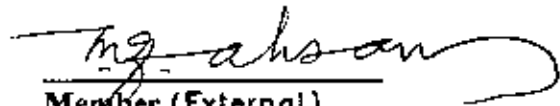
6. **Dr. Mominul Huq**  
**Assoc. Professor**  
**Dept. of Physics,**  
**B.U.E.T, Dhaka**

  
Member

7. **Prof. Dr. Sbabidul Islam Khan**  
**Dept. of Electrical and Electronics**  
**Engineering,**  
**B.U.E.T, Dhaka**

  
Member 28.10.95

8. **Prof. Md. Quamrul Ahsan**  
**Dept. of Electrical and Electronics**  
**Engineering,**  
**B.U.E.T, Dhaka**

  
Member (External)

9. **Dr. Anjali Krishnamurthy**  
**Assoc. Professor**  
**Department of Physics**  
**University of Rajasthan**  
**Jaipur, INDIA**

  
Member (External)

## CERTIFICATE

This is to certify that this thesis which the candidate has presented for a Ph.D.degree has been done by the candidate himself and does not contain any material extracted from elsewhere or from a work published by any body else. The work of this thesis has not been presented by the candidate for another degree or diploma in any other University. No other person's work has been used without due acknowledgement.

*Md. Faraz Alam Khan*

Candidate

*M. Ali Asgar*

Supervisor

*Dr. Nazim*

Co-Supervisor

## **Abstract**

Department of Physics  
Bangladesh University of Engineering and Technology  
**Doctor of Philosophy**

Magnetisation and magnetocrystalline anisotropy measurements of Ni-Mo and Fe<sub>2</sub>P alloys

by

**Md. Feroz Alam Khan**

This thesis describes the experimental investigation of magnetocrystalline anisotropy of Nickel-Molybdenum (Ni-Mo) single crystal alloys and of Fe<sub>2</sub>P single crystal. The first anisotropy constants of Ni-Mo system have been determined for compositions Ni<sub>1-x</sub>-Mo<sub>x</sub> x= 4,6,8,10 wt% at different temperatures down to 4.2K. The anisotropy constants have been determined by magnetisation measurements in different crystallographic directions as function of fields. The measurements are performed using both Vibrating Sample Magnetometer (VSM) and superconducting Quantum Interference Device (SQUID). The effect of alloying nickel with molybdenum is observed to be nearly straight forward dilution of magnetic system by non-magnetic atoms with slight non-linearity at higher concentration of molybdenum. The variation of magnetisation and the anisotropy constants due to change of composition and temperature have been analysed in the light of existing theories, none of which are completely supported by experimental results indicating the incompleteness of the present state of theoretical understanding of the magnetisation process of 3d transition metals and alloys. Our experimental results however agree favourably with the unpublished data obtained by torque magnetometer. The temperature dependence of magnetic anisotropy of Fe<sub>2</sub>P alloy is also determined by magnetisation measurements

using SQUID follows a third power law as observed in the case of iron. The a.c. susceptibility and the d.c. relaxation measurements have been performed on the anisotropic ferrimagnetic system  $\text{Fe}_3\text{O}_4$  Ferrofluid. It is revealed for the first time that the magnetisation in this anisotropic system decays with time i.e., the system ages

## **Acknowledgement:**

First and foremost I would like to thank my supervisor Professor Dr. M Ali Asgar for introducing me to the exciting field of magnetism and guiding me actively through to the end of this work. Without his able guidance and encouragement this work would have been impossible.

I would like to thank my co-supervisor Dr. Per Nordblad for guiding me actively during my experiment at the Department of Solid State Physics, Institute of Technology, Uppsala University, Sweden. His fruitful suggestions during difficult moments of my experiment enabled me to steer through my work successfully.

I would like to thank Professor Dr. Gias Uddin Ahmad, Head of the Department of Physics, Bangladesh University of Engineering and Technology for his valuable advice during the course of my work.

I am also thankful to Professor Dr. Tafazzal Hossain of the Department of Physics, B.U.E.T for his advice.

I would like to thank Professor Dr. Ajoy Kumar Roy of the Department of Physics, Dhaka University for his stimulating suggestions

I am thankful to Dr. Mominul Huq, Associate Professor of Physics, B.U.E.T for his advice.

I am also thankful to Professor Dr. Shahidul Islam Khan of the Department of Electrical and Electronics Engineering, B.U.E.T. for his advice

I am particularly grateful to Professor Dr. M A Taher Ali of the Department of Mechanical Engineering, B.U.E.T for his help in designing the rotating base of the magnet used in our Torque Magnetometer. I am also thankful to the technicians of the Mechanical Workshop of B.U.E.T who helped in the making of the base.

I am thankful to the Bangladesh University of Engineering and Technology for research grant.

I am thankful to late Professor Dr. Leif Lundgren for valuable advice during my experiments at Uppsala.

I am thankful to Dr. Peter Svedlinh for extending his helping hand during my work at Uppsala. Thanks are also due to Dr Per Granberg for his help during Laue Photography. I am thankful to Dr. Per.T. Norling for helping me in my Computer work. Thanks are also due to Mr. Tomas Jonsson for his helping hand at the a.c.Susceptometer and SQUID, to Mr.Claes Djurberg, Dr. Johan Mattsson and Dr. Anders Hjelm for advice; Miss.Malin Bjornander and Mr.Johan Magnusson who were very helpful while I was working at Uppsala. Thanks are also due to Mr.Bengt Gotesson for his technical assistance.

It is no formality to thank Dr. Lennart Hasselgren, Director, International Programs in the Physical Sciences (IPPS), Uppsala University, Sweden, who awarded me Fellowships to perform research at Uppsala University. Without these Fellowships this work would not have been possible. I am exclusively thankful to him for his constant



encouragement. Through Dr. Hasselgren I am thankful to the International Science Programs of Uppsala University for donating the Torque Magnetometer.

I am thankful to Dr. Garreth Bray for being helpful during my stay at Uppsala. I am indebted to Mrs. Asa Bergengren, Mrs. Mona Thorwaldsdotter and Mrs. Pravina Gajjar of the International Science Programs for taking care of all the official as well as family matters during my stay in Sweden.

I am thankful to Mr. Md. Shaif-Ul-Alam Lecturer in Physics, B.U.E.T for his help during Computer printout of this thesis

I am thankful to the members of Dhaka Material Science group and my colleagues in the Department of Physics for their help and co-operation

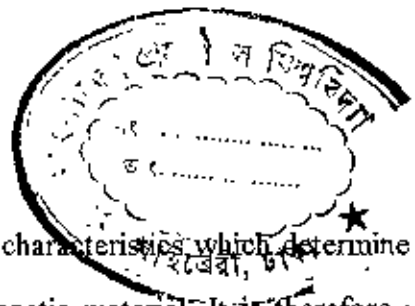
Finally, I am very much thankful to my beloved Wife Sadeka for working as a back-up for me during the last few years. And finally to my little daughter Silvia.

| <b>Contents</b>  |  |                 |
|------------------|--|-----------------|
| <b>Chapter</b>   |  | <b>Page No.</b> |
| <b>Chapter 1</b> | <b>Introduction</b>  | 1               |
| <br>             |  |                 |
| <b>Chapter 2</b> | <b>Magnetic Anisotropy</b>   |                 |
| Chap.2.1         | Paramagnetism  | 9               |
| Chap.2.2         | Ferromagnetism   | 10              |
| Chap.2.3         | Ferromagnetism in $Ni_{1-x}Mo_x$ alloys                            | 15              |
| Chap.2.4         | Physical origin of magnetocrystalline anisotropy                   | 15              |
| Chap.2.5         | Theories based on localized electron model                         | 19              |
| Chap.2.6         | Pair model of Magnetic Anisotropy                                  | 23              |
| Chap.2.7         | Single-Ion Model of Magnetic Anisotropy                            | 28              |
| Chap.2.8         | Band Model Theories  | 32              |
| Chap.2.9         | Composition dependence of magnetic anisotropy                      | 33              |
| Chap.2.10        | The Temperature dependence of magnetocrystalline anisotropy        | 35              |
| <br>             |  |                 |
| <b>Chapter 3</b> | <b>Measurement techniques</b>                                      |                 |
| Chap.3.1         | Experimental   | 43              |
| Chap.3.2         | Different methods of measurements of Magnetocrystalline Anisotropy | 43              |
| Chap.3.3         | Formulation of Magnetocrystalline anisotropy                       | 45              |
| Chap.3.4         | Sample preparation and orientation                                 | 46              |
| Chap.3.5         | The Vibrating Sample Magnetometer (V.S.M)                          | 46              |
| Chap.3.6         | The Detection Coil configuration                                   | 49              |

|                  |  |     |
|------------------|--|-----|
| Chap 3.7         | Calibration of the Magnetometer                              | 52  |
| Chap.3.8         | The Torque Magnetometer                                      | 53  |
| Chap 3 9         | Design and working principle of the Torque Magnetometer      | 55  |
| Chap.3.10        | The sample suspension  | 58  |
| Chap.3.11        | Calibration of the Torque Magnetometer                       | 58  |
| Chap.3.12        | The High Temperature Oven                                    | 63  |
| <b>Chapter 4</b> | <b>Measurements on Ni-Mo alloys</b>                          |     |
| Chap.4.1         | Magnetocrystalline Anisotropy in NiMo alloy                  | 66  |
| Chap.4 2         | Measurements of magnetization                                | 67  |
| Chap.4.3         | Evaluation of first anisotropy constant $K_1$                | 68  |
| Chap.4.4         | Results and Discussions                                      | 70  |
| <b>Chapter 5</b> | <b>Measurements on Iron Phosphide ( <math>Fe_2P</math> )</b> |     |
| Chap 5.1         | Introduction   | 92  |
| Chap.5 2         | $Fe_2P$ alloy  | 93  |
| Chap.5.3         | Magnetocrystalline anisotropy in $Fe_2P$                     | 98  |
| Chap 5.4         | Superconducting Quantum Interference Device (SQUID)          | 99  |
| Chap.5.5         | Experimental   | 103 |
| Chap.5.6         | Evaluation of the first anisotropy constant $K_1$            | 103 |
| Chap.5.7         | Results and Discussion                                       | 106 |

|                  |  |     |
|------------------|--|-----|
| <b>Chapter 6</b> | <b>Measurements on Ferrofluid ( <math>\text{Fe}_3\text{O}_4</math> )</b> |     |
| Chap.6.1         | Introduction   | 130 |
| Chap.6.2         | Review of previous works   | 131 |
| Chap.6.3         | Magnetism of ferrofluid  | 133 |
| Chap.6.4         | Static magnetization of ferrofluid                                       | 133 |
| Chap.6.5         | The effect of particle size distribution on the magnetization            | 135 |
| Chap.6.6         | The effect of magnetic anisotropy on magnetization                       | 136 |
| Chap.6.7         | Magnetic dipole-dipole interaction                                       | 138 |
| Chap.6.8         | The superparamagnetic relaxation   | 139 |
| Chap.6.9         | The Neel relaxation of interacting and non-interacting particles         | 139 |
| Chap.6.10        | Dynamic magnetization of ferrofluid                                      | 140 |
| Chap.6.11        | Superparamagnetism   | 141 |
| Chap.6.12        | Experimentals  | 143 |
| Chap.6.13        | Results and Discussion   | 144 |
| <b>Chapter 7</b> | <b>Findings and Conclusion</b>   |     |
| Chap.7.1         | Findings of this research  | 155 |
| Chap.7.2         | Conclusion   | 157 |
| References       |  | 161 |

## **Chapter 1**



### Introduction:

Magnetic anisotropy is one of the most important characteristics which determine the complex magnetization process of an ordered magnetic material. It is therefore very important in determining the technical properties of magnetic materials when they are tailored for their magnetically soft or hard characteristics. For example, silicon-iron is magnetically soft both because addition of silicon reduces magnetostriction and magnetic anisotropy of pure single crystals of iron. Again  $\text{SmCo}_5$  is eminently suitable for making permanent magnet because of its high uniaxial anisotropy, its anisotropy field is of the order of  $2.3 \times 10^7 \text{ A/m}$ . Therefore, it is important to understand the mechanism of magnetic anisotropy in order to control the magnetic hardness or softness of magnetic materials by manipulating magnetic anisotropy.

The present state of theoretical knowledge of the origin of magnetic anisotropy is not quite clear and since magnetism is basically an experimental science, the determination of magnetic anisotropy of magnetic alloys for their composition and temperature dependence through experiment is very important for checking the existing theories and controlling of magnetic anisotropy. Just as there are controversies in the theories of magnetic anisotropy, the experimental techniques used for determining anisotropy as also the choices of materials for the study of magnetic anisotropy are diverse.

In the present work we have chosen three different classes of anisotropic materials for their study. These are Nickel-Molybdenum( $\text{Ni-Mo}$ ), Iron-Phosphide( $\text{Fe}_2\text{P}$ ) and ferrofluid( $\text{Fe}_3\text{O}_4$ ). The methods used for determining the anisotropy of these materials are the measurement of magnetization by the Vibrating Sample Magnetometer (V.S.M), and the Superconducting Quantum Interference Device(SQUID), the a.c Susceptometer to measure the a.c.susceptibility of the anisotropic ferri-magnetic particles( $\text{Fe}_3\text{O}_4$ ) and the d.c.SQUID to measure the d.c.relaxation of the ferri-

magnetic particles. Finally a sensitive Torque Magnetometer is designed, built and set-up for measurements of torque. Some complimentary measurements are performed in the Torque Magnetometer.

Ferromagnetism is a co-operative phenomena where interactions between the magnetic moments of atoms or ions act in such a way that, below the Curie temperature, the moments begin to align parallel to each other creating a spontaneous magnetization. The coupling between the magnetic moments, can be represented empirically by a Weiss molecular field whose origin is quantum mechanical exchange force of isotropic nature. The atomic magnetic moments have two possible origins:

- (a) The orbital motion of the electrons around the nucleus,
- (b) The spin motion of the electron about its own axis.

From ferromagnetic resonance and gyromagnetic experiments the magnetic moments in nickel and other 3d ferromagnets are found to originate almost entirely from the electron spins. In these materials the orbital magnetic moment is quenched by the crystalline electric field created by surrounding atoms.

In a metal the motion of the electrons are affected by neighbouring atoms. The most tightly bound electrons are least affected and remain localized on separate nuclei. While the outermost electrons move through the lattice of positive ions, giving the metal its characteristic property of high electrical conductivity. In metals of the first transition series, and their alloys, the electrons responsible for ferromagnetism are those which remain in the unfilled 3d shell. Results of high-field magneto-resistance and Hall effect measurements(Fawcett,1964) indicate that the magnetic electrons in iron-group metals are itinerant with mobilities of the same order as the conduction electrons. Thus the electrons remain in states which are intermediate between localized and freely itinerant. That is they move through the lattice, but due to the strong

Coulomb repulsion's their motions are highly correlated. Molecular field models have been developed for two limiting cases:

- (i) the localized electron model, and
- (ii) the itinerant electron model.

The localized electron theories of ferromagnetism are governed by the work of Heisenberg(1928). According to Heisenberg the molecular field is the result of quantum mechanical exchange interactions between electron spins. Calculations of the Heisenberg exchange constant yield the values which are too small to account for ferromagnetism in the iron-group metals (Stuart and Marshall,1960). Van Vleck(1953), suggested that the d-electrons move between ions, changing the local electron configuration. Thus in nickel a mixture of magnetic  $3d^9$  electrons and non-magnetic  $3d^{10}$  electrons in the ratio 60:40 accounts for the observed magnetic moment per atom of  $0.6\mu_B$ .

The pioneering calculation of the interactions between itinerant electrons, by Bloch(1929), considered a free electron gas. It was shown that in this case, because of correlation effects, ferromagnetism is unlikely. Subsequent theories allow for the interaction between the electrons and the ion cores, as a result of which the electrons are confined to bands of permissible energy.

The collective electron theory proposed by Slater(1936) and Stoner(1933,1938,1939) is based on the following assumptions:

- (a) Ferromagnetism results from holes in the 3d energy band. This band is parabolic in shape.
- (b) The exchange interaction between the electrons may be represented by a molecular field proportional to the magnetization.
- (c) The electrons, or holes follow Fermi-Dirac statistics.



The theory predicts reduced magnetization and inverse susceptibility curves which are in reasonable agreement with the variations observed in real metals. One of its main achievements is the prediction of non-integral magnetic moments which agree well with experiment. Other authors have extended the collective electron theory to include a number of modifications (e.g. Wohlfarth, 1945, 1949, 1951; Band, 1946; Bell, 1952).

When compared with experimental measurements of magnetic and thermal properties and neutron diffraction studies of iron-group metals the collective electron approach is not necessarily found to be in better agreement than the more improved localized theories. In fact, while the band model provides good agreement for nickel the localized model fits better for iron.

More up-to-date theories attempt to include both itinerancy and the effect of correlations. The theories of Friedel et al. (1961) and Thompson et al. (1964) are based on an extension of the itinerant model which introduces spatial correlations. Others, proposed by Vansovsky (1946, 1953) and Zener (1951, 1953) start from the localized model and introduce an exchange interaction between the 3d and 4s electrons.

Magnetic anisotropy, which is the main aspect of the present research is not only evaluated from magnetization measurements but its variation with composition and temperature is also explained in terms of magnetization as a state variable.

The reason of undertaking this study is to understand the effect of alloying nickel with molybdenum in respect of saturation magnetization, magnetocrystalline anisotropy energy, magnetization process and the ferro-paramagnetic transition temperature. Nickel is a ferromagnetic element, on the other hand Molybdenum is a non-magnetic element. The idea of alloying Ni with Mo is to understand its effect on Ni in terms of its different measurable magnetic parameters. Nickel is used in its pure form or an alloy as a transformer core for which it is required to quench the material from high

temperature. Alloying nickel with a non-magnetic element like molybdenum eliminates the necessity of quenching and also reduces the magnetic hysteresis loss of the material. In this particular case the saturation magnetization becomes low and reduces its technological possibility, but is useful in understanding the effect of alloying on anisotropy. Nickel is also a major constituent of Permalloy and the binary alloy system Ni-Mo is relatively a simple material.

In this thesis Ni-Mo has been investigated from different angles and a comparative study have been performed to characterise this material in terms of different magnetic properties like magnetocrystalline anisotropy and magnetization process.

Since the orbit is rigidly coupled with the crystal, the magnetic anisotropy can talk about the crystal structure in general. Magnetic anisotropy can have different origins. There are stress induced anisotropy, anisotropy caused due to cold rolling of a material, shape anisotropy, anisotropy of magneto-strictive origin etc. In 3d elements anisotropy is caused due to holes in the 3d band.

The magnetocrystalline anisotropy originates from the spin-orbit coupling. Since a crystal is formed by the regular arrays of atoms, the atomic orbits are coupled with the crystal lattice. Therefore the crystal lattice are indirectly coupled to the spins of the electrons. As we know that magnetism is caused by the spins of the electrons, the magnetic anisotropy is a measure of the strength of the coupling between the spin and the orbit, also the coupling between the orbit and the lattice.

The aim of this work is to study the magnetocrystalline anisotropy of the binary alloy system Nickel-Molybdenum. The anisotropy of nickel have been studied before. But there are uncertainties in the experimental values of the anisotropy constants. As a part of the general problem of how the magnetic properties are affected when some non-magnetic solute atoms are added to the nickel matrix, the

magnetization of Nickel-Molybdenum single crystals  $Ni_{1-x}Mo_x$ ,  $x = 4, 6, 8, 10$  have been measured as a function of magnetic field, from which the anisotropy constants of these alloys have been calculated at liquid helium, and liquid nitrogen temperature. Although the magnetic anisotropy of Ni-Mo system have been done before by torque magnetometry, [private communication] there is no published data on this system. Review work on the conventional theory of magnetocrystalline anisotropy is discussed in Chap.2. This chapter also deals with the theories of temperature and composition dependence of the magnetic anisotropy and the different models on magnetic anisotropy. There are different methods of measurements of magnetocrystalline anisotropy e.g. the ferromagnetic resonance method in which the resonance frequency of precessing spin depends on the effective internal magnetic field which exerts a torque on the precessing spin system. Another method to determine the magnetic anisotropy is the torque method in which an anisotropic single crystal is suspended in a uniform magnetic field, a torque acts on it tending to align an easy direction of magnetization along the field direction. The third method is the measurements of area under the magnetization curves of a single crystal. The shape of the magnetization curve for a magnetic field applied in a particular crystallographic direction depends on the values of the anisotropy constants. These methods of determining the magnetic anisotropy are discussed in chapter 3. Also the mode of operation of a Vibrating Sample Magnetometer (VSM) is described in this chapter. The working principle of the Torque Magnetometer is also discussed in this chapter.

The technique of evaluating the anisotropy constants is discussed in Chapter 4 which also contain the results and discussion.

Iron phosphide ( $\text{Fe}_2\text{P}$ ) is a very interesting material to study. There are different parameters of this material which are under continuous investigation for years together and still calls for further investigations. The most disputed parameters are the ferro-paramagnetic transition temperature (Curie temperature), the saturation moments etc. There is no systematic investigation of the anisotropy constants of this material. In this work a detail investigation is performed on this system, e.g. the determination of the transition temperature, the saturation magnetization and the magnetocrystalline anisotropy constants. There is no previous data on the temperature dependence of the magnetocrystalline anisotropy constants on this system. We have studied the temperature dependence of the anisotropy constants upto the Curie temperature by the SQUID magnetometer. Also a theoretical fitting of the temperature dependence of the anisotropy constant is done on this system. This is described in chapter 5.

As an interesting current research problem ferrofluid is included as a third magnetic system in the present work in Chap.6. A ferrofluid is a system of fine magnetic particles suspended in a carrier liquid e.g. hydro-carbon oil. This particles are anisotropic in nature and goes through different magnetic phenomenon which is very interesting from the point of view of understanding the nature of a very dilute magnetic system. To avoid agglomeration the particles are coated with surfactants. In this system there are particles which are super-paramagnetic and blocked in nature. These terms are explained in chapter.6. To study the nature of this particle system the a.c. susceptibility and the d.c.relaxation experiments are performed by the a.c. Susceptometer and the d.c. SQUID. Possible interpretations are given for both the states ( dilute and frozen ) , and an overall magnetic characteristics and the

dynamics of this system is described in terms of a single particle as well as a system of particles.

In chapter 7 which is the concluding chapter, the salient features of the present work and the conclusion arrived at are presented alongwith some suggestions for future research.

**Chapter 2**  
**Magnetic Anisotropy**

## 2.1 Paramagnetism:

When the magnetic atoms in a substance are non-interacting and are not affected by any spontaneous internal field it is said to be in a paramagnetic state.

Paramagnetism is thus found in those materials where the individual atoms, ions or molecules have a permanent magnetic dipole moment but no molecular field. When a magnetic field is applied to these materials, the atomic moments tend to align themselves along the field direction whereas the thermal agitation tends to misalign them. The perfect alignment is classically possible at infinite magnetic field.  $Mn^{2+}$ ,  $Gd^{3+}$ ,  $U^{4+}$  are the examples of paramagnetic materials. According to Hund's rule, in a partly filled transition metal, the various orbital states are filled first by electrons of one spin, then by the other, so that pairing of electron spins is the least possible and the spin magnetic moment is maximized. It is this type of exchange interaction that is responsible for spin alignment in paramagnetic materials. Paramagnetism may also arise from atoms, ions or molecules with a net magnetic dipole moment. It is observed experimentally that for many materials in weak magnetic fields, the susceptibility is inversely proportional to temperature. This dependence of susceptibility on temperature  $T$  is known as Curie's law. According to this law the susceptibility  $\chi$  is defined as

$$\chi_{para} = \mu_0 \frac{M}{B} = \frac{C}{T}$$

where  $C$  is the Curie constant,  $M$  is the magnetisation,  $B$  is the magnetic flux density and  $\mu_0$  is the permeability constant.

## 2.2 Ferromagnetism.

An alloy is composed of atoms. The magnetic moment of an atom is associated with the spin motion of its electrons and their orbital motion around the nucleus. The magnetic orbital quantum number  $m_l$  and the magnetic spin quantum number  $m_s$  determines the quantum state of an atom. For a filled shell of an atom the contribution from both the orbital and spin motion is zero, i.e.  $\sum m_l = 0$  and  $\sum m_s = 0$ . This is the situation for complete diamagnetism where all the atomic shells are full. On the other hand in the case of 3d transition elements the shells are not completely filled and there are resultant  $\sum m_l$  and  $\sum m_s$  which are non zero.

This means that they have a resultant magnetic moment. These materials when subjected to external magnetic field exhibit very large magnetization. This magnetization is not reversible and persists even after the magnetic field is withdrawn. When cooled below a certain critical temperature, the magnetic moments of the atoms are ordered to a certain degree even in the absence of an external magnetic field. Ferromagnetic materials are characterized by the presence of spontaneously magnetized regions called domains and the existence of internal molecular field  $B_i$  as proposed by Weiss (1907). The origin of the molecular field was explained by Heisenberg (1924) and the existence of domains was explained by Landau and Lifshitz. At  $0^\circ K$  or at infinite magnetic field the alignment of the spins is complete and the magnetization attains its maximum value. Materials like transition metals Fe, Co, Ni and some rare-earth metals like Gd and oxides  $CrO_2$ , ErO are examples of ferromagnetic materials

The field seen by an atomic dipole is the sum of the applied field  $B_0$  and the internal field  $B_i$  i.e.,

$$B = B_0 + B_i \quad \dots \dots \dots (2.1)$$



$$B = B_0 + \lambda M \quad \dots\dots\dots (2.1)$$

where  $B_0 = \lambda M$ , and  $\lambda$  is known as the Weiss constant

If  $B$  is such that  $\frac{g\mu_B B}{k_B T}$  is small, where  $g$  is the Lande 'g'-factor,  $\mu_B$  is the Bohr

magneton and  $k_B$  is the Boltzmann constant. Then we can write

$$\begin{aligned} \chi_{ferro}^m &= \mu_0 \frac{M}{B_0} = \frac{Ng^2 \mu_B^2 J(J+1)}{8k_B T} \left(1 + \frac{\lambda M}{B_0}\right) \\ &= \frac{C}{T} \left(1 + \frac{\lambda \chi_{ferro}^m}{\mu_0}\right) \quad C = \frac{Ng^2 \mu_B^2 J(J+1)}{8k_B} \\ \text{or } \chi_{ferro}^m &= \frac{C}{T - T_C}, \quad \text{where } T_C = \frac{C\lambda}{\mu_0} \quad \dots\dots\dots (2.2) \end{aligned}$$

$T_C$  is the Curie temperature at which the susceptibility tends to infinity. This means that  $M$  has a finite value when  $B_0$  is zero which is an evidence of spontaneous magnetization.

From the quantum theory of paramagnetism we can write the equation for spontaneous magnetization as

$$M = Ng\mu_B J B_J(y) \quad \dots\dots\dots (2.3)$$

$$\text{where } y = \frac{g\mu_B JB}{k_B T} \quad \dots\dots\dots (2.4)$$

and  $B_J(y)$  is the Brillouin function defined by

$$B_J(y) = \left(\frac{2J+1}{2J}\right) \coth\left[\frac{(2J+1)}{2J}y\right] - \frac{1}{2J} \coth\left(\frac{y}{2J}\right) \quad \dots\dots\dots (2.5)$$

Thus eq(2.3) can be written as

$$\begin{aligned} M &= Ng\mu_B J B_J \left[ \frac{Ng\mu_B J}{Nk_B T} (B_0 + \lambda M) \right] \\ &= M_s(0) B_J \left[ \frac{M_s(0)}{Nk_B T} (B_0 + \lambda M) \right] \quad \dots\dots\dots (2.6) \end{aligned}$$

where  $M_s(0) = Ng\mu_B J$  represents the maximum value of magnetization at  $0^\circ K$ . When there is no magnetic field,  $B_0 = 0$  and we get

where  $y$  is given by eq(2.4), in case of ferromagnetic materials, as

$$y = \frac{g\mu_B J}{k_B T} B = \frac{g\mu_B J}{k_B T} (B_0 + \lambda M) \quad \dots\dots\dots(2.8)$$

In case of no magnetic field,  $B_0 = 0$  and hence

$$M = \frac{k_B T y}{g\mu_B J \lambda} \quad \dots\dots\dots(2.9)$$

Since  $M$  satisfies both eq(2.7) and eq(2.9), the two  $M$  versus  $y$  curves are plotted in Fig.(2.1) Eq(2.9) is a straight line between  $M$  and  $y$  and for various temperatures i.e  $T < T_c, T = T_c$  and  $T > T_c$  is shown in Fig.(2.1). Eq(2.7) represents a curve which intersects the straight line for  $T < T_c$  at point P. This gives a non-vanishing value of  $M$  even if the external field  $B_0 = 0$ . This spontaneous magnetization below the Curie temperature is shown in Fig (2.2) where the magnetization decreases from a saturated value  $M = M_c(0)$  at  $T = 0$  to zero at  $T = T_c$ . At  $T = T_c$ , the straight line given by eq(2.9) is the tangent to the curve eq(2.7) at the origin. Thus there is no spontaneous magnetization for  $T \geq T_c$ .

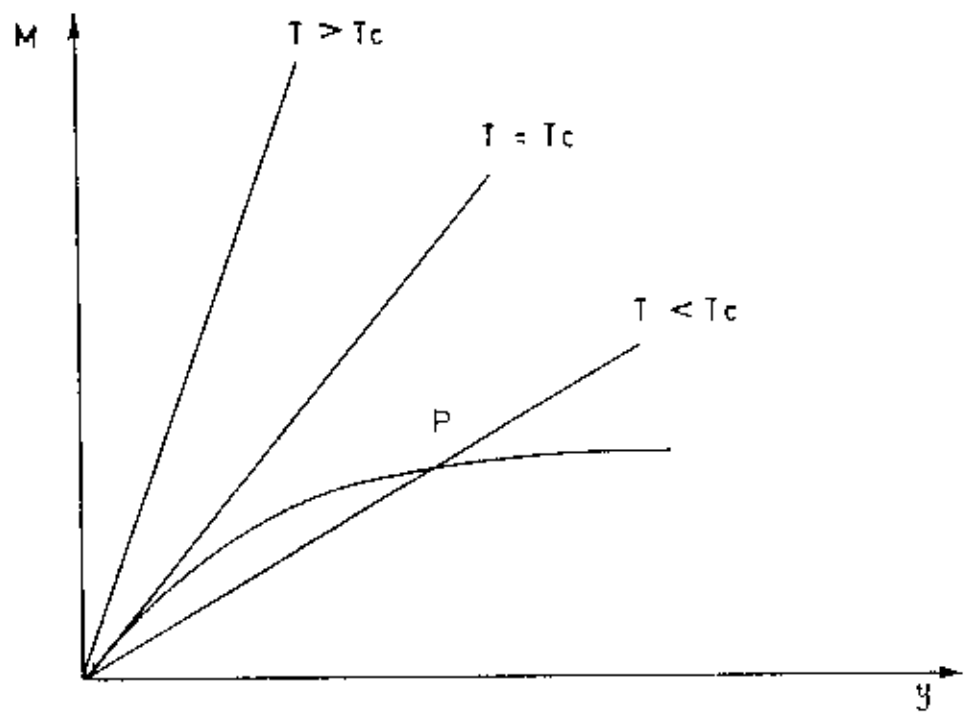


Fig. 2.1 Graphical solution of equations 2.7 and 2.9

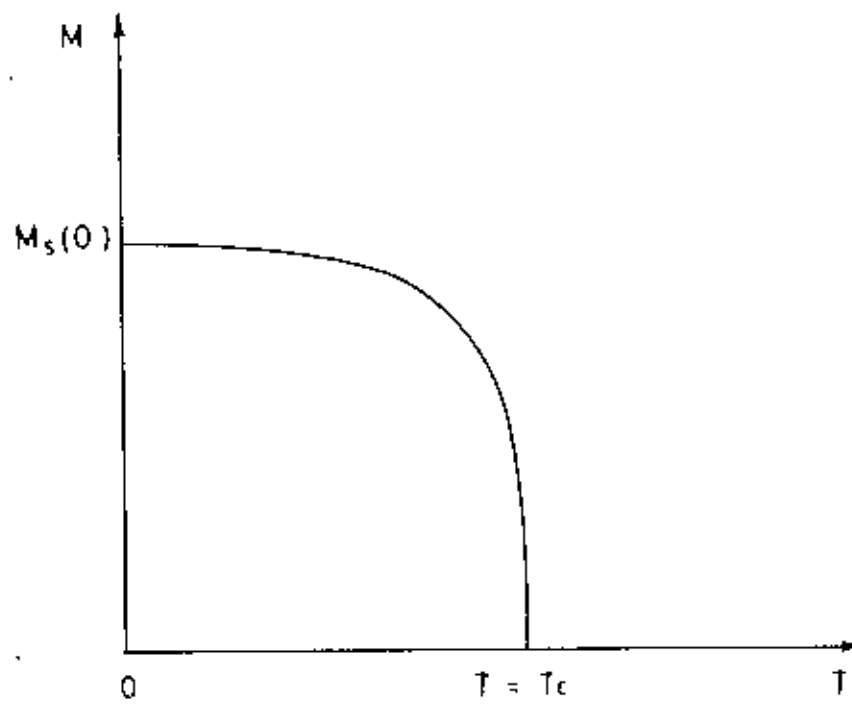


Fig. 2.2 Spontaneous magnetization below the Curie temperature.

### 2.3 Ferromagnetism in $Ni_{1-x}Mo_x$ alloys

The present object of investigations are dilute solid solutions of non-ferromagnetic metal molybdenum in nickel. Ni-Mo alloys exhibit variations of spontaneous magnetization with temperature that are smooth, and decrease monotonically with increasing temperature. They also show a systematic decrease in the value of the magnetic moment per atom as a function of increasing solute concentration. It is found that the decrease in the magnetic moment of the alloy per solute atom added is approximately equal to the number,  $n$ , of valence electrons of the solute atom ( $n=1$  for Cu and  $n=6$  for Mo). This behaviour can be explained by assuming that the valence electrons of the solute atom enter the 3d band to fill up the 0.6 holes per atom of nickel until no unpaired spins remain and the alloys cease to be ferromagnetic. This model fits the experimental data well.

In general, these alloys also show a decrease in the Curie temperature,  $T_C$ , with increasing solute concentration which is nearly linear and becomes slightly non-linear as we go higher in the concentration of Mo. The variation of  $T_C$  with solute concentration is similar to that of the average atomic moment and is, for most alloys, in proportion to the number of valence electrons of the added element. The Ni-Mo alloys investigated in the present work falls in the typical alloy system mentioned above.

### 2.4 Physical origin of magnetocrystalline anisotropy:

Phenomenologically magnetic anisotropy of a ferromagnetic single crystal is usually expressed in terms of a free energy  $E_a$ , which is assumed to be a function of the direction cosines  $\alpha_1$ ,  $\alpha_2$  and  $\alpha_3$  of the magnetization vector  $M$  with respect to the

crystallographic axes. Considering cubic symmetry and the fact that the total Hamiltonian of a given system is invariant under the time reversal transformation in the absence of an external magnetic field, we can write

$$E_a = K_0 + K_1(\alpha_1^2\alpha_2^2 + \alpha_2^2\alpha_1^2 + \alpha_3^2\alpha_1^2) + K_2(\alpha_1^2\alpha_2^2\alpha_3^2) + \dots$$

for a cubic crystal.

For a crystal of uniaxial anisotropy the corresponding equation is

$$E_a = K_{u1} \sin^2 \phi + K_{u2} \sin^4 \phi$$

where  $\phi$  is the angle between the axis of easy magnetization and the direction of magnetization vector.

Crystal anisotropy originates mainly from the spin-orbit coupling. Dy coupling is meant a kind of interaction which keeps the moments either parallel or anti parallel to each other. Crystal anisotropy may be regarded as a force which tends to bind the magnetization to directions of a certain form in the crystal. Thus we could speak of the exchange interaction between two neighbouring spins parallel or anti-parallel to one another. But the associated exchange energy is isotropic and it depends only on the angle between the adjacent spins, but not on the direction of the spin axis relative to the crystal lattice. The spin-spin coupling therefore cannot contribute to the crystal anisotropy. The orbit-lattice coupling is also strong. This follows from the fact that orbital magnetic moments are almost entirely quenched. This means, in effect, that the orientations of the orbits are fixed very strongly to the lattice, because even large fields cannot change them.

There is also a coupling between the spins and the orbital motion of the electrons when the orbital angular momentum remains partially unquenched. When an external field tries to reorient the spin of an electron, the orbit of that electron also tends to be reoriented. But the orbit is strongly coupled to the lattice and therefore resists the

attempt to rotate the spin axis. The energy required to rotate the spin system of a domain away from the easy direction, which we call the anisotropy energy, is just the energy required to overcome the spin-orbit coupling. This coupling is relatively weak because fields of a few hundred gauss are usually strong enough to rotate the spins. Inasmuch as the "lattice" is really constituted by a number of atomic nuclei arranged in space, each with its surrounding cloud of orbital electrons, we can also speak of a spin-lattice coupling and conclude that it too is weak. The strength of the anisotropy in any particular crystal is measured by the magnitude of the anisotropy constants  $K_1, K_2$ , etc. Although there is no doubt that crystal anisotropy is due to spin-orbit coupling, the details are different, and it is not yet possible to calculate the value of the anisotropy constants from first principles.

As the theory of ferromagnetism in nickel and other 3d metals is still not understood fully, the origin of magnetic anisotropy in these materials remain, to a considerable extent, phenomenological. Brief review of theories follow that the attempts to explain the temperature dependence of magnetic anisotropy have completely dominated the minds of the theoreticians. However the problem of producing a theory of the temperature dependence of magnetic anisotropy in 3d metals is enormous.

The anisotropy energy depends on the direction of magnetization relative to the crystal lattice. Thus their magnetic moments must be coupled to the crystal lattice in some manner. In the iron-group ferromagnetic materials the magnetic moments, due to spin moments of the 3d electrons are coupled indirectly to the lattice via spin-orbit and orbit-lattice couplings. The extent of the influence of lattice symmetry on a magnetic ion will depend strongly on its electronic structure.

In rare-earth metals and compounds, on the other hand, the magnetic moments consist of both spin and orbital contributions because of the strong spin-orbit coupling. The magnetic anisotropy therefore arises from a direct orbital-lattice coupling.

The 3d electrons responsible for the magnetic moments in iron group ionic crystals are well localized about each lattice site, so that it is possible to treat the disturbing effects of surroundings as small perturbations on a free-ion state. Thus the magnetic anisotropy can be calculated on the basis of Van Vleck's theory.

In 3d metals and alloys, the orbital moments are quenched by a mechanism which differs somewhat from that in insulators; this is due to electron transfer or hopping. Nevertheless magnetic anisotropy is caused by orbital moments induced by spin-orbit coupling, and the mechanism for anisotropy must be essentially the same as in insulators. For this reason, theories based on localized electron model (Van Vleck, 1937, Zener, 1954, and others) provide a qualitative understanding of magnetic anisotropy.

The observed temperature variation of the anisotropy constants of metals such as nickel is very rapid. On the other hand, the magnetostrictive energy the origin of which is the spin-orbit coupling shows a very much slower variation with temperature. Thus according to Zener (1954), the decrease in the anisotropy constant with increasing temperature cannot be due to a weakening of the spin-orbit coupling.

The 3d shells of 3d transition metals and alloys are the most exposed except for the 4s conduction electrons. The energy levels of these electrons, responsible for ferromagnetism, is perturbed due to overlapping of the 3d shells of neighbouring atoms. This perturbation gives rise to a spread in the energy levels of 3d electrons to form an energy band. The description of magnetic anisotropy and magnetostriction cannot therefore be obtained in the strict sense on the basis of localized electron model



which has relatively more success for insulators and rare-earth metals. On the other hand, the description of these phenomena in the band theory of ferromagnetism in terms of the effects of crystalline field and spin-orbit interaction as attempted by Fletcher and Katayama becomes inexact due to the difficulty of treating different electron spin correlation functions correctly

The theory of temperature dependence of magnetostriction constants of nickel does not agree satisfactorily with the experimental results (Asgar 1970) and the same is expected to be the case with Ni-Mo alloys whose basic temperature characteristics are not likely to be changed much from those of nickel when reduced temperature  $T/T_c$  is considered in place of  $T$ .

The effect of alloying a ferromagnetic metal is to change its electronic structure which in its turn changes the magnetic anisotropy, magnetostriction and other secondary phenomenon of the resultant alloy. A magnetic material can thus be tailored if the effect of alloying on anisotropy and magnetostriction can be understood quantitatively.

### 2.5 Theories based on the localized electron model:

Akulov (1936) is the pioneer to derive the first theoretical expression for the temperature dependence of magnetic anisotropy constant  $K_1$ . Using a simple classical argument and assuming a system of independent spins, Akulov assumed that each spin had a free energy of the form  $K_1 = (\alpha_1^2 \alpha_2^2 + \alpha_2^2 \alpha_3^2 + \alpha_3^2 \alpha_1^2)$ , where the direction cosines  $\alpha_1$  refer to a particular spin. A simple statistical calculation gives the relationship

$$\frac{K_1(T)}{K_1(0)} \approx \left[ \frac{M(T)}{M(0)} \right]^{10} \quad \dots \dots \dots (2.10)$$

between  $K_1$  and the spontaneous magnetization  $M$ .

The number 10 arises from the structural combination of the direction cosines in the usual expression for the anisotropy energy; a combination dictated solely by the symmetry of the crystal. The power law holds well for many insulators and rare-earth metals, for which the localized electron model is particularly applicable. But agreement with the experimental data for nickel and iron is not satisfactory; for example, in nickel the temperature variation of  $K_1$  exhibits a dependence of the 50th power of the magnetization (Carr 1958).

In a further classical treatment of magnetic anisotropy Zener (1954), generalised the 10th power law to an  $\frac{n}{2}(n+1)$  law assuming a system of independent spins. Zener showed that, if the anisotropy energy  $E_a$  is written in terms of spherical harmonics,

$$E_a = \sum_n k_n(T) Y_n^m(\alpha), \quad \dots \dots \dots (2.11)$$

then

$$\frac{k_n(T)}{k_n(0)} \approx \left[ \frac{M(T)}{M(0)} \right]^{n/2(n+1)}$$

Here the  $k_n(T)$  are linear combinations of the  $K_n(T)$ , and in particular

$$k_2(T) = K_1(T) + \frac{1}{11} K_2(T) + \dots \quad \text{and} \quad k_3(T) = K_2(T) \quad \dots \dots \dots (2.12)$$

The two assumptions basic to Zener's derivation are:

- (i) the existence of regions of short-range order of spins around each atom, inside which the anisotropy constants are temperature independent. Thus the only effect of

raising the temperature is to introduce small perturbations in the direction of the local magnetization.

(ii) the distribution of spins within each region is random so that the local anisotropy energy may be averaged over all directions.

The basis for a quantum theory of magnetic anisotropy was laid by Van Vleck(1937) in a paper on anisotropy in metals using the localized electron model. Van Vleck's approach is based on an anisotropic contribution to the exchange energy, which appears when the spin-orbit interaction is considered as a perturbation. The second order term is of the same form as a classical dipole-dipole interaction energy, and the fourth order term appears as quadrupole-quadrupole interaction. These two terms provide two models for magnetic anisotropy. The pseudo-dipolar model applied to cubic crystals predicts that anisotropy will vanish if all the dipoles are parallel; quantum mechanically this does not occur, even at 0°K. The pseudo-quadrupolar model requires that the spin quantum number be greater than  $\frac{1}{2}$ , which is unlikely in nickel.

Van Vleck used a Weiss molecular field to portray the exchange interactions. The results of his calculations on each of the two models are as follows:

**(a) Dipolar model:**

$K_1$  is of the order of  $10^4$  joule/m<sup>3</sup>, negative for f.c.c. and positive for h.c.c. crystals. This is in agreement with the experimental data for nickel and iron. The temperature variation of  $K_1$  should be according to the square of magnetization.

**(b) Quadrupolar model:**

$K_1$  for nickel is of the correct order of magnitude, but the sign is indeterminate. The temperature dependence is as a 5th or 6th power of magnetization. From dimensional

consideration  $K_2$  should be about  $10^{-3}$  to  $10^{-2}$  times as great as  $K_1$ . For nickel the experimental value of  $K_2$  is found to be of the same order as  $K_1$ .

The use of a molecular field by Van Vleck assumed no correlation between neighbouring spins. Keffer(1955) replaced the molecular field by a cluster theory, which restored the spin correlation. With this modification, Van Vleck's theory gives the temperature dependence of  $K_1$  as the 10th power of the magnetization at very low temperatures, changing to a 6th power at temperatures where the spin correlations are disrupted.

More improved calculations than Van Vleck's, using spin wave theory(Keffer, 1955, Turov and Mitsek, 1959) give the same  $\frac{n}{2}(n+1)$  power dependence for the temperature variation of the anisotropy. In these cases the anisotropy energy must be written in terms of spherical harmonics, and so the anisotropy constants appearing in the theory are linear combinations of the usual constants.

The use of a molecular field theory can, in fact, give a tenth power law for the temperature variation of  $K_1$ , as was shown by Carr(1958). By expressing the anisotropy energy in terms of the Coulomb energy only, Carr(1957) concluded one of the principal mechanisms of anisotropy to be different from those discussed by Van Vleck. Carr obtained the anisotropy constants in terms of electric multipole moments and crystalline potential constants. The electric multipole moments arise from the spin-orbit coupling inducing an orbital moment. Interaction between the orbital moment and the lattice crystalline potential provides a coupling between the spin and the charge distribution. Anisotropy results from distortion of the charge distribution which may occur in a sufficiently inhomogeneous crystalline potential. Carr's theory gives reasonable values of  $K_1$  and  $K_2$ , and it appears that in nickel and cobalt the dominant

part of  $K_1$  comes from the interaction of the charge distribution with the crystalline field.

### 2.6 Pair Model of Magnetic Anisotropy:

The physical mechanisms responsible for magnetic anisotropy are dipole-dipole, crystal field or single ion, and anisotropic exchange interactions. Starting from these approaches different calculations have been performed to determine the magnitude, sign and temperature dependence of anisotropy constants.

Magnetic anisotropy describes the circumstance that the energy of a system changes with a rotation of magnetization. The relation between the change in energy of a system with the change in energy of atomic pairs is called the pair model of anisotropy. Van Vleck (1937) first developed this theory. The most important interaction between the atomic magnetic moments is the exchange interaction. This energy is only dependent on the angle between the neighbouring atomic moments, independently of their orientation relative to their bond direction. In a view to explain magnetic anisotropy we may assume that the pair energy is dependent on the direction of the magnetic moment,  $\phi$ , as measured from the bond direction. In general we express the pair energy by expanding it in Legendre polynomials;

$$w(\cos \phi) = g + f \left( \cos^2 \phi - \frac{1}{3} \right) + g \left( \cos^4 \phi - \frac{6}{7} \cos^2 \phi + \frac{3}{15} \right) + \dots \quad \dots\dots(2.13)$$

The first term is independent of  $\phi$ ; hence the exchange energy is to be included in this term. The second term is called the dipole-dipole interaction term.

If the pair energy were due exclusively to magnetic dipolar interaction, it should follow that

$$I = -\frac{3M^2}{4\pi\mu_0 r^3} \quad \dots\dots(2.14)$$

The actual value of  $I$  can be evaluated from the uniaxial crystal anisotropy. In most cases the estimated value is  $10^2$  to  $10^3$  times larger than that given by eq(2.14). The origin of this strong interaction is believed to be the combined effect of spin-orbit interaction and exchange or Coulomb interaction between the neighbouring orbits. That is if there are small amounts of orbital magnetic moment remaining unquenched by the crystalline field, a part of the orbit will rotate with a rotation of the spin magnetic moment because of a magnetic interaction between the two, and the rotation of the orbit will, in turn, change the overlap of the wave functions between the two atoms, giving rise to a change in the electrostatic or exchange energy. This type of interaction is termed as the anisotropic exchange. It should be noted here that the dipolar term of eq(2.13) does not contribute to the interaction energy  $E_e$ , since the spins are perfectly parallel. The dipole terms between the atomic pairs with different bond directions cancel out as long as their distribution maintains cubic symmetry. If, however, the crystal has a lower symmetry than the cubic crystal, as in a hexagonal crystal, the dipole-dipole interaction gives rise to magnetic anisotropy.

Van Vleck pointed out that the dipole-dipole interaction does give rise to cubic anisotropy since the perfect parallelism of the spin system is disturbed by the dipolar interaction itself. Thus if  $I < 0$  and all the spins are parallel, the dipole-dipole interaction gives rise to a large pair energy for  $\phi = \frac{\pi}{2}$ . In such case, a more stable

configuration of the spin pair will be an antiparallel alignment. Some of the spins will therefore take the anti parallel direction in an equilibrium state

According to Van Vleck's calculation, the cubic anisotropy constants for an f.c.c system due to dipole-dipole interaction are

$$K_1 = -\frac{9NI^2}{8SMH_m} \quad \text{at } T = 0^\circ K \quad \dots\dots(2.15)$$

where  $S$  is the total spin quantum number,  $M$  the atomic magnetic moment, and  $H_m$  the molecular field. In the classical picture,  $K_1$  should vanish by letting  $S \rightarrow \infty$ .

Now, since  $NMH_m \approx 10^9 J/m^3$  and  $NI \approx 10^7 J/m^3$ , the order of magnitude of  $k_1$  due to dipole-dipole interaction is

$$K_1 \approx \frac{(NI)^2}{NMH_m} \approx \frac{(10^7)^2}{10^9} \approx 10^5 J/m^3$$

This is sufficient to explain the magnitude of the observed anisotropy energy.

Judging from the origin of anisotropy, it would be practical to suppose that the anisotropy constant decreases with increasing temperature and disappears at the Curie Point. Actually this does happen, and the temperature dependence is more drastic than that of spontaneous magnetization. Zener treated this problem in a simple way and explained the temperature dependence fairly well. He assumed that the pair energy is given by eq(2.13) even for the thermally perturbed spin system, since the neighbouring spins maintain an approximately parallel alignment upto the Curie point, where, because of the strong exchange interaction, parallel spin clusters prevail in the spin system.

Carr followed this method to calculate the crystal anisotropy constant for iron, nickel and cobalt.

Let  $(\alpha_1, \alpha_2, \alpha_3)$  denote the direction cosines of the average magnetization, and  $(\beta_1, \beta_2, \beta_3)$  are the direction cosines of the local magnetization. Since we assume local parallelism in the spin system, the anisotropy energy should be given by the average of the local anisotropy energies, so that

$$E_a(T) = K_1(0) \langle \beta_1^2 \beta_2^2 + \beta_2^2 \beta_3^2 + \beta_3^2 \beta_1^2 \rangle \quad \dots\dots\dots(2.16)$$

where  $K_1(0)$  is the anisotropy constant at  $T = 0^\circ K$  and  $\langle \rangle$  denotes the average over all possible orientations of local magnetization. Using the polar co-ordinates  $(\theta, \phi)$ , where  $\theta$  is the angle between the local spin and the average magnetization, and  $\phi$  the azimuthal angle around the magnetization direction. Thus,

$$E_a(T) = K_1(0) \frac{\int_0^\pi \left[ \left( \frac{1}{2\pi} \right) \int_0^{2\pi} (\beta_1^2 \beta_2^2 + \beta_2^2 \beta_3^2 + \beta_3^2 \beta_1^2) n(\theta) d\theta d\phi \right]}{\int_0^\pi n(\theta) d\theta} \quad \dots\dots\dots(2.17)$$

where  $n(\theta)d\theta$  is the number of spins which point in the solid angle between  $\theta$  and  $(\theta+d\theta)$ .

Since

$$\begin{aligned} \frac{1}{2\pi} \int_0^{2\pi} (\beta_1^2 \beta_2^2 + \beta_2^2 \beta_3^2 + \beta_3^2 \beta_1^2) d\phi \\ = \frac{1}{5} [1 - P_4(\cos \theta)] + P_4(\cos \theta) (\alpha_1^2 \alpha_2^2 + \alpha_2^2 \alpha_3^2 + \alpha_3^2 \alpha_1^2) \quad \dots\dots\dots(2.18) \end{aligned}$$



where  $P_4(\cos \theta)$  is the fourth order Legendre polynomial. Thus eq(2.17) becomes

$$E_a(T) = K_1(0) \langle P_4(\cos \theta) \rangle (\alpha_1^2 \alpha_2^2 + \alpha_2^2 \alpha_3^2 + \alpha_3^2 \alpha_1^2) \quad \dots \dots \dots (2.19)$$

where

$$\langle P_4(\cos \theta) \rangle = \frac{\int_0^\pi P_4(\cos \theta) n(\theta) d\theta}{\int_0^\pi n(\theta) d\theta} \quad \dots \dots \dots (2.20)$$

This can be expressed in a polynomial series in

$$\frac{1}{\alpha} = \frac{kT}{MH_m}$$

where  $H_m$  is the molecular field.

$$\langle P_4(\cos \theta) \rangle = 1 - \frac{10}{\alpha} + \frac{45}{\alpha^2} - \frac{105}{\alpha^3} + \dots \dots \dots (2.21)$$

On the other hand

$$M(T) = M(0) \left( \coth \alpha - \frac{1}{\alpha} \right) \approx M(0) \left( 1 - \frac{1}{\alpha} \right) \quad \dots \dots \dots (2.22)$$

so that

$$\left[ \frac{M(T)}{M(0)} \right]^{10} \approx 1 - \frac{10}{\alpha} + \frac{45}{\alpha^2} - \frac{120}{\alpha^3} + \dots \dots \dots (2.23)$$

comparing eq(2.21) and eq(2.23) we get

$$\left[ \frac{K_1(T)}{K_1(0)} \right] = \left[ \frac{M(T)}{M(0)} \right]^{10} \quad \dots \dots \dots (2.23 a)$$

Relation(2.23 a) holds good for the temperature dependence of  $K_1$  of iron Carr also explained the temperature dependence of  $K_1$  for nickel and cobalt by taking into

consideration the effect of thermal expansion of the crystal lattice. But, in contrast to Zener's theory, Van Vleck obtained a much more gentle temperature dependence of magnetic anisotropy. Keffer investigated this point and showed that the Zener's theory is valid at least at low temperature, while Van Vleck's theory is valid at high temperature.

### 2.7 Single-Ion Model of Magnetic Anisotropy:

The orbital state of magnetic ions plays an important role in determining the magnetic anisotropy. In order to discuss this phenomenon, we must first learn how the orbital state of a magnetic ion is influenced by a given crystalline field and how the resultant orbital state gives rise to magnetic anisotropy. This phenomenon is described by the single-ion model of magnetic anisotropy. This model has been successful in interpreting the magnetic anisotropy of various anti-ferromagnetic and ferrimagnetic crystals.

In free atomic states, every 3d electronic state has the same energy; in other words their energy levels are degenerate. When the atom is placed in a cubic field, the orbital states of 3d electrons are split into two groups. One is the triply degenerate  $d_{\epsilon}$  orbitals, the spatial distributions of which are expressed by  $xy, yz$  or  $zx$ . The other is the doubly degenerate  $d_{\gamma}$  orbitals whose distributions are expressed by  $2z^2 - x^2 - y^2$  and  $x^2 - y^2$ . Fig.2.3 explains that the  $d_{\epsilon}$  orbitals extend to  $\langle 110 \rangle$  directions, while the  $d_{\gamma}$  orbitals extend along the co-ordinate axes. In octahedral sites, the surrounding anions are found on the three co-ordinate axes, so the  $d_{\gamma}$  orbitals, which extend towards the anions, have a much higher energy than  $d_{\epsilon}$  orbitals because of the electrostatic repulsion

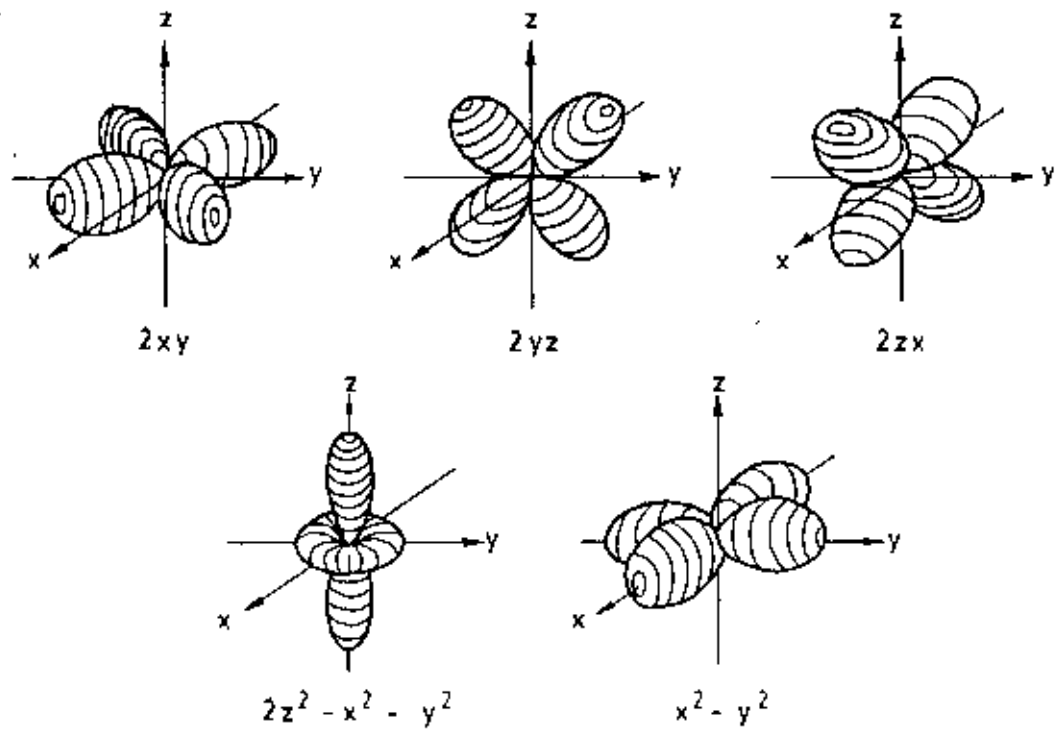


Fig. 2.3 Spatial distribution of  $d_e$  and  $d_\gamma$  orbitals

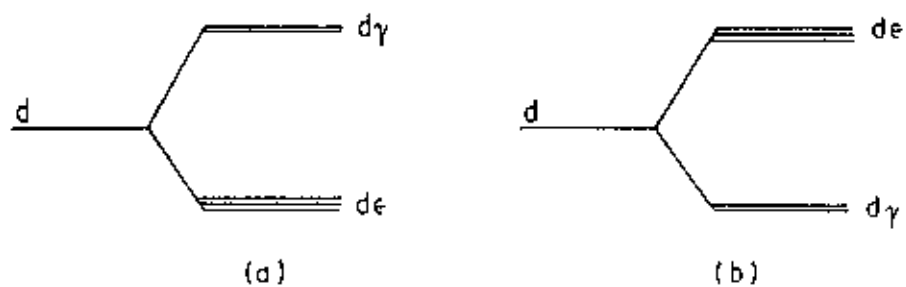


Fig 2.4 Energy levels of  $d_e$  and  $d_\gamma$  electrons in (a) octahedral and (b) tetrahedral sites

between anions and  $d$  orbitals. For tetrahedral sites  $dy$  orbitals are more stable than  $dx$  orbitals (Fig 2.4)

Let us consider the case of the  $d$  electrons occupying the  $3d$  energy levels. First let us assume that the magnetic ion has only one  $3d$  electron. This electron will naturally occupy the lowest energy level. Now as the three  $dx$  levels have the same energy, the lowest orbital state is triply degenerate (triplet). Such an orbital degeneracy plays an important role in determining the magnetic anisotropy. If there are additional  $3d$  electrons, they should occupy exclusively the plus spin levels, because the exchange interaction between these  $3d$  electrons is much larger than the energy separation between the  $dy$  and  $dx$  levels. In the case of  $(3d)^1$ , the three electrons occupy the three  $dx$  levels, so that the ground state is non-degenerate (singlet). For  $(3d)^4$ , three electrons occupy the  $dx$  levels and the remaining one occupies one of the two  $dy$  levels, thus the state is doubly degenerate (doublet). In the case of  $(3d)^5$ , all electrons occupy plus spin levels, so that the ground state is a singlet. When there are more than five electrons, the first five fill up the plus spin levels while the remaining electrons occupy the minus spin levels in the same way as for the plus spin levels.

As for the  $Fe^{2+}$  ion, the sixth electron should occupy the lowest singlet state, so that the ground state is non-degenerate. On the other hand, the  $Co^{2+}$  ion has seven electrons, so that the last one should occupy the doublet. In such a case the orbit has the freedom to change its state in the plane which is normal to the trigonal axis, so that it has an angular momentum parallel to the trigonal axis. Now since the angular momentum is fixed in direction, it tends to align the spin magnetic moment parallel to the trigonal axis through the spin-orbit interaction. The energy of this interaction can be expressed as  $-\lambda LS \cos \theta$ , where  $\lambda$  is the spin-orbit parameter,  $L$  and  $S$  are the orbital and spin angular momentum and  $\theta$  is the angle between the magnetization and

the trigonal axis. This model was first proposed by Slonczewski, who explained the magnetic annealing effect in *Co* ferrite by this model. He also explained the temperature dependence of the anisotropy constant of cobalt-substituted magnetite. In the normal, or non-magnetically annealed state,  $Co^{2+}$  ions should be distributed equally among the four kinds of octahedral sites each of which has its trigonal axis parallel to one of the four  $\langle 111 \rangle$  directions, so that the cubic anisotropy can be obtained by averaging the anisotropy energy  $-\lambda LS^2 |\cos \theta_i|$  over four directions of trigonal axes.

If the ground orbital state is non-degenerate, we cannot expect any orbital angular momentum so long as the atom stays in the ground state; in other words, the orbital angular momentum is quenched by the crystalline field. In such a case we cannot expect an anisotropy as large as that of the  $Co^{2+}$  ion in an octahedral site. There are, however, various sources which result in a fairly small magnetic anisotropy, which is nevertheless sufficiently large to account for the observed values. Yosida and Tachiki calculated the various types of anisotropy and applied their results to the *Mn*, *Fe* and *Ni* ferrites, which contain  $Mn^{2+}$ ,  $Fe^{3+}$ ,  $Fe^{2+}$  and  $Ni^{2+}$  ions. Firstly, they found that the magnetic dipole-dipole interaction is too weak to account for the observed magnitude of anisotropy. The main source of anisotropy is thought to be the distortion of the  $3d$  shell from spherical symmetry. In a distorted  $3d$  shell the intra-atomic dipole-dipole interaction between the spin magnetic moments may depend on the direction of magnetization; this is similar to the dependence of the magneto static energy on the direction of magnetization in a fine elongated single domain particle, and gives rise to anisotropy energy.

The anisotropy is also induced through spin-orbit interaction. That is, some amount of orbital angular momentum can be induced by spin-orbit interaction by exciting

additional orbital states. In a distorted  $3d$  shell this excitation is dependent on the direction of magnetization, giving rise to anisotropy. Yosida and Tachiki showed that the anisotropy due to these mechanisms should vanish for  $S = \frac{1}{2}, 1,$  and  $\frac{3}{2}$ , where  $S$  is the total spin angular momentum, and that anisotropy of this type cannot be expected for  $Ni^{2+}$  and  $Co^{2+}$  ions. Accordingly, the main source of the anisotropy of  $Mn, Fe$  and  $Ni$  ferrites is considered to be the  $Mn^{2+}, Fe^{3+}$ , and  $Fe^{2+}$  ions. Since  $Ni^{2+}$  ion has no effect on the magnetic anisotropy in  $Ni$  ferrite, the difference in anisotropy energy between  $Fe$  and  $Ni$  ferrites must be explained by the anisotropy due to  $Fe^{2+}$  ions. Yosida and Tachiki also calculated the temperature dependence of the anisotropy constant for  $Mn$  ferrites and fitted the theory with experiment.

### 2.8 Band Model Theories:

Brooks(1940) treated the magnetic anisotropy of nickel and iron from the collective electron approach. in an attempt to calculate the anisotropy constants with a more explicit model than that of Van Vleck. In the collective electron model of Bloch, Stoner and Slater each electron is considered as belonging to the metal as a whole and moving in a self-consistent field. Although, this is a poor approximation for the tightly bound  $d$  electrons, it gives rise to magnetic anisotropy in a straight forward manner.

According to Brook's theory, spin-orbit coupling together with the quenching of the orbital causes anisotropy. The quenching arises naturally from the hopping of electrons between adjacent atoms. This hopping takes place, even in the  $d$  band, with sufficient frequency to destroy any orientation in an external magnetic field. So each electron moves in a field which has the symmetry of the crystal.

The structure of the d band was represented by the Bloch tight-binding approximation, which is reasonably reliable since the overlapping of the shells is small. Using this and by treating the spin-orbit interaction as a small perturbation Brooks calculated  $K_1$  for nickel and iron. His values of  $K_1$  were of the correct signs and orders of magnitude. Fletcher(1954) re-calculated  $K_1$  for nickel by Brooks method, using new data on the energy distribution of the d-electrons. His value of  $K_1$  at 0°K is about 50 times greater than the accepted experimental values.

### 2.9 Composition dependence of magnetic anisotropy:

In the present work, the variation of the anisotropy energy as a function of the concentration of a non-magnetic solute, e.g. molybdenum, in nickel is of particular interest. The saturation magnetization of Ni-Mo alloys decreases linearly with increasing molybdenum content in Ni, being zero at about 10 at% Mo.(Fig.4.4). Since the anisotropy energy is related to the magnetization, the anisotropy constants will also decrease with increasing molybdenum, as some function of the saturation magnetization.

On a single-ion model of anisotropy it seems reasonable to expect, by a simple dilution process, that the anisotropy energy will decrease in the same manner as the magnetization, i.e., linearly with increasing solute concentration.

From Van Vleck's theory of magnetic anisotropy, according to Bozorth(1951),  $K_1(0)$  of alloys such as Ni-Mo decreases with increasing solute content as:

(a) dipolar model

$$K_1(0) \propto M(0)$$

and

(b) quadrupolar model

$$K_1(0) \propto [M(0)]^2$$

A simple model of the composition dependence of  $K_1$  is given by Enoch and Fudge(1966). They consider a localized model in which magnetic anisotropy arises from magnetic Ni-Ni interactions; they assume that the basic mechanism of anisotropy is unaffected by the presence of atoms of Cu or Mo. On this model increasing the amount of solute should reduce  $K_1$  by

(a) a simple dilution process where a magnetic nickel atom is replaced by a non-magnetic solute atom,

(b) dilution caused by the presence of neutralised nickel atoms. Thus  $K_1(0)$  should be proportional to the probability of Ni-Ni interactions occurring, i.e.,

$$K_1(0) \propto (C_{Ni} - kC_{So})^2$$

where  $C_{Ni}$  and  $C_{So}$  are the atomic concentrations of nickel and solute respectively, and  $k$  is the number of nickel atoms neutralised by the addition of one atom of solute

Results of neutron scattering experiments (Comly, Holden and Low, 1968) examine the spatial distribution of the magnetic moment disturbance around an impurity atom in dilute alloys of nickel and suggest that the composition dependence of Ni-Cu and Ni-Mo alloys may be rather complicated, especially for low concentrations. Comly et. al. found that the addition of small concentrations of copper or molybdenum to nickel lead to a widespread magnetic disturbance in the neighbourhood of the impurity atom, extending some 5Å into the nickel matrix. Since the lattice constant of nickel is about 3.5Å, the range of the disturbance is considerable, and might be expected to give rise to a rapid decrease in the anisotropy energy with small additions of the solute to the pure metal.



Further work by Hicks et al.(1969) on Ni-Cu alloys near the critical composition (about 60% Cu) indicate that in this region the behaviour of the anisotropy energy may be complicated by the presence of giant magnetic moments. Using neutron scattering techniques, these workers found, in the weakly ferromagnetic Ni-Cu alloys, the low temperature spontaneous magnetization to be inhomogeneously distributed in magnetic polarisation clouds of large total moment (over  $8\mu_B$ ) extending over many atoms. It seems reasonable that a similar situation exists in Ni-Mo alloys in the region near 10 atomic% Mo.

### 2.10 The Temperature dependence of magnetocrystalline anisotropy:

The temperature dependence of magnetocrystalline anisotropy is established by theoretical arguments with increasing generality(Callen and Callen 1966)to follow the general  $\frac{n}{2}(n+1)$  power law, i.e.

$$\frac{K(T)}{K(0)} = \left[ \frac{M(T)}{M(0)} \right]^{\frac{n}{2}(n+1)}$$

where  $K(0)$  is the anisotropy constant at  $0^\circ K$  and  $K(T)$  is the anisotropy constant at  $T^\circ K$ .  $M(0)$  is the magnetization at  $0^\circ K$  and  $M(T)$  is the magnetization at  $T^\circ K$ .

The  $\frac{n}{2}(n+1)$  power law of the temperature dependence of the magneto-crystalline anisotropy at low temperature is derived in general fashion by Callen and Callen(1966). The problem of temperature dependence of anisotropy energy takes its beginning from the famous tenth power law, formulated for the first time by Akulov. Callen and Callen have reviewed the origin of the tenth power law.

The magnetocrystalline anisotropy is defined in terms of the dependence of the free energy on the direction of the magnetization. For a cubic ferromagnet the free energy is usually expanded in a power series in the direction cosines  $\alpha_1, \alpha_2, \alpha_3$  of the

magnetization direction relative to the crystallographic axes. Symmetry dictates that this power series take the form

$$F = K_0(T) + K_1(T) [\alpha_1^2 \alpha_2^2 + \alpha_2^2 \alpha_1^2 + \alpha_3^2 \alpha_1^2] + K_2(T) \alpha_1^2 \alpha_2^2 \alpha_3^2 \dots \dots (2.24)$$

Akulov showed by a simple classical argument that

$$\frac{K_1(T)}{K_1(0)} \cong 1 - 10\delta n \cong [1 - \delta n]^{10} \cong [m(T)]^{10} \dots \dots (2.25)$$

where  $m(T)$  is the reduced magnetization  $\left( = \frac{M(T)}{M(0)} \right)$  and where  $\delta n(T) \cong 1 - m(T)$ .

The Akulov result applies only at temperatures sufficiently low that  $\delta n \ll 1$ . The Akulov derivation is based on the assumption of independent classical spins, each of which has an energy of the form of eq(2.24). The power 10 in eq(2.25) arises not from a particular model but rather from the peculiar structural combination of the direction cosines in eq(2.24). This combination is completely dictated by the symmetry of the crystal. Thus the Akulov derivation, did identify the source of the 10th power law. Akulov compared the theoretical result with the data of Honda et al. on iron, and concluded that the law was quite accurately obeyed upto  $T \approx 0.65T_c$ .

In 1955 Keffer recognised that the paradox posed by the disagreement of Akulov's theorem and Van Vleck's molecular field calculations arose from the violence that molecular field theory does to spin correlations. He therefore recalculated the anisotropy of pseudo-quadrupolar origin, substituting a cluster theory for molecular field theory. This cluster theory had been incidentally introduced by Van Vleck in 1937. This concept was later fully exploited by Oguchi. Keffer then found that the pseudo-quadrupolar interaction would give a 10th power law at low temperatures, changing rapidly to Van Vleck's 6th power dependence as increasing temperature

disrupts the spin correlations. Keffer also rederived the Zener  $\frac{n}{2}(n+1)$  generalisation, using the classical single-ion mechanism and molecular field theory. At this point it was clear that the single-ion terms in the Hamiltonian were completely consistent with the  $\frac{n}{2}(n+1)$  power law, and Keffer's cluster calculation was generally accepted as establishing the theorem for pseudo-quadrupolar interactions.

Peculiarly in the very paper in which Keffer established the  $\frac{n}{2}(n+1)$  law for the single-ion and pseudo-quadrupolar terms and identified the crucial role of spin correlations, he also briefly remarked that a spin-wave analysis of the dipolar terms would probably give a power even lower than two. Kasuya then carried out just such a spin-wave calculation for the pseudo-dipolar terms and found a 16th power. Charap and Weiss found an error of a factor of 2 in Kasuya's calculation and concluded that the 8th power was correct. Finally Keffer and Oguchi added certain terms omitted by Charap and Weiss, regained the 10th power and stressed that correlations ensure the 10th power law in all cases.

In 1959 Turov and Mitsek deduced the  $\frac{n}{2}(n+1)$  power dependence from the spin-wave approach of Kasuya. In 1966 Callen and Callen showed that this law can be generalised to higher anisotropy constants of arbitrary crystal symmetry, to a quantum mechanical treatment, to two ion as well as one ion mechanism and to arbitrary temperatures.

The theory predicts that for cubic crystals the anisotropy constants are related to magnetization as,

$$\frac{K_2^0(T)}{K_2^0(0)} = \left[ \frac{M(T)}{M(0)} \right]^{10}, \quad \frac{K_4^0(T)}{K_4^0(0)} = \left[ \frac{M(T)}{M(0)} \right]^{21} \dots \dots \dots (2.26)$$

And for hexagonal crystal

$$\frac{K_2^0(T)}{K_2^0(0)} = \left[ \frac{M(T)}{M(0)} \right]^3 ; \frac{K_4^0(T)}{K_4^0(0)} = \left[ \frac{M(T)}{M(0)} \right]^{10}$$

and

$$\frac{K_n^0(T)}{K_n^0(0)} = \frac{K_n^0(T)}{K_n^0(0)} = \left[ \frac{M(T)}{M(0)} \right]^{21} \dots \dots \dots (2.27)$$

When these coefficients are expressed in terms of anisotropy constants  $K_1, K_2, \dots$  which are generally measured in the analysis of the torque curve, the expressions (2.24) and (2.25) become

For cubic crystal

$$K_1(T) = \left[ K_1(0) + \frac{1}{11} K_2(0) \right] \left[ \frac{M(T)}{M(0)} \right]^{10} - \frac{1}{11} K_2(0) \left[ \frac{M(T)}{M(0)} \right]^{21} \dots \dots \dots (2.28)$$

$$K_2(T) = K_2(0) \left[ \frac{M(T)}{M(0)} \right]^{21} \dots \dots \dots (2.29)$$

For hexagonal crystals

$$K_1(T) = \left[ K_1(0) + \frac{8}{7} K_2(0) + \frac{8}{7} K_3(0) \right] \left[ \frac{M(T)}{M(0)} \right]^3 - \left[ \frac{8}{7} K_2(0) + \frac{144}{77} K_3(0) \right] \left[ \frac{M(T)}{M(0)} \right]^{10} + \frac{8}{3} K_3(0) \left[ \frac{M(T)}{M(0)} \right]^{21} \dots \dots \dots (2.30)$$

$$K_2(T) = \left[ K_2(0) + \frac{18}{11} K_3(0) \right] \left[ \frac{M(T)}{M(0)} \right]^{10} - \frac{18}{11} K_3(0) \left[ \frac{M(T)}{M(0)} \right]^{21} \dots \dots \dots (2.31)$$

$$K_3(T) = K_3(0) \left[ \frac{M(T)}{M(0)} \right]^{21} \quad \dots\dots (2.32)$$

$$K_4(T) = K_4(0) \left[ \frac{M(T)}{M(0)} \right]^{21} \quad \dots\dots (2.33)$$

However, neither of the expressions (2.26) or (2.27) is found to be in good agreement with the observed behaviour of the iron group elements. For iron (cubic)  $K_1(T)$  varies as approximately as the sixth power of  $\frac{M(T)}{M(0)}$ , whilst in nickel the variation is much faster than  $\left[ \frac{M(T)}{M(0)} \right]^{10}$  and nearly follows  $\left[ \frac{M(T)}{M(0)} \right]^{20}$  at lower temperature

From all the model discussed so far, it is evident that the ferromagnetic anisotropy is caused by an anisotropic term in the exchange energy. The anisotropic exchange is caused by the spin-orbit coupling which relates the spin to the dependence of inter-atomic energy on the orientation of the orbital wave functions. The origins of magnetic anisotropy, mainly with reference to insulators, are reviewed by Yosida(1968), Kanamori(1963), and Callen and Callen(1966).

The  $\frac{n}{2}(n+1)$  power law for the temperature dependence of the anisotropy constants, in particular the 10th power law for  $K_1$ , obtains in all the theories that can treat the temperature variation of the anisotropy energy. It may be derived quite generally, both quantum mechanically and classically(Van Vleck, 1956). In either case the law is valid at low temperatures only, because classically it is assumed that the spin deviations are small, and quantum mechanically only the ground and the first excited states are occupied.

On the other hand, it has been found by many workers that a highly satisfactory fit to experimental data is given by the empirical relationship of Bryuchatov and Kirensky(1937).

$$\frac{K_1'(T)}{K_1'(0)} = \exp(-aT^2) \quad \dots\dots\dots (2.34)$$

which is frequently used to determine  $K_1(0)$  by extrapolation. This holds for nickel up to room temperature. A thermodynamic argument has been given in favour of this relationship by Stato and Tino (1956)

The mathematical expression of the behaviour of the anisotropy constants at low temperatures, derived theoretically, is

$$\frac{K_n(0) - K_n(T)}{K_n(0)} = \frac{n}{2}(n+1) \left[ \frac{M(0) - M(T)}{M(0)} \right] \quad \dots\dots\dots (2.35)$$

i.e 
$$\frac{K_n(T)}{K_n(0)} = 1 - \frac{n}{2}(n+1) \delta M(T) \quad \dots\dots\dots (2.36)$$

where 
$$\delta M(T) = \frac{M(0) - M(T)}{M(0)}$$

Since the anisotropy is assumed to vanish at the Curie temperature the linear expression of equation(2.30) can not be exact. Hence it represents the first two terms of a binomial expansion,

$$\frac{K_n(T)}{K_n(0)} = [1 - \delta M(T)]^{\frac{n}{2}(n+1)} = \left[ \frac{M(T)}{M(0)} \right]^{\frac{n}{2}(n+1)} \quad \dots\dots\dots (2.37)$$

At temperatures sufficiently far from the Curie temperature

$$\frac{K_u(T)}{K_u(0)} = \exp\left[-\frac{n}{2}(n+1)\delta M(0)\right] \quad \dots\dots\dots (2.38)$$

If the low temperature variation of the spontaneous magnetization is taken to be

$$\frac{M(T)}{M(0)} = 1 - A\left(\frac{M}{T_c}\right)^m \quad \dots\dots\dots (2.39)$$

then

$$\frac{K_u(T)}{K_u(0)} = \exp\left[-B\left(\frac{M}{T_c}\right)^m\right] \quad \dots\dots\dots (2.40)$$

where

$$B = \frac{n}{2}(n+1)A$$

From spin wave theory  $m = \frac{3}{2}$  at low temperatures and equation(2.39) has been confirmed to a high accuracy (Pugh and Argyle,1962) for nickel. The derived constant of  $\frac{A}{T_c^{\frac{1}{2}}}$  is of order  $4 \times 10^{-6}$ . It must be admitted that the temperature dependence of  $\frac{K_1(T)}{K_1(0)}$  for Ni does not follow the expression in equation(2.34) with  $m = \frac{3}{2}$ , nor the initial slope of a graph of  $\log\left[\frac{K_1(T)}{K_1(0)}\right]$  in agreement with the predicted value of  $\frac{n}{2}(n+1)AT_c^{\frac{1}{2}}$ . However it has been the common experience of many experimentalists that equation (2.39) does fit experimental magnetization data with  $m = 2$  over a large temperature range. However none of the theories of anisotropy can explain the change in sign of  $K_1$  of nickel that is found experimentally to occur about 200°C. A change in sign of  $K_1$  would apparently suggest a change in sign of the magnetization which is incorrect. It is possible that if corrected to constant volume  $K_1$  may be found to remain negative.

These developments in the theoretical understanding of temperature dependence of anisotropy however fails to explain our results of Ni-Mo alloys satisfactorily as we shall see in Chapter 4.



**Chapter 3**  
**Measurement Techniques**

### 3.1 Experimental

For the measurements of magnetization a Vibrating Sample Magnetometer (VSM) with the facilities of connecting a Cryostat for measurements at low temperature and a high temperature Oven for the measurements at high temperature is used. Also a Super Conducting Quantum Interference Device (SQUID) with a computer controlled data acquisition system is used for measurements of magnetization. For the measurements of a.c susceptibility an a.c. Susceptometer with a Computer controlled data acquisition system is used. For the measurements of d.c. relaxation measurements a r.f. SQUID with a Computer controlled data acquisition system is used.

### 3.2 Different methods of measurements of Magneto-crystalline Anisotropy:

#### (1) Ferromagnetic resonance

The resonance frequency depends on the effective internal magnetic field which exerts a torque on the precessing spin system. Magnetic anisotropy contributes a torque on a spin system if the spins point in other than the easy or hard directions, thus affecting the resonance frequency. The equation of motion of the magnetization vector is given by

$$\left(\frac{1}{\gamma}\right)\left(\frac{dM}{dt}\right) = M \times H + \text{torque due to anisotropy energy}$$

By calculating the frequency of the small oscillation of  $M$  around the equilibrium position one can express the resonance frequency in terms of  $B$  and anisotropy constant.  $\gamma$  is the gyro-magnetic ratio.

This method enables measurements of the anisotropy to be made on very small single crystal specimens. It also offers information about the magnitude of the local anisotropy, as distinct from the bulk anisotropy determined by other methods.

### (2) Torque Curves

When an anisotropic single crystal is suspended in a uniform magnetic field, a torque acts on it tending to align an easy direction of magnetization along the field direction. The torque exerted per unit volume of the specimen is

$$L = -\frac{dE_a}{d\phi} \quad \dots\dots\dots (3.1)$$

where  $\phi$  is the angle of rotation of the easy direction of magnetization, from which the anisotropy constants may be evaluated. This method has the advantage that contributions to the torque from sources other than the magnetic anisotropy can generally be distinguished in the torque curves.

### (3) Magnetization curves of a single crystal:

The shape of the magnetization curve for a magnetic field applied in a particular crystallographic direction depends on the values of the anisotropy constants. The theoretical expressions for the magnetization in terms of the magnetic field and the anisotropy energy can be calculated, and comparison with experimental values enables the anisotropy constants to be determined.

### 3.3 Formulation of Magneto-crystalline anisotropy:

When a ferromagnetic material is magnetised in an applied magnetic field  $H$ , the energy  $E_a$  stored in the system is represented by

$$E_a = \int_0^{M_s} H \cdot dM \quad \dots\dots\dots(3.2)$$

where  $M_s$  is the saturation magnetization. The quantity  $\int_0^{M_s} H \cdot dM$  represents the area under the magnetization curve and is related to the magnetic anisotropy energy

$$E_a = K_1 (\alpha_1^2 \alpha_2^2 + \alpha_2^2 \alpha_3^2 + \alpha_3^2 \alpha_1^2) + K_2 \alpha_1^2 \alpha_2^2 \alpha_3^2 + \dots\dots\dots(3.3)$$

where  $\alpha$ 's are the direction cosines of the magnetization vector with respect to the crystallographic axes and  $K_1$  and  $K_2$  are the first and the second anisotropy constants respectively. If  $\phi$  is the angle made by the internal magnetization measured in the plane of the specimen. For magnetization confined to a (001) plane of a cubic crystal, we can write  $\alpha_1 = \cos \phi$ ,  $\alpha_2 = \sin \phi$  and  $\alpha_3 = 0$ , if  $\phi$  is measured from the [100] direction.

Then the first term of eq(3.3) becomes

$$E_a = K_1 \cos^2 \phi \sin^2 \phi = \frac{1}{4} K_1 \sin^2 2\phi \quad \dots\dots\dots(3.4)$$

and hence from eq(3.1)

$$L = -\frac{1}{2} K_1 \sin 4\phi \quad \dots\dots\dots(3.5)$$

where  $L$  is the torque.

For a (100) surface the anisotropy energy is given by [Chikazumi]

$$E_a = -K_1 \cos^2(\phi - \phi_0) + \frac{K_1}{32} [7 - 4 \cos 2(\phi - \phi_0) - 3 \cos 4(\phi - \phi_0)] + \frac{K_2}{128} [2 - \cos 2(\phi - \phi_0) - 2 \cos 4(\phi - \phi_0) + \cos 6(\phi - \phi_0)] \quad \dots\dots\dots(3.6)$$

$$E_{a(111) \parallel (100)} = \frac{K_1}{3} + \frac{K_2}{27} \quad \dots\dots\dots(3.7)$$

$$E_{\sigma_{110-100}} = \frac{K_1}{4} \dots \dots \dots (3.8)$$

For a hexagonal system the anisotropy energy may be written as

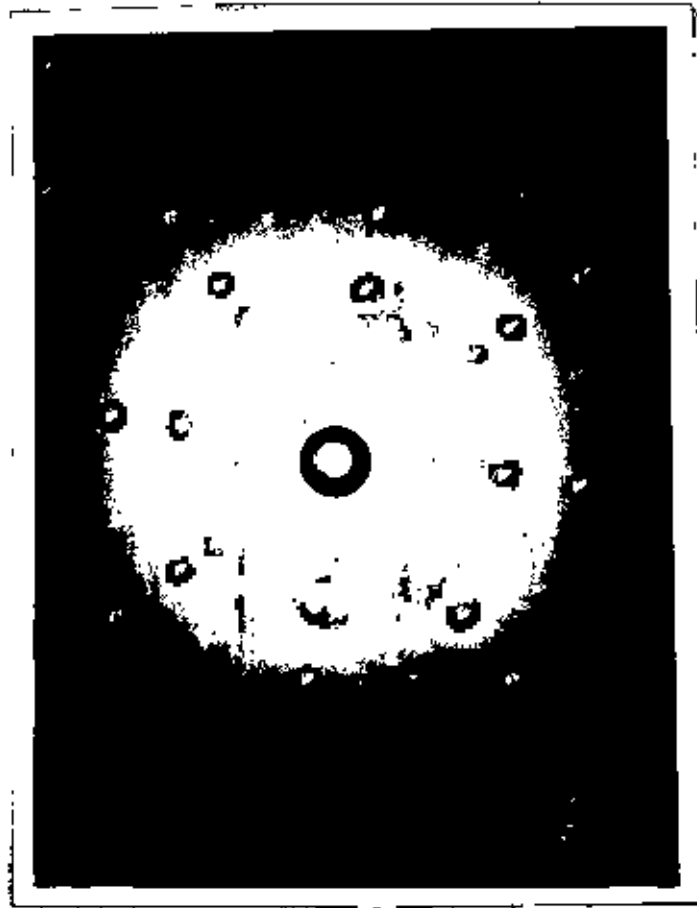
$$E_a = K_{a1} \sin^2 \phi + K_{a2} \sin^4 \phi + \dots \dots \dots (3.9)$$

### **3.4 Sample preparation and orientation:**

A 5X5X5 mm<sup>3</sup> sample is cut from the bulk Ni-Mo specimen and then turned into a rough sphere by using a polishing machine. The sample is then put into a ball milling machine for several hours. After several hours of milling the sample is turned into a perfect sphere. After that the sample is etched by dilute HNO<sub>3</sub> for a couple of hours to remove strains. The etched sample is then glued to a Goniometer head for Laue photography. The sample is then oriented in the (110) crystallographic plane within the accuracy of  $\pm \frac{1}{2}^\circ$ . This plane contains all the three principal crystallographic directions, [111], [110] and [100] respectively within an accuracy of  $\pm \frac{1}{2}^\circ$ .

### **3.5 The Vibrating Sample Magnetometer (V.S.M):**

A vibrating sample magnetometer (VSM) is a device which measures the magnetic moment of a sample when it is vibrated perpendicularly to a uniform magnetising field. With this instrument, changes as small as 10<sup>-6</sup>-10<sup>-7</sup> e.m.u can be detected and a stability of one part in 10<sup>4</sup> may be attained. This instrument is simple, inexpensive, and versatile, yet permits precision magnetic moment measurements to be made in a uniform magnetising field as a function of temperature, magnetising field and crystallographic orientation.



**Laue photograph of the Ni-Mo single crystal in the [100] crystallographic direction**

The novel features of this magnetometer are, firstly, the sample motion is perpendicular to the applied field, and secondly, the detection coil configurations with effective area turns non-symmetrically distributed about the axis of vibrations, which permit the oscillating dipole field to be observed. The basic instrument is shown in Fig 3.1.

The sample is vibrated perpendicularly to the applied field by the loudspeaker(diaphragm) assembly with a selected frequency. The oscillating magnetic field of the vibrating sample induces a voltage in the stationary detection coils, and from measurements of this voltage the magnetic properties of the sample are deduced. A second voltage is induced in a similar stationary set of reference coils by a reference sample which is a small permanent magnet or a vibrating coil in the field of permanent magnets. Since the sample and the reference are driven synchronously by a common member, the phase and the amplitude of the resulting voltages are directly related. The known portion of the voltage from the reference coils is phased to balance the voltage from the detection coils, which is then proportional to the magnetic moment of the sample.

By this procedure the measurements can be made insensitive to changes of vibrational amplitude, vibration frequency, small magnetic field instabilities, magnetic field non-uniformity, amplifier gain, or amplifier linearity. The measurements are made insensitive to the exact sample position by employing suitable pairs of coils. To do this for the coils, the sample is first centrally positioned between the coils by visual inspection. The sample is then positioned about the z-axis for maximum signal output. The output is then insensitive to small changes in position about this axis. The sample is then translated in the x-direction for a minimum output, and then along the y-

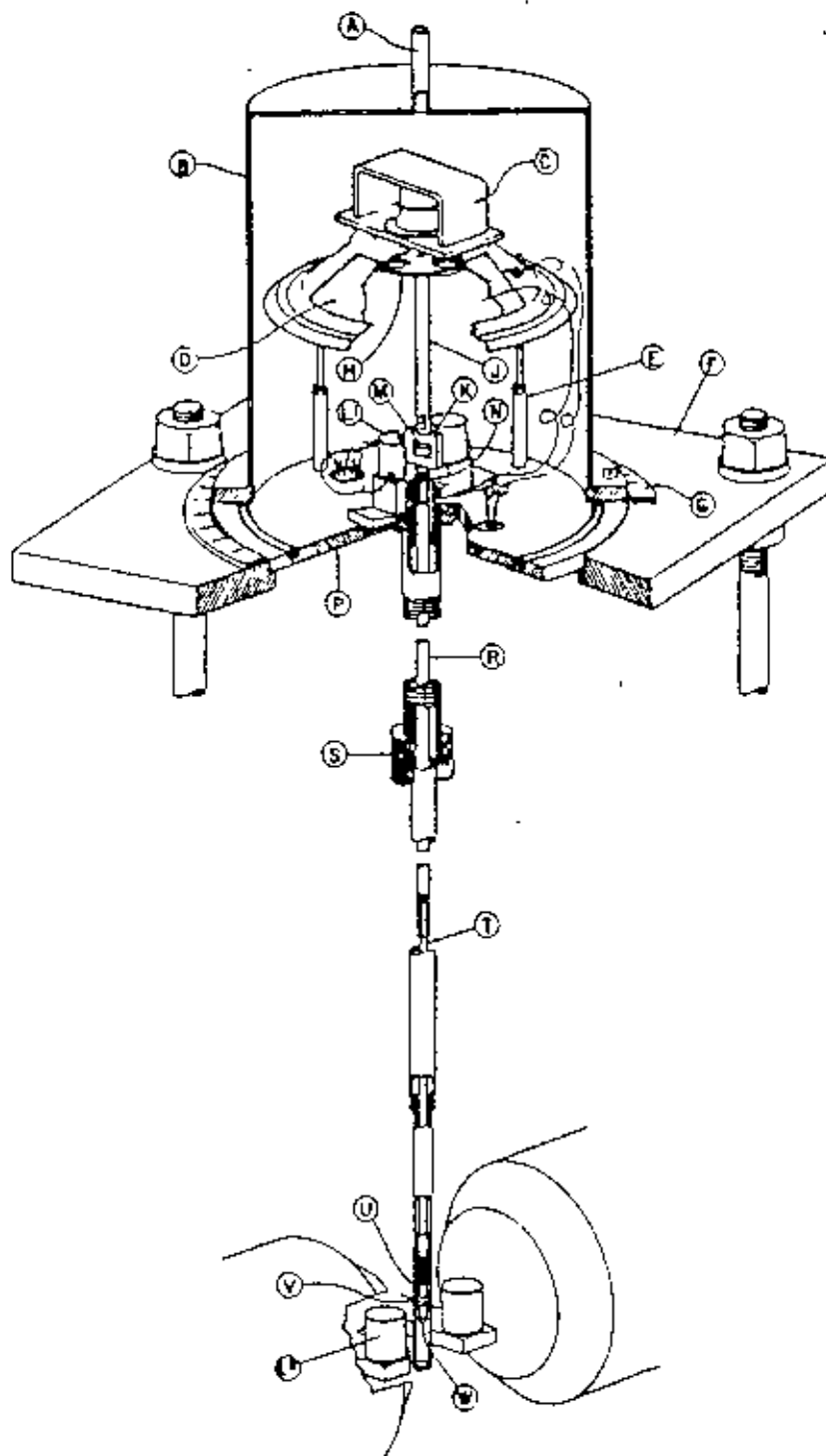


**Fig. 3.1 Schematic diagram of the Vibrating Sample Magnetometer**



direction for a maximum output. The sample is now located at the 'saddle point'. The output signal is independent of small displacements of the sample in any direction

### 3.6 The Detection Coil configuration

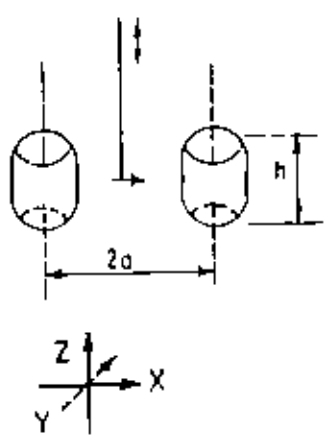
All the magnetic induction measurements involve observation of the voltage induced in a detection coil by a flux change when the applied magnetic field, coil position, or sample position is changed. The advantages of sample vibration perpendicularly to the applied magnetic field can be realised only if suitable detection coil arrangements can be devised. In practice many satisfactory coil configurations can be found. This is easily seen if we consider the time varying part of the vibrating dipole field. The scalar potential of a fixed dipole  $m$  at the origin and pointed along the  $X$  direction is  $\phi = \frac{mX}{r^3}$ . If  $m$  is vibrated in the  $Z$  direction with sufficiently small amplitude, the time varying potential in the surrounding space will be  $\phi_1 e^{i\omega t}$  where  $\phi_1 = -a \left( \frac{\partial \phi}{\partial Z} \right) = \frac{amXZ}{r^5}$ .

The flux pattern of the time varying part of the field is given by  $-\text{grad}\phi_1$ .

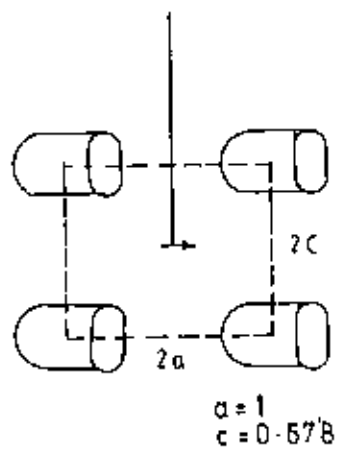
Appropriate placement of pick up coils to sense this flux may be visualised easily. A general feature of all the useful coil configurations is that each effective area-turn is non symmetrically distributed about the axis of vibration. Pairs of coils are employed in order to minimise effects of sample position or external field variations. In a similar way, the effect of slight nonuniformities of the magnetising field, which causes  $m$  to vary during vibration, may be examined. In general, the pickup coil dimensions are not small compared to their distance from the sample. Furthermore, the coil geometries

often do not follow the symmetries of the time varying field. For these reasons, the voltage induced in most useful pickup coils can not be calculated in closed form

One of the most convenient detection-coil arrangements is the double coil shown in Fig.3 2. The spatial variations of relative output signal for a typical double coil assembly is plotted in Fig.3 2 a.



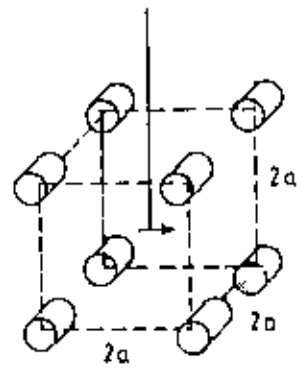
(a)



(b)

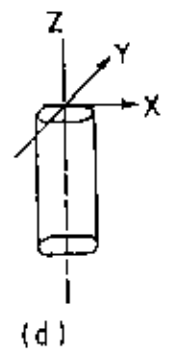
$$a = 1$$

$$c = 0.578$$



(c)

$$a = b = c = 1/\sqrt{2}$$



(d)

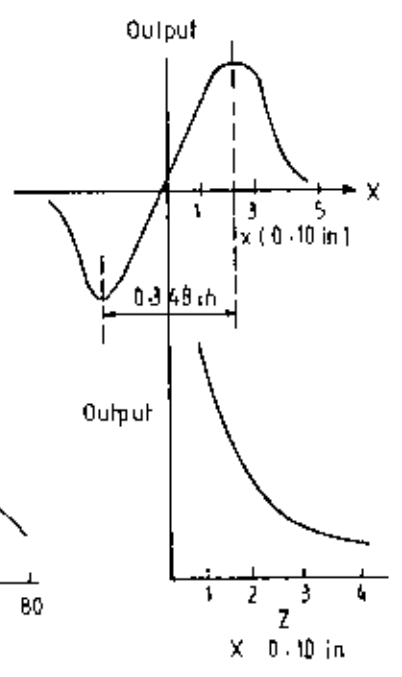
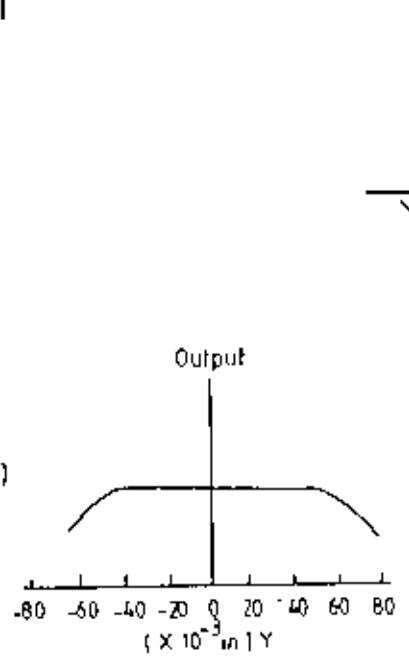
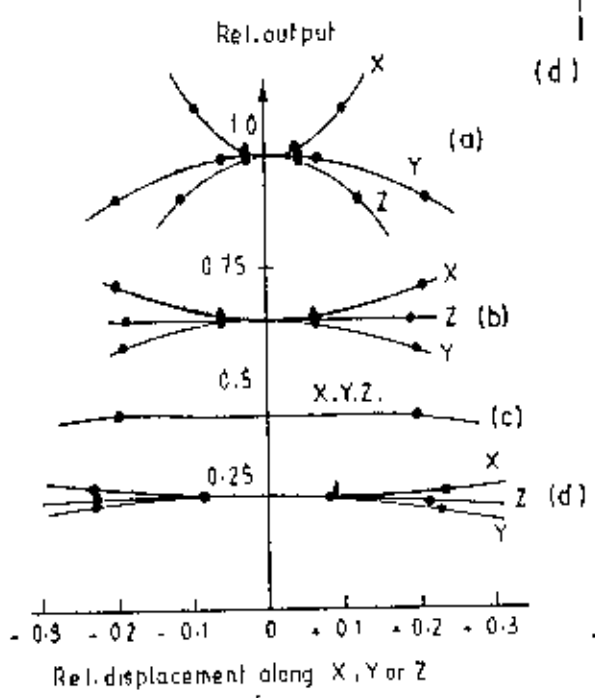
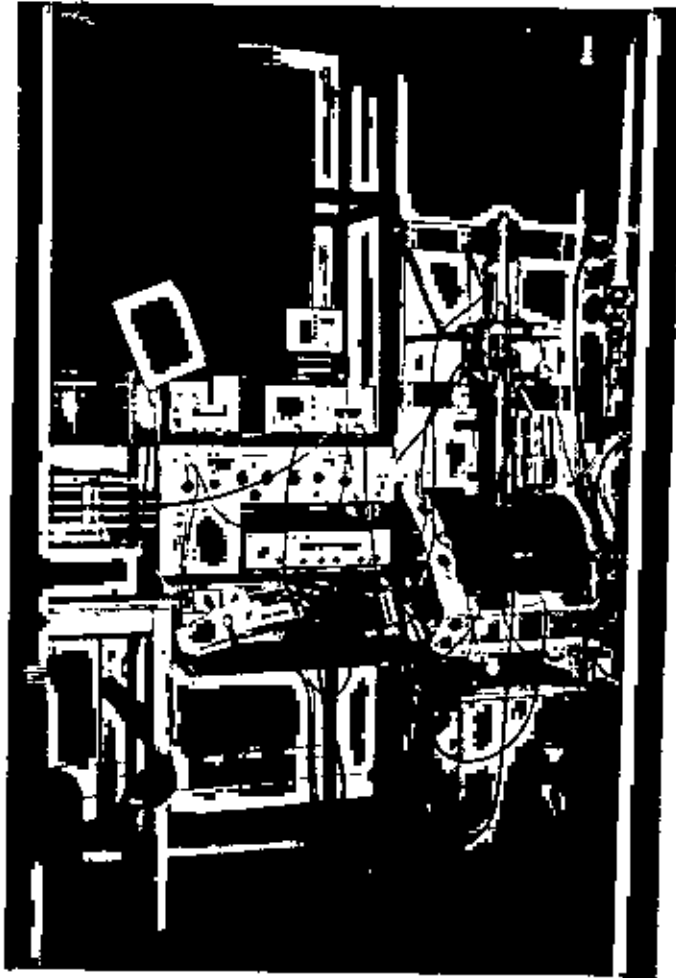


Fig 3.2 Transverse detection coil configuration

Two coils are wound each of resistance about 8 kilo Ohm. The coils are positioned on the two pole faces of the electromagnet. These coils are tested experimentally by observing the output signal due to the magnetic moment of a small magnetically saturated nickel sphere as it is positioned at various points in space by a suitable micrometer arrangement. An additional feature of this double-coil system is that the two coils are connected series-opposing in order to obtain a net output signal. This arrangement to a large extent eliminates the effects of the background noise due to magnetic field instability or mechanical vibrations of the magnet and coil system. This coil configuration is employed extensively for almost all magnetic measurements and is proved to be suitable for our measurements as it is versatile, easy to assemble and most convenient in operation.

### 3.7 Calibration of the Magnetometer.

For the calibration of the V.S.M a standard nickel sphere of mass 57 mg from National Board of Standards is obtained. The sphere is put in a small plastic cup of about 5mm diameter. Some cotton is put on top of the sphere to avoid free vibration of the sample. Then the sample cup alongwith the sample is fixed at the end of the quartz sample rod and is joined with the upper part of the sample rod. A small alternating voltage is applied by a Phillips Signal Generator to vibrate the sample rod with a selected frequency (in this experiment 37 Hz). The magnet power supply is connected to a Magnetic Field Sweeping unit. The magnetic field is then gradually increased to record the magnetization. The field is continued to increase until the nickel sphere is magnetically saturated. The output is measured in volts by a voltmeter. Then using the



**Photograph of the Vibrating Sample Magnetometer**

saturation moment of nickel the magnetometer is calibrated. The calibration constant of the V.S.M. is

$$\text{Volt} = 2.3e.m u$$

### **3.8 The Torque Magnetometer:**

A torque magnetometer for the measurement of torque in the range of  $10^{-10}$ Nm to  $5.0 \times 10^{-4}$ Nm has been constructed. The torque compensation is achieved by feedback from a photo-detector into a Proportional Integrating Differentiating (PID) regulator system which generates a current through a compensation coil located in the field of permanent magnets. Measurements can be made in the temperature range 300K to 1100K.

#### **Introduction:**

The inherent property of a magnetic material in a static magnetic field is to align itself in order to minimise its energy. The energy variation with respect to sample orientation is represented by a torque exerted on the sample. The torque  $L$  exerted along an axis perpendicular to the magnetic field is related to the total anisotropy energy  $E_a$  by

$$L = -\frac{dE_a}{d\phi} \quad \dots\dots\dots(3.10)$$

where,  $\phi$  is the angle between a fixed direction in the sample and the direction of the magnetic field. Thus it is evident that by measuring the torque from a sample in a magnetic field we can gain information about the magnetic anisotropy energy of a

material. For ferromagnetic substances the anisotropy constants can be deduced from a Fourier analysis of the torque data as a function of the angle  $\phi$  between the magnetic field and a direction fixed in the crystal

Akulov (1929) showed that  $E_a$  can be expressed in terms of a series expansion of the direction cosines of  $M_s$  (saturation magnetization) relative to the crystal axes. In a cubic crystal, let  $M_s$  makes angles  $a, b, c$  with the crystal axes and let  $\alpha_1, \alpha_2, \alpha_3$  be the cosines of these angles, then

$$E_a = K_0 + K_1(\alpha_1^2\alpha_2^2 + \alpha_2^2\alpha_3^2 + \alpha_3^2\alpha_1^2) + K_2(\alpha_1^2\alpha_2^2\alpha_3^2) \quad \dots \dots (3.11)$$

where  $K_0, K_1, K_2, \dots$  are the anisotropy constants. The first term, which is simply  $K_0$ , is independent of angle and is usually ignored, because normally we are interested only on the change in energy  $E_a$  when the  $M_s$  vector rotates from one direction to another. When  $K_2$  is zero, the direction of easy magnetization is determined by the sign of  $K_1$ . If  $K_1$  is positive, then  $E_{100} < E_{110} < E_{111}$  and  $\langle 100 \rangle$  is the direction of easy magnetization. If  $K_1$  is negative,  $E_{111} < E_{110} < E_{100}$ , and  $\langle 111 \rangle$  is the direction of easy magnetization.  $K_1$  is negative for nickel.

The anisotropy energy expression for a hexagonal crystal can be written as

$$E_a = K_0 + K_1 \sin^2 \theta + K_2 \sin^4 \theta + \dots \dots (3.12)$$

The expression for the torque can be obtained by using eq(3.10). From eq(3.10) the  $\theta$  dependent part of the anisotropy energy may be written neglecting  $K_2$  as

$$E_a = K_1 \sin^2 \theta \quad \dots \dots (3.13)$$

When the energy of a system depends on an angle, the derivative of the energy with respect to the angle is a torque. Thus  $\frac{dE_a}{d\theta}$  is the torque exerted by the crystal on  $M_s$ , and  $-\frac{dE}{d\theta}$  is the torque exerted on the crystal by  $M_s$ . Then the torque on the crystal per unit volume is

$$L = -\frac{dE}{d\theta} \dots\dots\dots (3.14)$$

or  $L = -2K_1 \sin \theta \cos \theta$

or  $L = -K_1 \sin 2\theta \dots\dots\dots(3.15)$

**3.9 Design and working principle of the Torque Magnetometer:**

A simple form of torque compensation can be achieved by suspending the sample from a fibre with known torsional constant. When a magnetic field is applied, the torque from the crystal will twist the fibre, thus we can measure, by how much we have to rotate the upper point of suspension of the fibre to bring the crystal back to its original position.

Instead of using a torsion fibre a balancing torque can be generated with a compensation coil in a static magnetic field. The torque from the coil is proportional to



the current through the coil over a wide range of currents. Thus we measure the current needed for the crystal to keep its orientation.

The principal drawing of a torque magnetometer with an automatic compensation system is shown in Fig.3.3. The sample is rigidly connected to a mirror and the compensation coil. The whole assembly is freely suspended in a thin quartz fibre and the coil is located in a field produced by a pair of permanent magnets. Now if a laser beam is shined on the mirror, the image of the beam will move as soon as some torque acts on the crystal and thus turns the mirror. The principle is to let a photo-detector detect the movement of the reflected beam via an amplifier generating a current through the compensation coil which inhibits the motion of the suspension.

The simplest type of electronic compensation system with a photo-sensitive feedback have been designed(Westerstrandh et al.). The simplest way is to let the current through the compensation coil be directly proportional to the signal from the detector. Such a feedback system is often referred to as a proportional (P) regulator. If a torque acts on the crystal the turning of the mirror gives rise to a deflection of the beam shining on the detector. The deflection from the centre of the detector can be made small by increasing the amplifier gain. Nevertheless the contribution from the rigidity of the suspension may seriously affect measurements of small torques. Neither the gain of the feedback could be increased too much since the system will then become unstable. To improve the stability we have used the oil damping. The viscosity of the oil damps oscillations so that we can increase the amplifier gain. To enhance the electronic damping a differentiating amplifier has been used in parallel with the proportional amplifier and hence improve the stability of the system. This type of compensation system can be characterised as a proportional differentiating regulator(PD). Since the

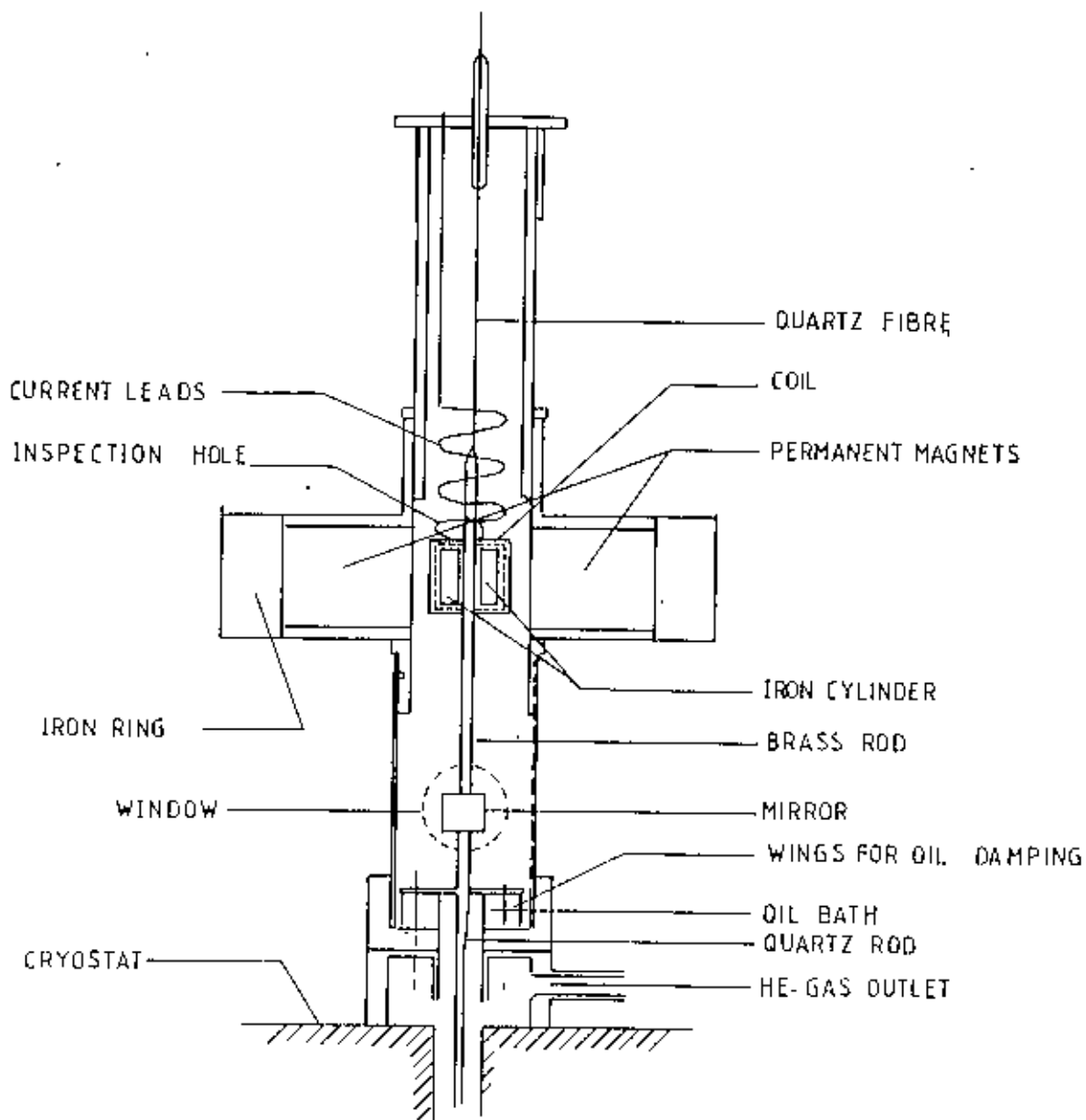


Fig 3.3 Cross section of the upper part of the torque magnetometer

large deflection of the suspended system is a problem, the introduction of a differentiating unit allows a very high gain and a small angular deflection.

### **3.10 The sample suspension:**

The sample is mounted at the end of a thin quartz rod. Quartz is a suitable material for this purpose as it is diamagnetic and has a low thermal conductivity. The upper end of the quartz rod is attached to a brass rod, to which the mirror and the compensating coils are fixed. The whole assembly is suspended in a quartz fibre. The quartz fibre is very suitable because of its large tensile strength and small torsional constant. Typical values of the torsional constant are  $5-20 \times 10^{-7} \text{ Nm/rad}$ . The elasticity in the longitudinal direction is very low, which prevents low frequency oscillation along the axis of suspension. The compensation coils have 10 layers of 100 turns of 0.06mm copper wire. To minimise influence from the stiffness of the copper wire, the leads to the coils have been spiralized. Below the coil there is besides the mirror, an arrangement for oil damping, effective against self oscillations.

### **3.11 Calibration of the Torque Magnetometer:**

The torque magnetometer is designed at the Department of Solid State Physics, University of Uppsala in Sweden by Professor M.Ali Asgar and late Professor Leif Lundgren. The magnetometer is built in the Workshop of the Department of Solid

State Physics, Uppsala University and is financed by the International Science Programs of the University of Uppsala, Sweden. The magnetometer is later donated to the Material Science group of the Department of Physics, Bangladesh University of Engineering and Technology (BUET) by the International Science Programs (ISP), University of Uppsala, Sweden. The magnetometer is assembled and installed at the Solid State Physics laboratory in BUET. The rotating base of the magnetometer is designed by Professor M. Abu Taher Ali of the Department of Mechanical Engineering, BUET, and is constructed at the Engineering Workshop of BUET.

The main parts of the magnetometer is described in section 3.9. For the calibration of the magnetometer a thin nickel single crystal disc is chosen. The disc is of mass 45 mg and is oriented in such a way that the (100) crystallographic plane lies on the plane of the disc. The sample is glued to the quartz rod and is suspended from the quartz fibre. A three kilo gauss magnetic field which is strong enough to saturate the nickel specimen is applied along the plane of the disc and measurements of torque is taken in steps of  $10^\circ$  for a complete  $360^\circ$  rotation of the magnetic field. A total of 36 points are obtained from a complete rotation of the magnetic field. The whole process of measurements is repeated for applied magnetic field of 3.5 kilo gauss and 4.0 kilo gauss.

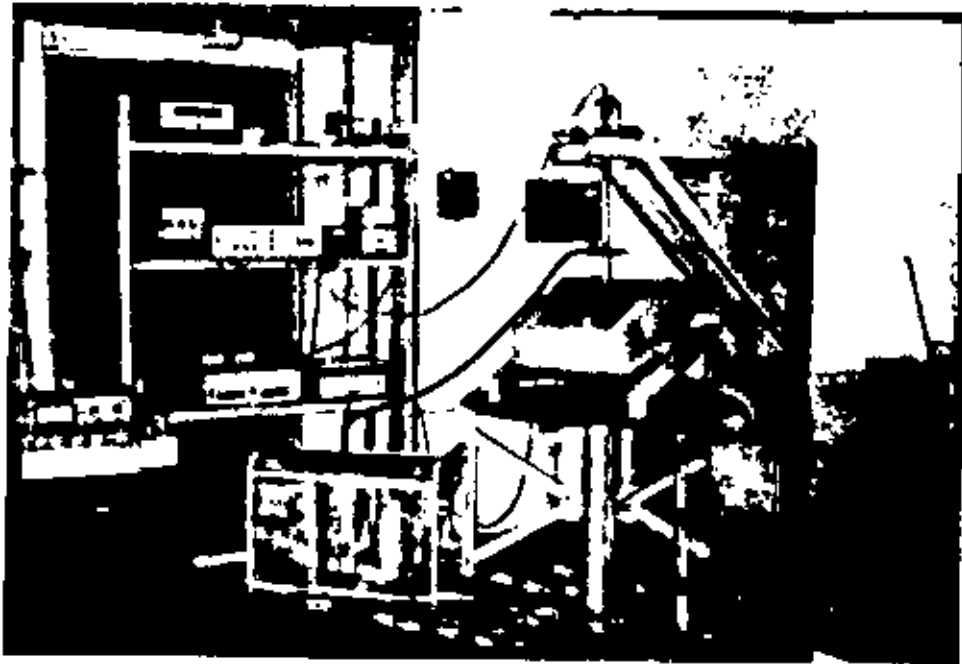
The torque on the specimen is given by

$$\tau = A \sin 2\theta + B \sin 4\theta$$

where  $A = -\left(\frac{K_1}{4} + \frac{K_2}{64}\right)$  and  $B = \left(\frac{3K_1}{8} + \frac{K_2}{16}\right)$  for (110) crystallographic plane of rotation.

The experimental torque data are then fitted with a theoretical expression using a least square fit. The Fourier coefficients  $A$  and  $B$  are calculated using the known values of  $K_1$  and  $K_2$ .

Fig 3 4 shows the torque curve at 300<sup>o</sup>K of a nickel disc oriented in the (100) crystallographic plane. And Fig.3 5 shows the torque curve of a spherical shaped sample of Ni-Mo<sub>6</sub>% at 300<sup>o</sup>K oriented in the (110) crystallographic plane



**Photograph of the Torque Magnetometer**

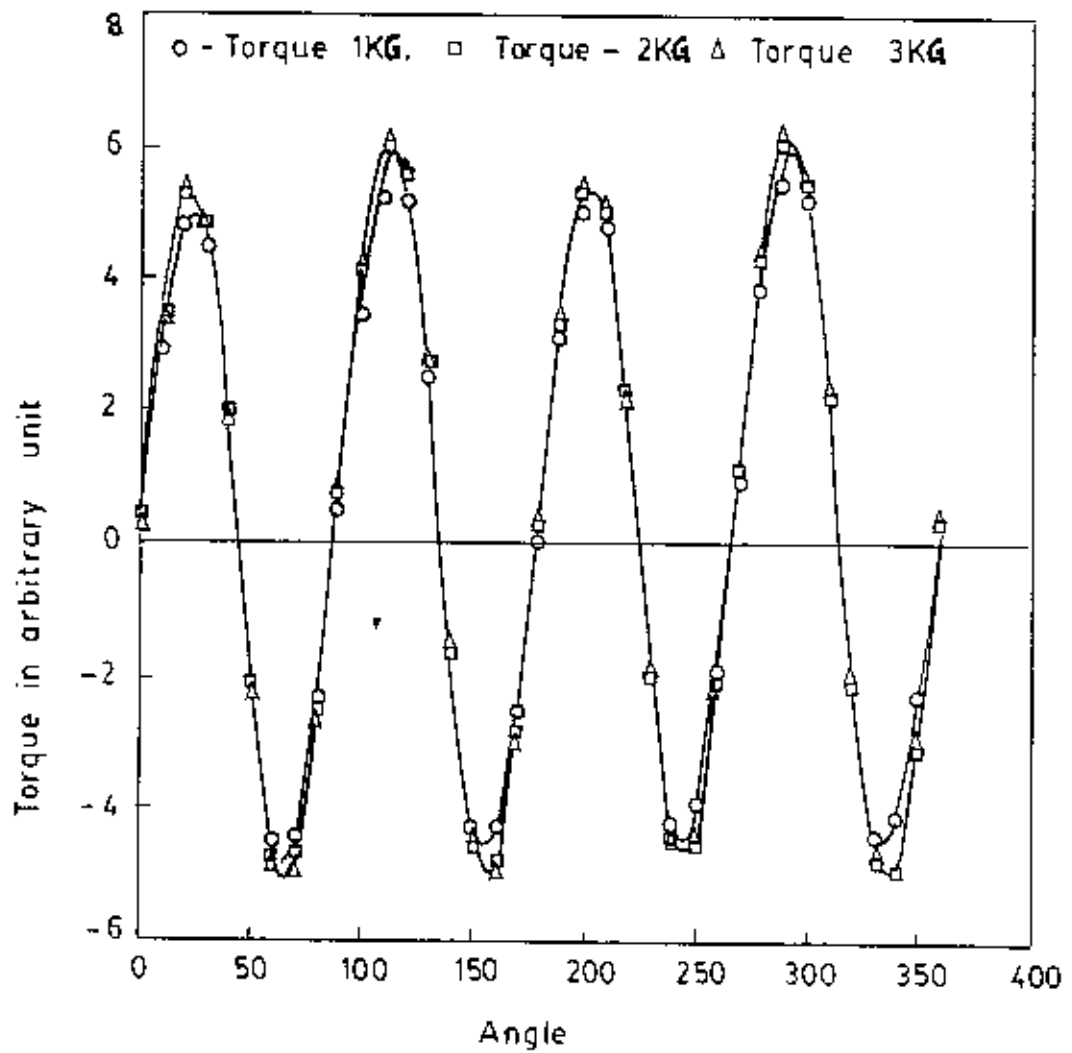


Fig 3.4 Torque curve for a single crystal of Nickel disc in (100) crystallographic plane at 300 K.

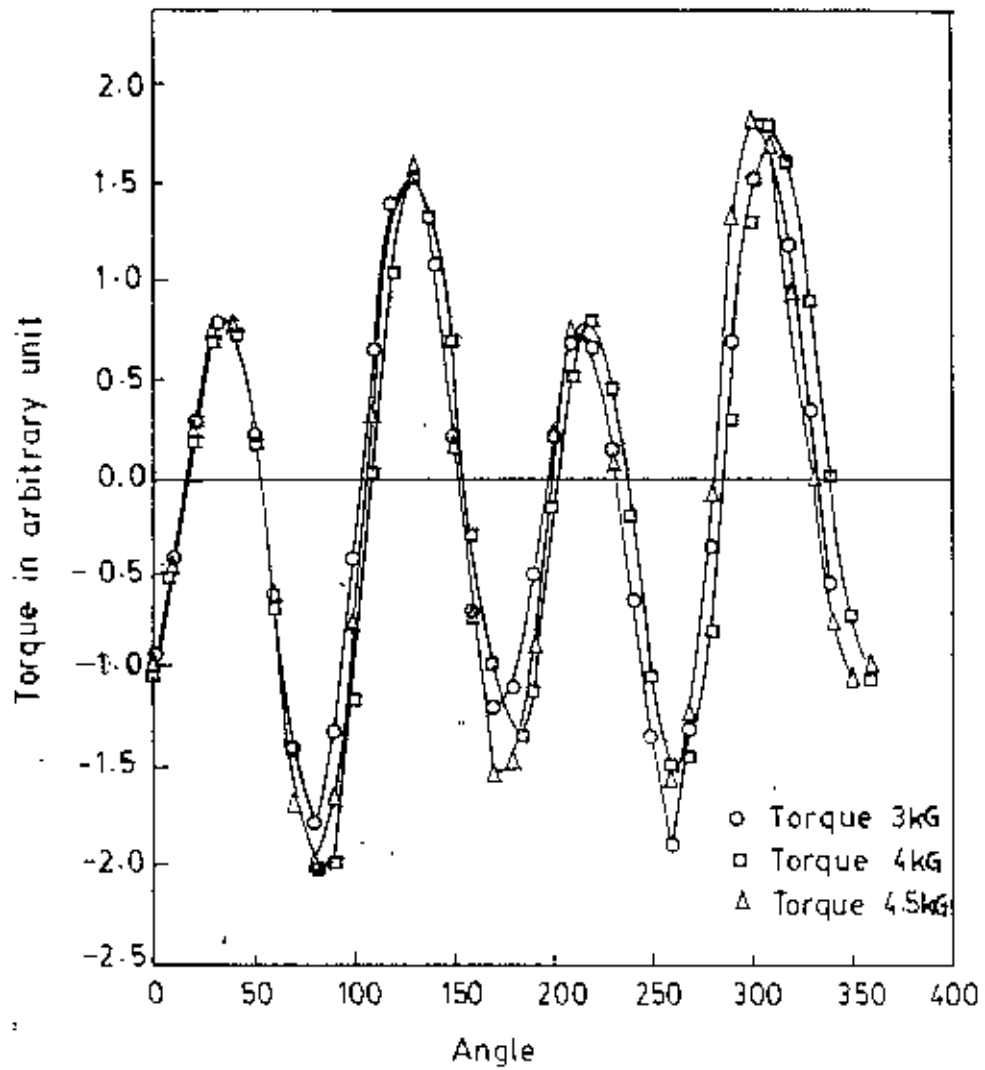


Fig. 3.5 Torque curve for NiMo<sub>6%</sub> Single crystal in (110) crystallographic plane at 300 K



### 3.12 The High Temperature Oven:

The high temperature oven is constructed by Dr.Per Nordblad and late Prof.Leif Lundgren of the Department of Technology, Uppsala University, Sweden. The schematic diagram of the oven is shown in Fig.3.6. The most important feature in the construction of the oven is that the inner stainless steel tube extends throughout the oven and the thermocouple unit is introduced from the bottom end with the thermocouple junction placed immediately below the sample.

The heater is wound directly on the inner tube. The heater consists of a MgO insulated Chromel-Constantan thermocouple with a stainless steel cover ( O.D. 1mm, length 1.3m, manufactured by OMEGA Corp. This thermocouple is flexible and to obtain a firm contact between the heater and the inner sample tube, the thermocouple is first wound on a tube with a somewhat smaller diameter and the resulting spiral is afterwards squeezed on to the sample tube. The thermal contact between the heater and the sample tube is improved by adding some silver paint. The lower ends of the heater wires are electrically connected by means of silver paint. Copper wires, connecting an external power supply, are soft soldered on the upper ends of the heater wires. The silver paint is dried out at ordinary atmosphere by passing some current through the heater. The advantages to use this Chromel-Constantan thermocouple as a heater for this oven are that it is readily available, non-magnetic, insulated, easily formed gives a bifilar winding and close thermal contact with the sample tube. The heater has a resistance of 75 ohms at room temperature

Five radiation shields, consisting of 50  $\mu$ m stainless steel foils are located outside the heater. These are tied directly on to the heater using reinforced glass fibre threads. The outer tube is at the bottom end connected to the inner tube via a phosphor-bronze bellow in order to allow for the difference in length of the two tubes at higher

89349

temperatures. O-ring couplings are used throughout to enable easy disassembling of the oven in case of any fault.

Both the oven and the thermocouple are adjustable in height with respect to the sample. This gives a possibility to find a position of the sample in the warmest region of the oven which gives a minimum temperature gradient between the sample and the thermocouple junction. The temperature gradient  $\frac{\nabla T}{T - T_0}$  over 10mm of length in the

warmest part of the oven is approximately 0.1% and independent of the temperature.

The special characteristics of the oven are

(1) the oven can be heated from room temperature to 1043 K in less than 15 minutes with a temperature difference between thermocouple and sample of less than 1 K at the final temperature

(2) at a constant heating or cooling rate of 5K/minute a temperature difference of the order of 1K is established.

Due to small thermal mass of the oven, it cools from 1150 K to 600 K in about 30 minutes which enables a fast interchange of samples.

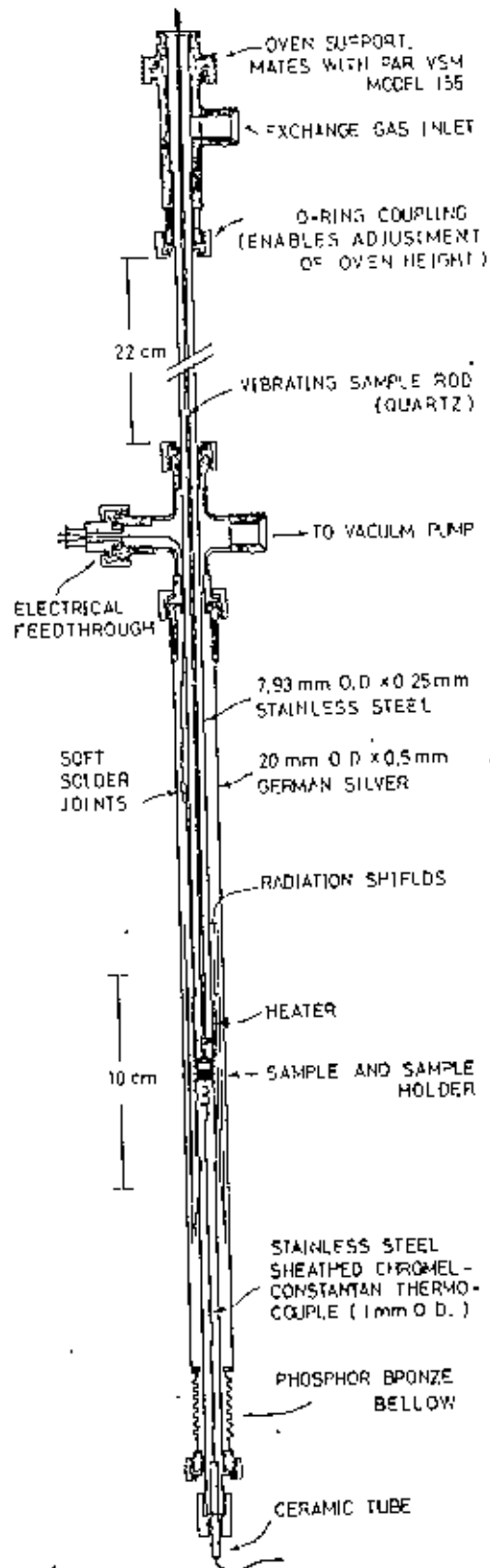


**Fig. 3.6 Schematic diagram of the high temperature oven**

**Chapter 4**  
**Measurements on Ni-Mo alloys**

#### 4.1 Magnetocrystalline Anisotropy in Ni-Mo alloy:

The Ni-Mo single crystals are prepared by the British Post Office Research station, Dollis Hill and have been made available for this investigation through private communication between Prof.E.W.Lee and Prof.M.A.Asgar. The single crystals are of high quality as can be seen from the magnetization curves. The equilibrium phase diagram of this alloy system indicates a continuous f.c.c structure upto 16 at% of Molybdenum (Fig.4.1). The magnetization curves at different temperatures are used to calculate the magnetocrystalline anisotropy energy of different samples. The saturation magnetization is estimated by scaling the magnetization axis using the demagnetising line of the magnetization curves. The  $K_1$  values are estimated by using the relevant equation for the chosen crystallographic plane. The  $K_1$  values are plotted as a function of different molybdenum concentrations at 4.2K and 77K (Fig 4.15). These values are although negative, decreasing in magnitude with increasing molybdenum concentration and goes to zero at about 10 at%. The effect of alloying nickel with molybdenum is interesting both from the point of view of magnetic anisotropy and magnetization. Also a weak alloying of Ni by non-magnetic solute might improve the properties of some Nickel-ferrite and avoid quenching from high temperature of these alloys. The temperature dependence of magnetic anisotropy is also an interesting property to understand these materials. According to Zener the effect of temperature upon magnetic anisotropy arises solely from the introduction of local deviations in the direction of magnetization. This deviation in an elementary region is the resultant of very large number of independent deviations. The influence of these local deviations upon the magnetic anisotropy is most conveniently expressed by representing the magnetic energy as a series of surface harmonics. The coefficient of the  $n$ th harmonic is found to vary with temperature as  $\left[ \frac{M_s(T)}{M_s(0)} \right]$  raised to the power  $\frac{n(n+1)}{2}$ . The first

two exponents for cubic crystals have the values of 10 and 21, respectively. The exponent 10 expresses almost precisely the observed temperature dependence of  $K_1$  in iron. In nickel the anisotropy decreases much more rapidly than predicted. According to Franse J.J.M. et al the dependence of the anisotropy energy of nickel on the impurity concentration can be described in terms of a nearly temperature independent parameter. In Ni-Mo the addition of molybdenum has no effects other than simply diluting the system. Hence it may be argued that the same temperature dependence of anisotropy and magnetization holds for Ni-Mo alloys

#### 4.2 Measurements of magnetization:

For the measurements of magnetization, the Cryostat is first evacuated by an Edwards high vacuum pump. The vacuum pump is kept running until the pressure in the Cryostat dropped to about  $10^{-4}$  torr. The vacuum line is then disconnected and the Cryostat is filled with liquid Nitrogen. The oriented sample in the Goniometer is then glued to the quartz rod with Araldite. After some time the glue became hard. The sample rod is then fixed with the upper portion of the vibrating part of the V.S.M. An a.c. signal is then fed to the coil of the vibrating diaphragm from a Phillips signal generator so that the sample rod alongwith the sample vibrates with a definite frequency ( 37 Hz in this case ) The induced signal (signal A ) is then measured by a Voltmeter. The position of the sample is changed vertically and horizontally with the help of adjustable screws fixed on the support of the V.S.M until the signal is maximised and the sample is on the 'saddle point'. The induced signal is then fed into the A terminal of the Princeton Applied Research (PAR) Lock-in-Amplifier. The

reference signal from the reference coil is fed into the B terminal of the Lock-in-Amplifier. The phase, sensitivity, and the time constant of the signals are adjusted until the output of the Lock-in-Amplifier was zero. The output of the Lock-in-Amplifier (A-B) is fed into the input of the P.I.D. regulator which is in the reverse bias mode. The output of the P I D (Proportional Integrating Differentiating) regulator is connected to the Y-terminal of the X-Y recorder. The X-terminal of the recorder is connected to the Hall-probe of the Electro-magnet (Varian Electro-Magnet) across a resistor. The magnet power supply is connected to an automatic magnetic field sweeping unit. The magnetic field is then swept up gradually and the sample is magnetised in a particular crystallographic direction. The magnetic field is kept sweeping until the sample is saturated in a particular crystallographic direction. The output is measured in a X-Y recorder. The saturation magnetization is then measured. The magnetic field is swept down gradually and the sample is demagnetised. The sample is then rotated in the other crystallographic directions and then magnetised in the same procedure. The whole procedure is repeated in liquid Helium temperature.

#### 4.3 Evaluation of first anisotropy constant $K_1$ :

The first anisotropy constant  $K_1$  is evaluated using the magnetization curves of the different samples at 77K and 4.2K. The magnetization curves are scaled using the demagnetisation factor of the sample N. For a sphere, the demagnetisation factor is  $\frac{1}{3}$  and the slope of the magnetization curve is proportional to the reciprocal of the

demagnetisation factor . Thus the magnetization axes are scaled and the magnetisation values are calculated in  $\frac{A}{m}$ . The magnetic field axes are measured in tesla. The areas between the magnetization curves are integrated and the anisotropy energy  $E_a$  is calculated in  $J/m^3$ . After calculating the anisotropy energy, the anisotropy constants are calculated using the relevant equations for different crystallographic planes.

Table.4.1

| Molybdenum at% | $K_1$ (Joules/m <sup>3</sup> ) at 77 K | $K_1$ (Joules/m <sup>3</sup> ) at 4.2 K |
|----------------|--|---|
| 0.61           | $-6.1 \times 10^4$                     | $-8.07 \times 10^4$                     |
| 2.66           | $-2.65 \times 10^4$                    | $-3.85 \times 10^4$                     |
| 3.12           | $-2.41 \times 10^4$                    | $-3.34 \times 10^4$                     |
| 3.76           | $-1.78 \times 10^4$                    | $-2.72 \times 10^4$                     |
| 3.99           | $-1.64 \times 10^4$                    | $-2.37 \times 10^4$                     |
| 4.84           | $-9.3 \times 10^3$                     | $-1.54 \times 10^4$                     |
| 5.33           | $-7.82 \times 10^3$                    | $-12.82 \times 10^3$                    |
| 6.11           | $-3.05 \times 10^3$                    | $-7.22 \times 10^3$                     |
| 6.66           | $-2.07 \times 10^3$                    | $-4.95 \times 10^3$                     |
| 7.39           | $-3.1 \times 10^2$                     | $-2.22 \times 10^3$                     |
| 9.05           | $-1.0 \times 10^1$                     | $-3.20 \times 10^2$                     |



#### 4.4 Results and Discussion:

In Fig.4.1 the equilibrium phase diagram of Ni-Mo alloy system is given. In Figure 4.2 a typical  $M$  vs  $T$  curve at low applied field near the  $T_C$  is shown. The transition to paramagnetic state is similarly sharp for all the samples. The Curie temperature of the samples are determined from such curves using the kink-point method. Figure 4.3 shows the variation of  $T_C$  with molybdenum concentration. Almost a linear decrease of  $T_C$  is observed at low molybdenum concentration. At higher Mo concentrations the decrease becomes more rapid and an extrapolation to  $T_C = 0$  yields a concentration of 10 at% of Mo.

In Fig.4.4 the saturation magnetisation ( $M_S$ ) at 4.2K is plotted against Mo concentration. Also included in the figure is  $M_S$  of pure Ni. The decrease of  $M_S$  with Mo concentration is closely linear at low concentrations but becomes non-linear with stronger dilution and  $M_S$  goes to zero at about 10 at% of Mo. This linear decrease of both  $T_C$  and  $M_S$  with concentration of Mo is in accordance with the typical behaviour of the ferromagnetic 3d transition metals when they are diluted with non-magnetic elements. In Figure.4.5 the saturation magnetisation of the Ni-Mo samples are plotted vs temperature.  $M_S = 0$  is in the figure marked at the measured  $T_C$  for different samples. The fall of saturation magnetisation with temperature is non-linear for different concentrations. Fig 4.6-4.13 show the  $M$  vs  $H$  curves for samples with different Mo concentrations at 4.2 and 77K. The magnetisation curves for different crystallographic directions are quite sharp which is an indicative of the high quality of the samples. In Fig.4.14 a room temperature curve for Ni(3.99at%Mo) is shown. Using these curves the first anisotropy constants ( $K_1$ ) of the different Ni-Mo samples are calculated. In Figure.4.15  $K_1$  is plotted as a function of Mo concentrations at two temperatures 4.2 and 77K. Both the curves show quite rapid decrease of  $K_1$  with Mo

concentration There is no published data on magnetization and magnetic anisotropy of Ni-Mo single crystal alloys to be compared with our results. However, anisotropy constants of Ni-Mo alloy single crystal measured by Janet by torque magnetometry (obtained by private communication) is plotted alongwith our results in Fig.4.15. The data obtained from the two different methods compare nicely both in magnitude and for temperature dependence. Also the data compare favourably with concentration dependence of anisotropy constants for the different samples.

The room temperature magnetization measurements are done on Ni-Mo<sub>3.99at%</sub>. Other samples did not show any measurable anisotropy at room temperature. The values of  $K_1$  remain althrough negative decreasing in magnirude with increasing molybdenum concentration. The general shape of the curves for the alloys is similar to that for pure nickel.

Puzei (1949) determined  $K_1$  for some Ni-Mo and Ni-Cu alloys at temperatures above 90K by measuring the approach to saturation of the polycrystalline specimens. He calculated that, at a first approximation, the temperature dependence of  $K_1$  was independent of composition. It is found by many workers that a highly satisfactory fit to experimental data is given by empirical relationship by Bryuchatov and Kirensky(1937),

$$\frac{K_1(T)}{K_1(0)} = \exp(-\alpha T^2) \quad \dots\dots\dots(4.1)$$

This equation is frequently used to determine  $K_1(0)$  by extrapolation and is found to hold for nickel upto room temperature. Hence according to Puzei, for temperatures far from the Curie point, the constant  $\alpha$  in the eq(4.1) may be considered to be independent of the alloy composition.

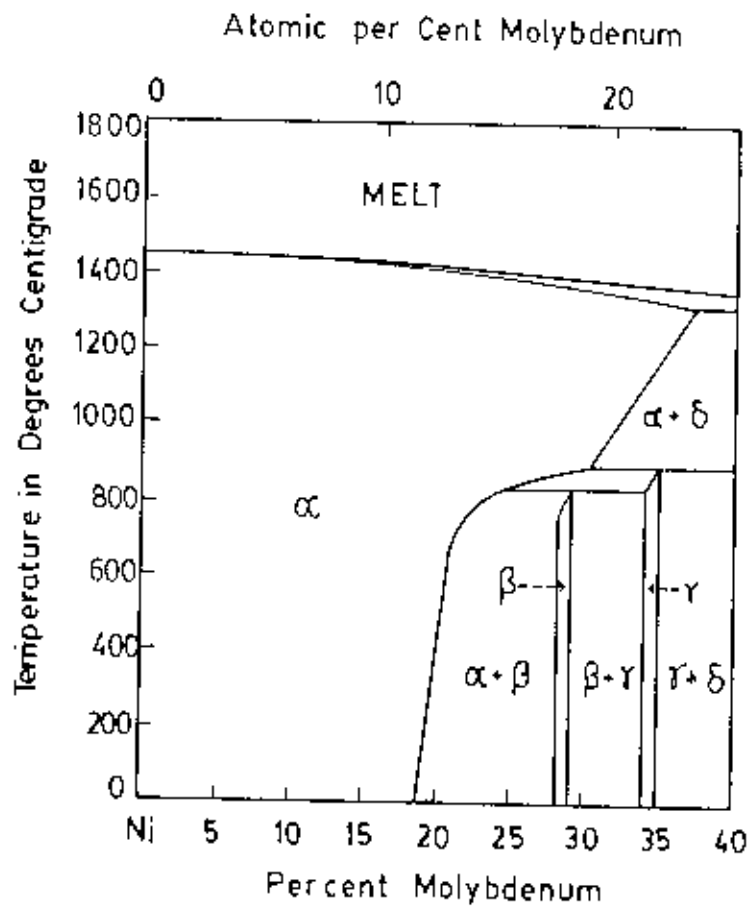


Fig. 4.1 Equilibrium phase diagram of Ni-Mo alloys

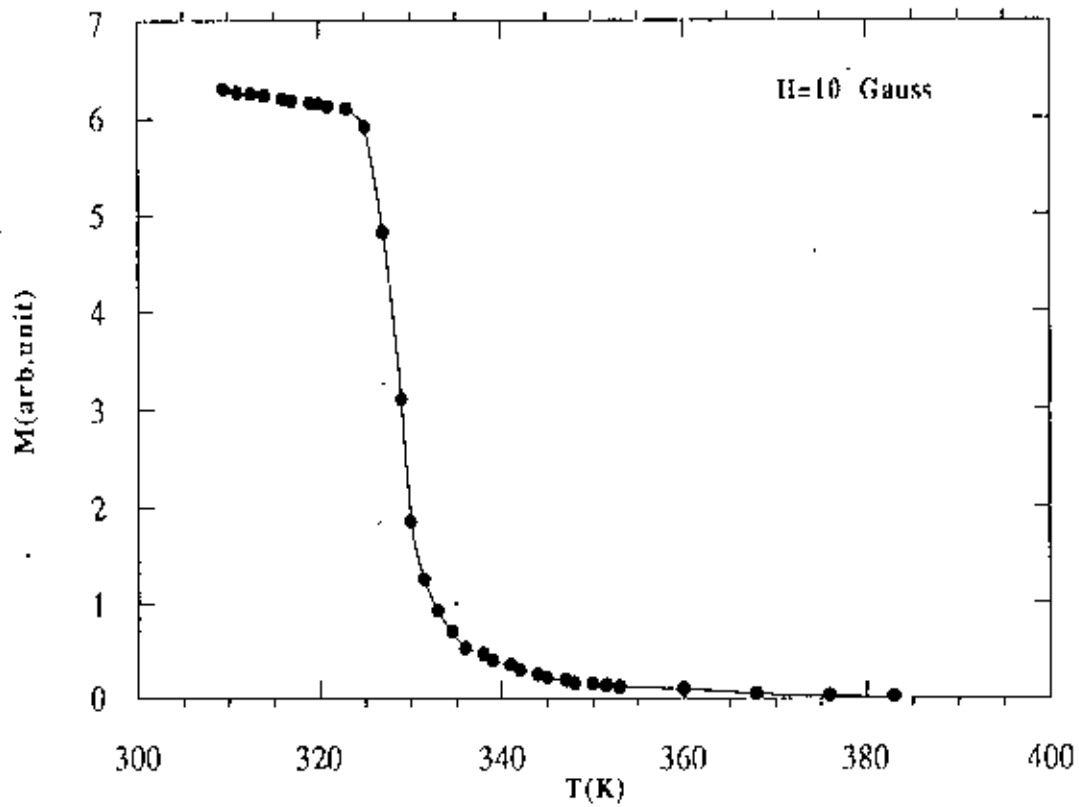


Fig. 4.2 M vs T curve of Ni-Mo 8%

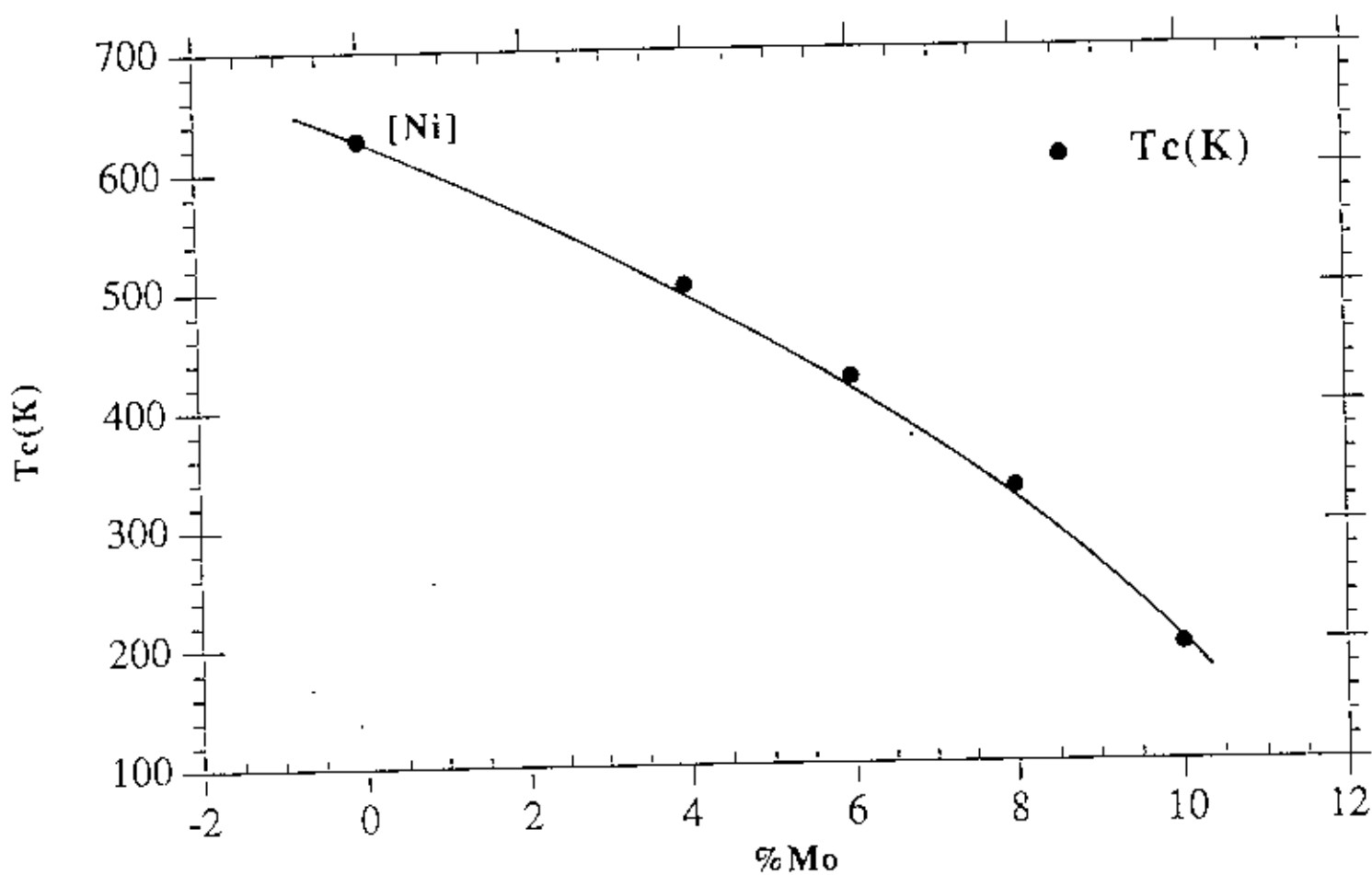
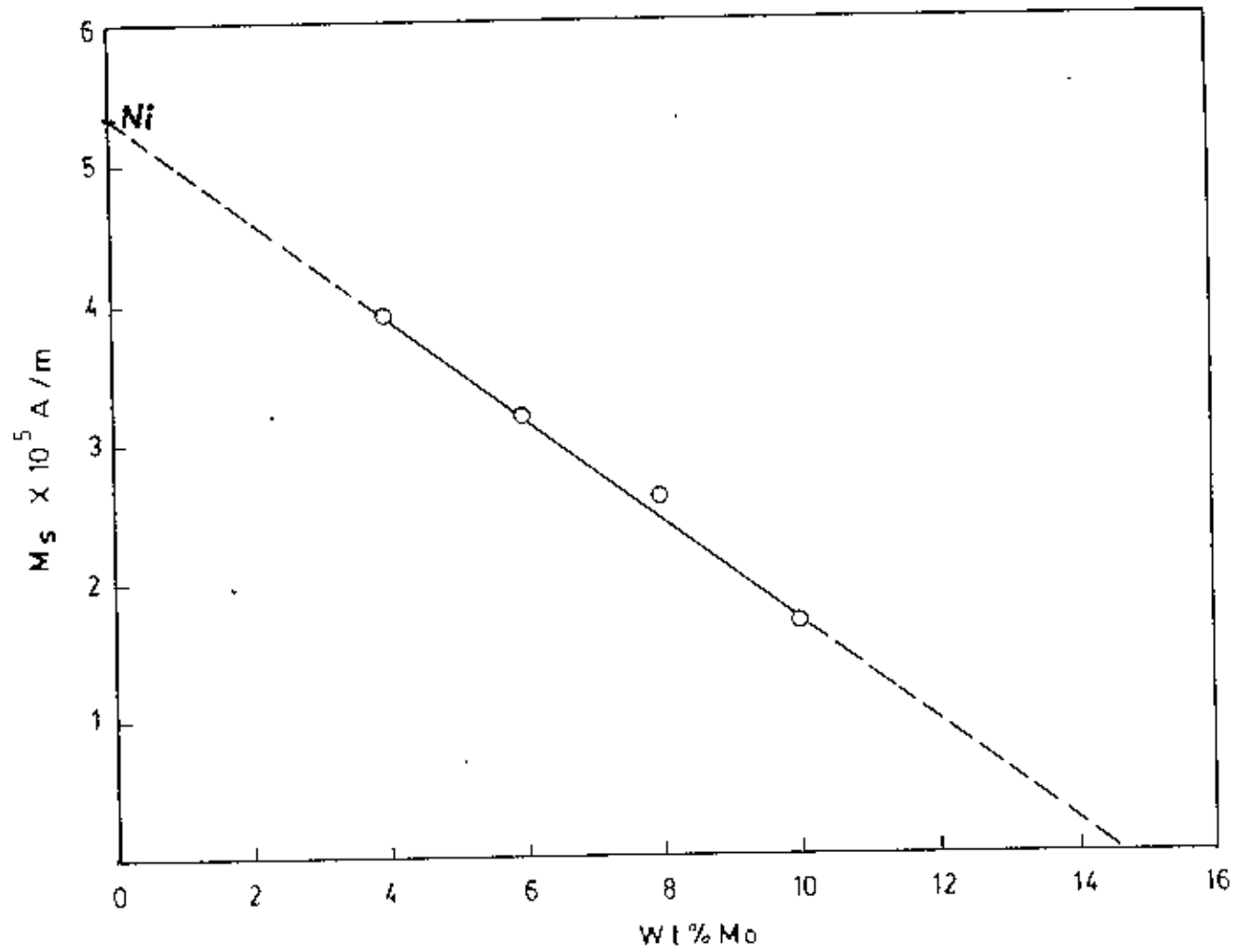


Fig. 4.3 Change of Curie temperature with increasing Mo concentration in Ni.



**Fig. 4.4** Variation of saturation magnetisation  $M_s$  with Mo concentration

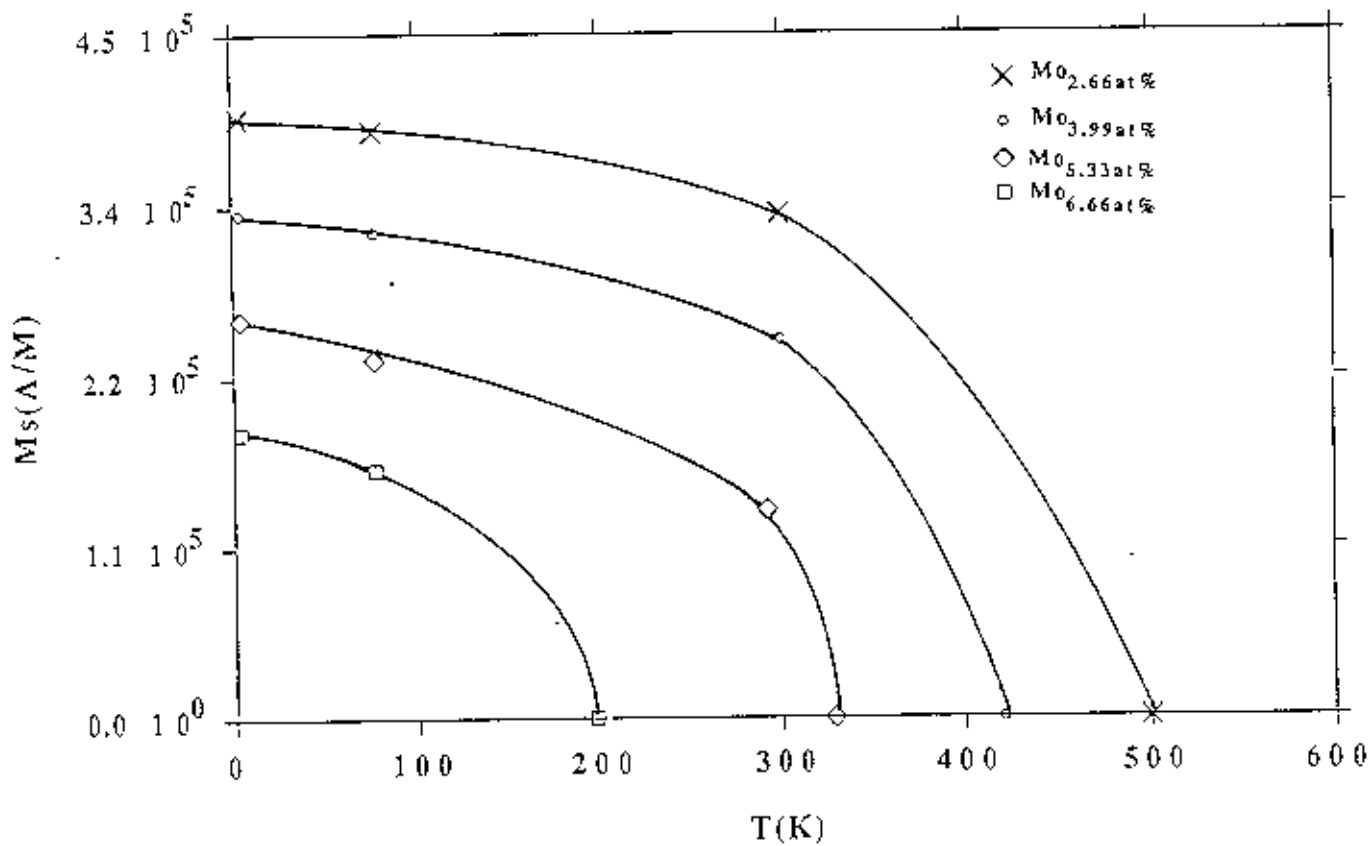


Fig. 4.5 Temperature dependence of saturation magnetization for Ni-Mo single crystal.

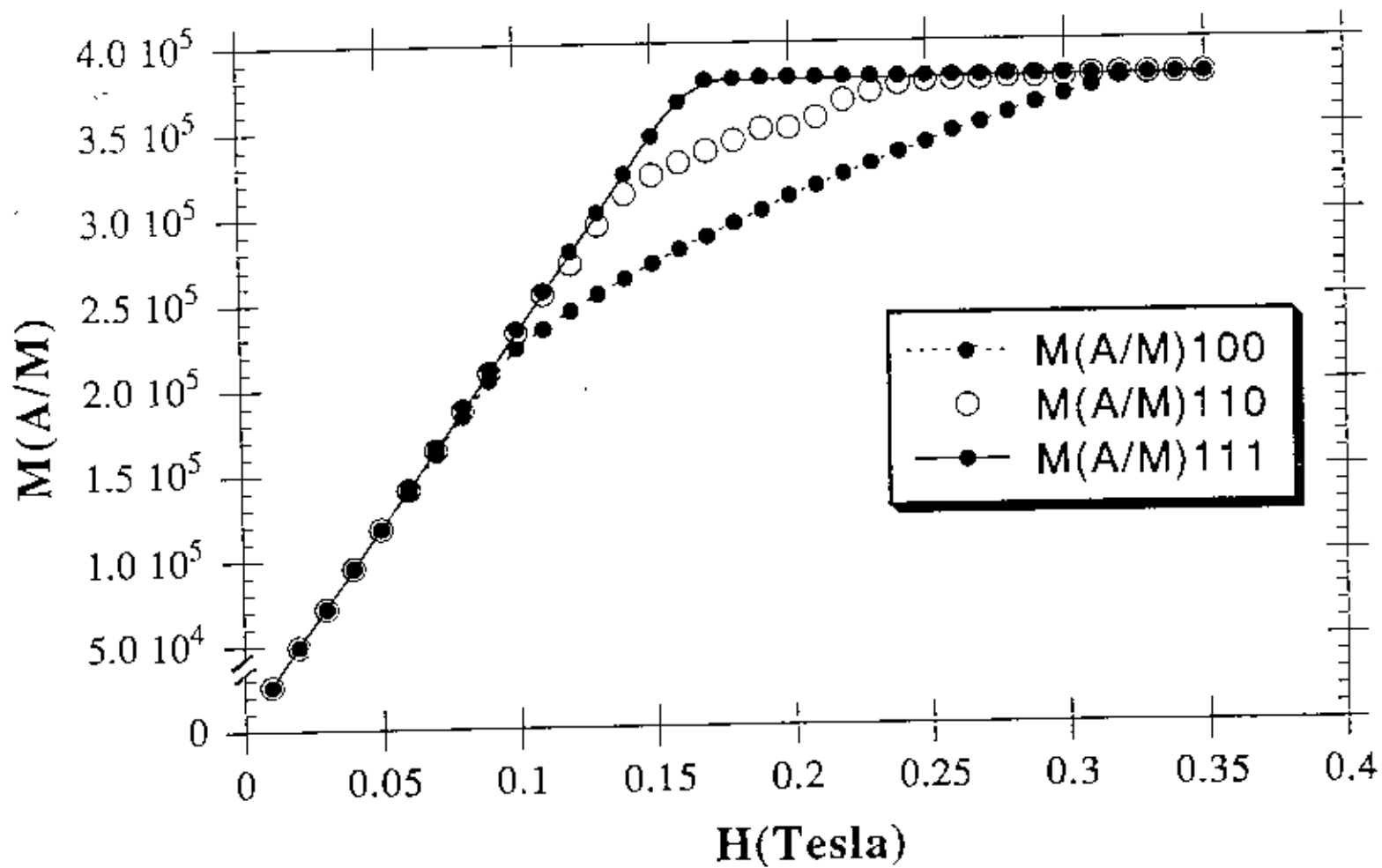


Fig. 4.6 M vs H curve of  $Ni-Mo_{4\%}$  single crystal for three principal crystallographic directions at  $77K$ .



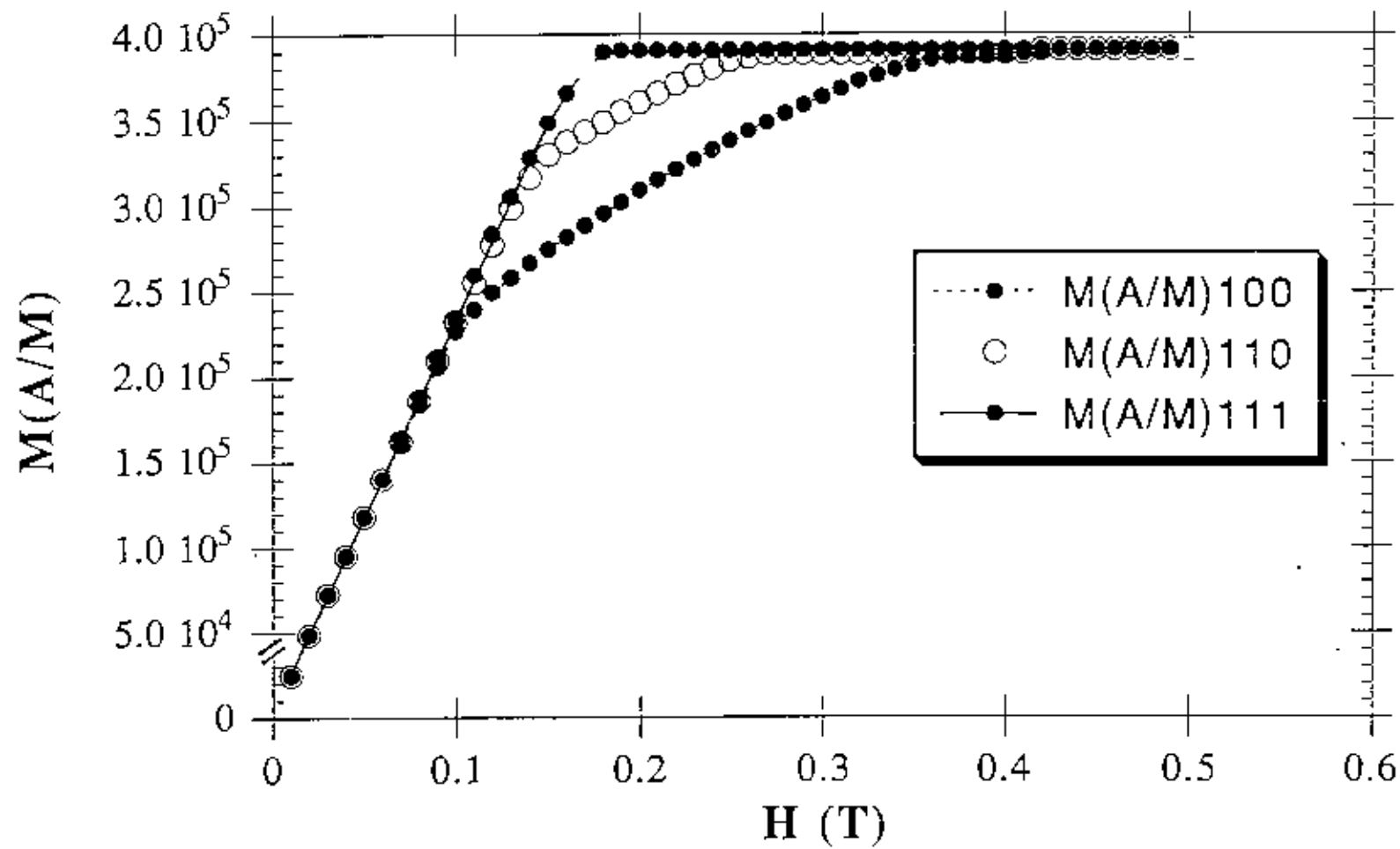


Fig. 4.7 M vs H curve of Ni-Mo<sub>4%</sub> single crystal for three principal crystallographic directions at 4.2 K.

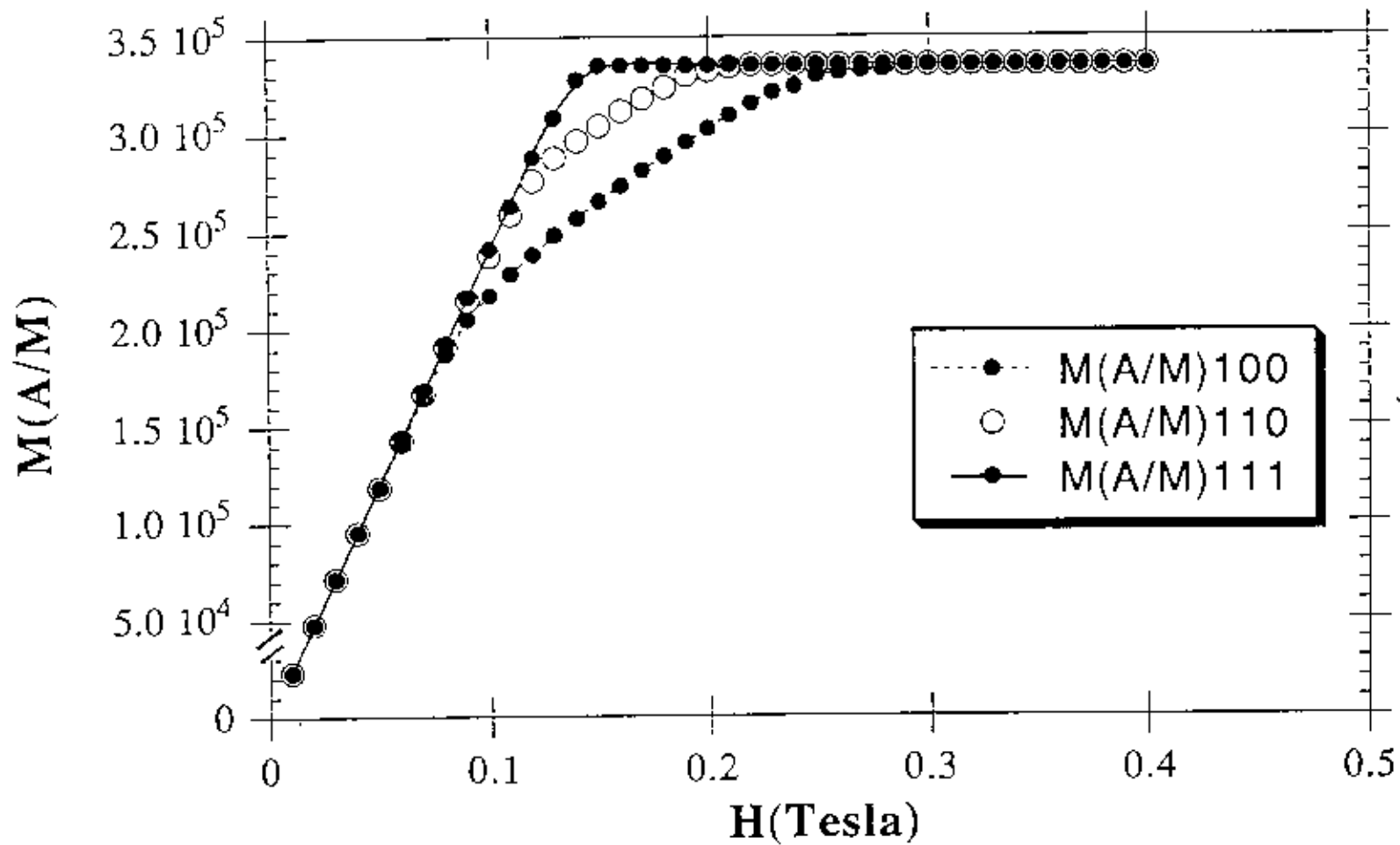


Fig. 4.8 M vs H curve of  $Ni-Mo_{6\%}$  single crystals for three principal crystallographic direction at  $77K$ .

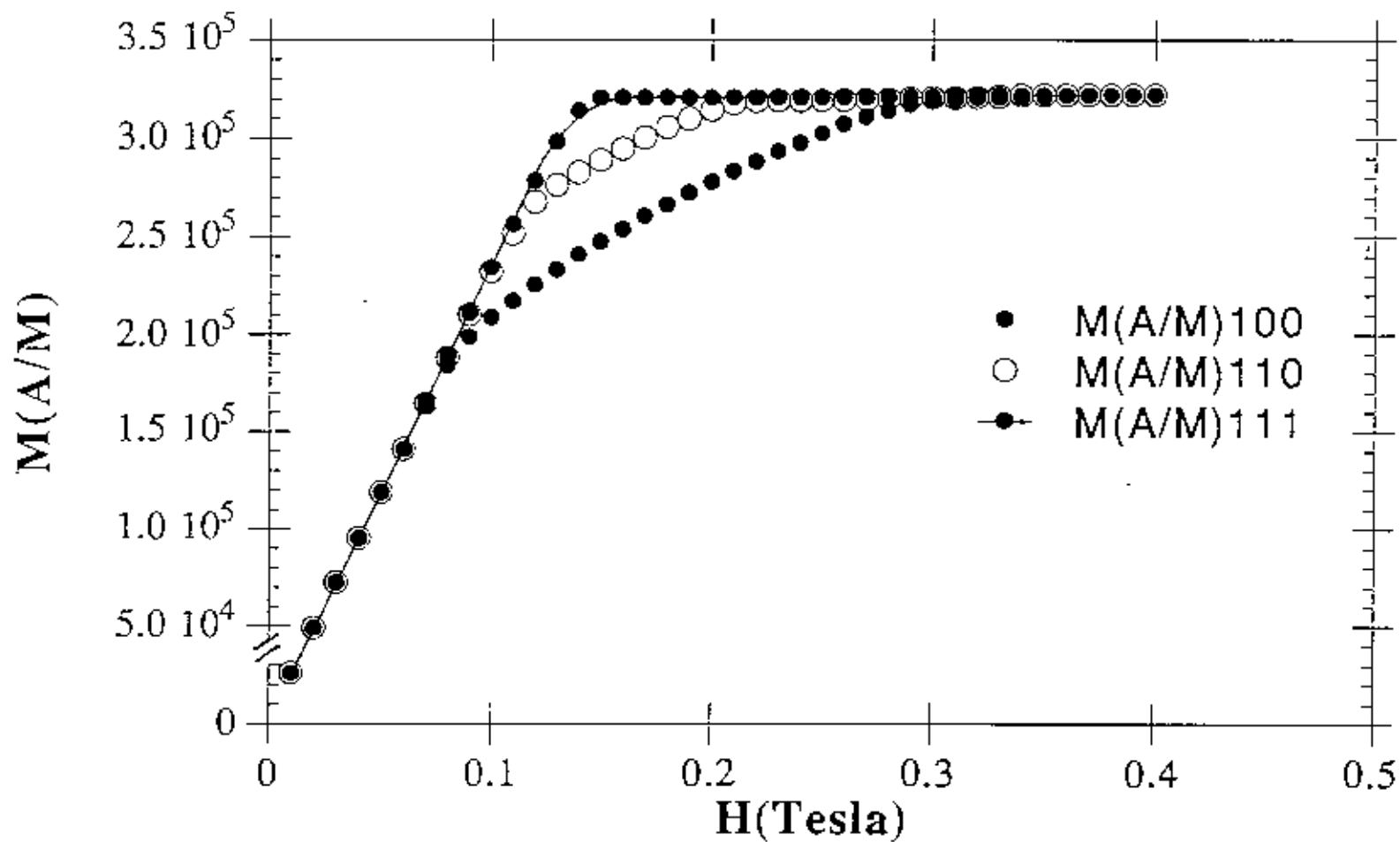


Fig. 4.9  $M$  vs  $H$  curve of  $Ni-Mo_{6\%}$  for three principal crystallographic directions at  $4.2\text{ K}$ .

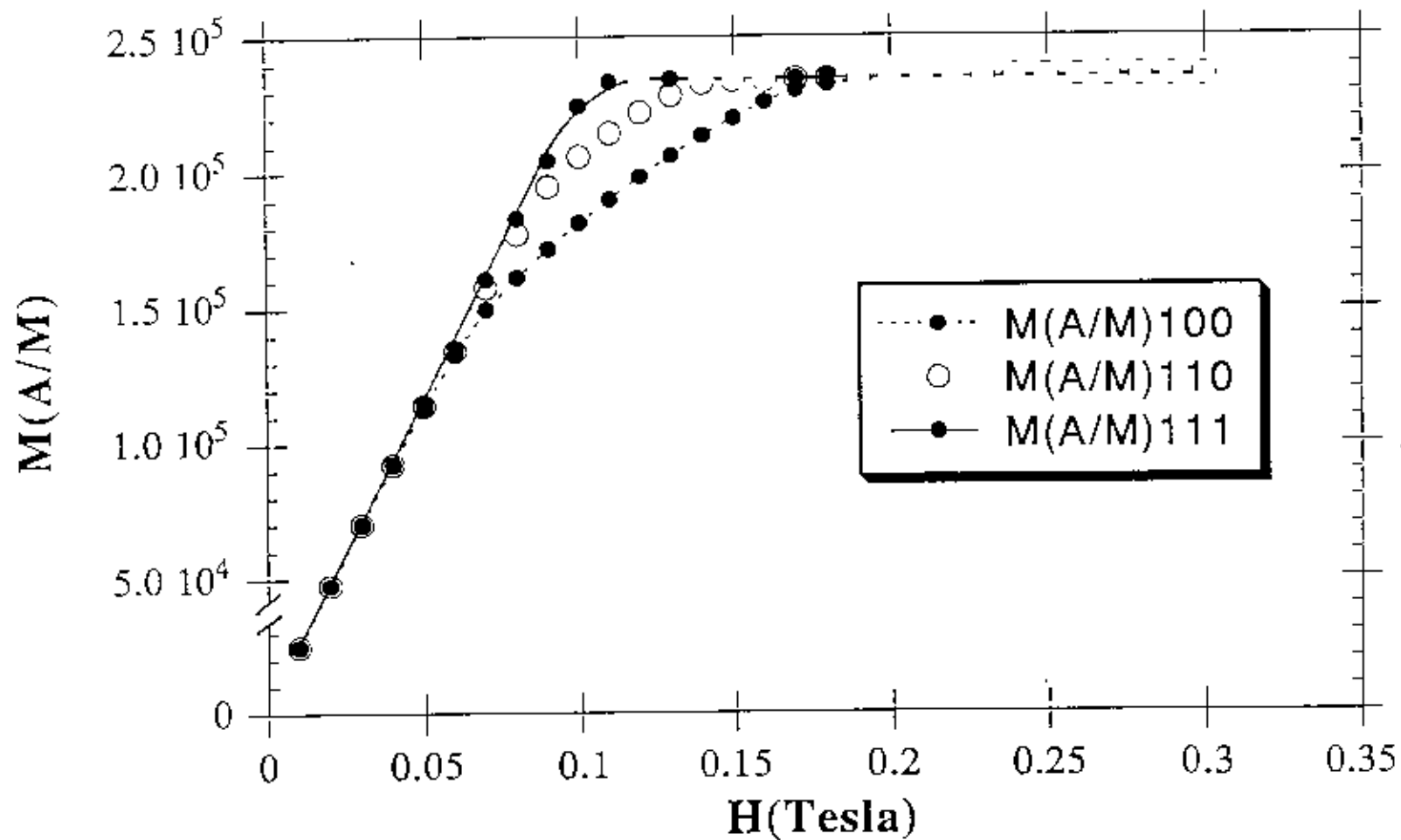


Fig.4.10 M vs H curve of Ni-Mo8% single crystal for three principal crystallographic directions at 77K.

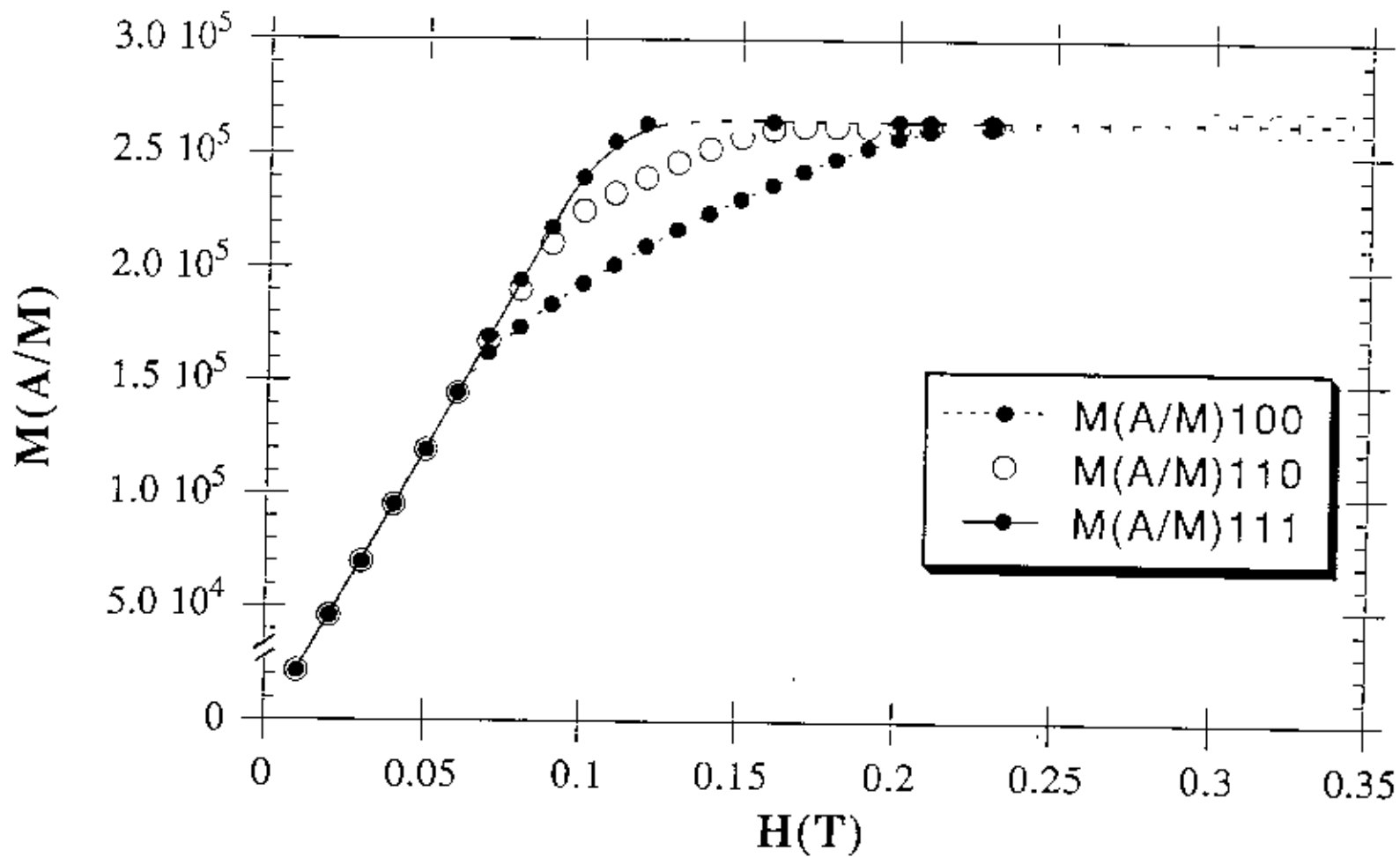


Fig. 4.11 M vs H curve of Ni-Mo8% single crystal for three principal crystallographic directions at 4.2K

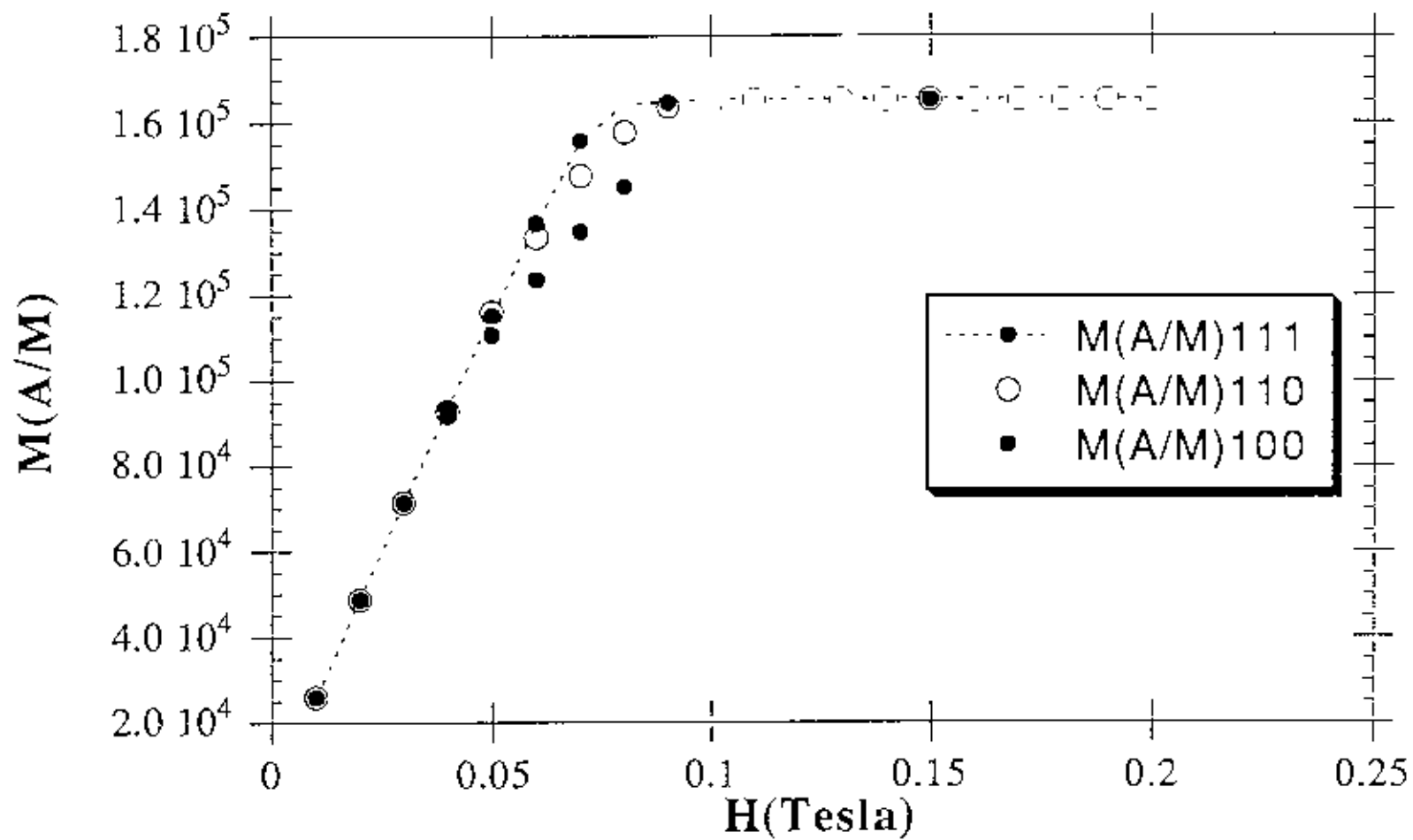


Fig. 4.12 M vs H curve of Ni-Mo<sub>10%</sub> single crystal for three principal crystallographic directions at 77K.

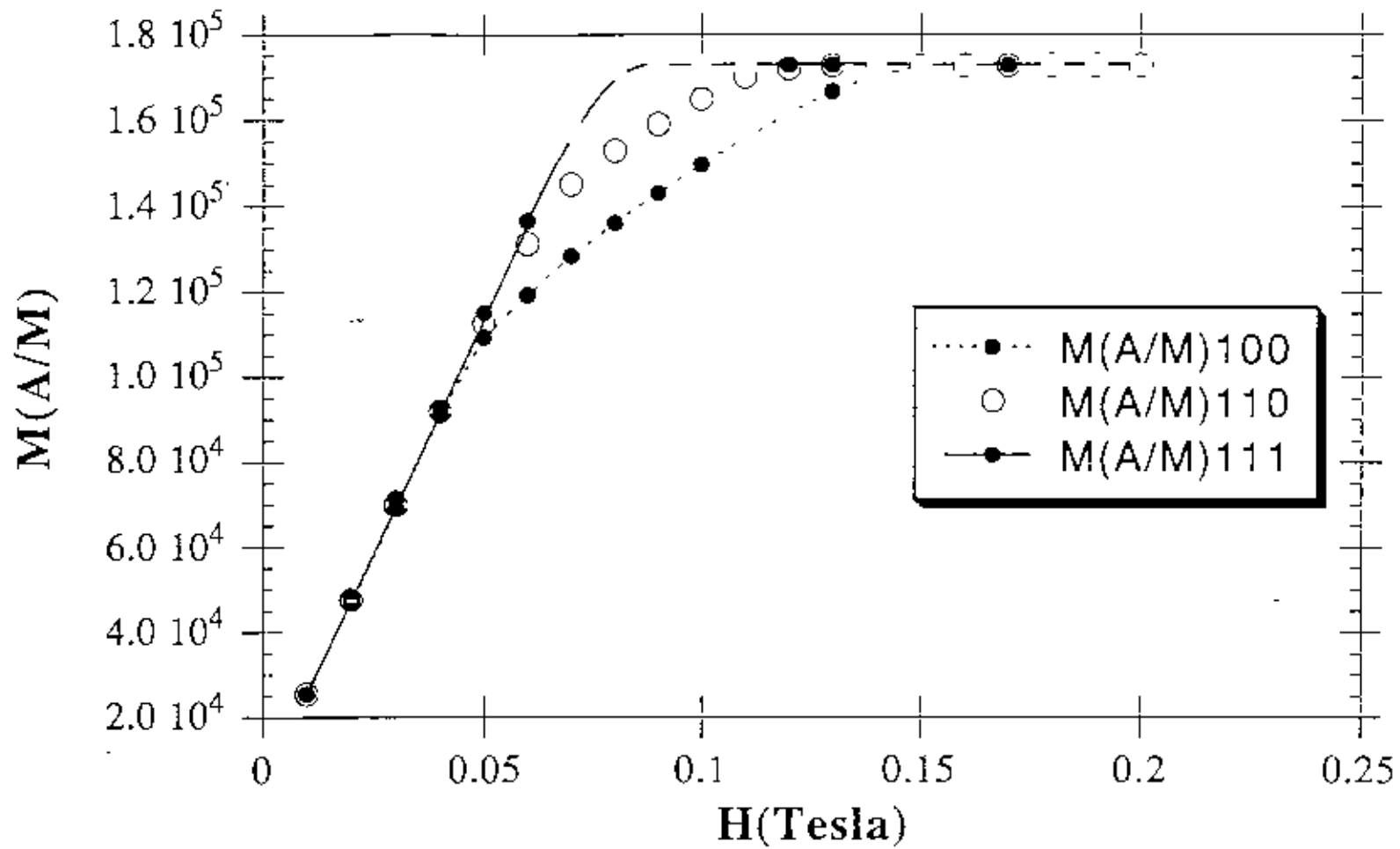


Fig. 4.13 M vs H curve of Ni-Mo<sub>10%</sub> single crystal for three principal crystallographic directions at 4.2K.

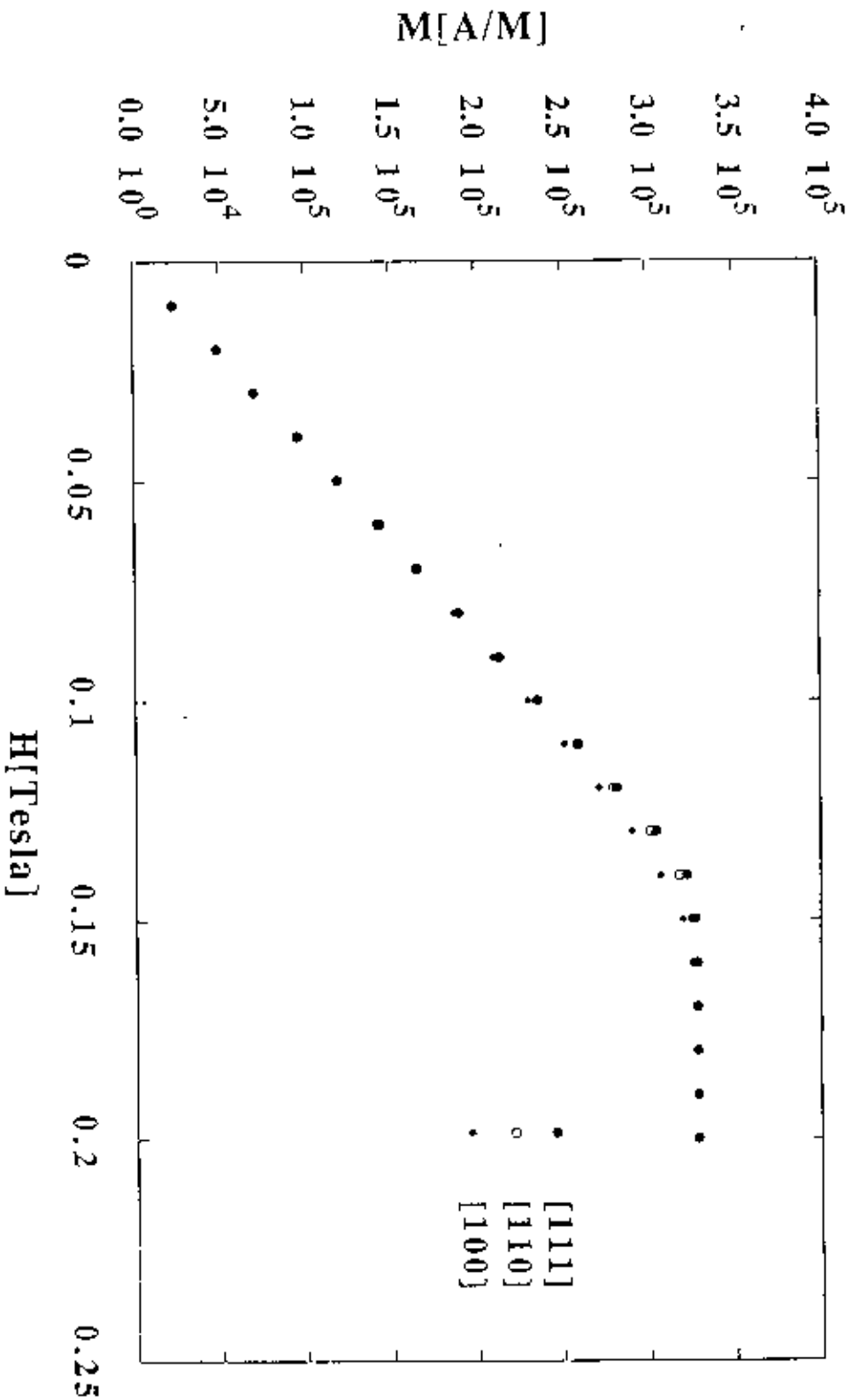


Fig. 4.14 M vs H curve of Ni-Mo6% for three principal crystallographic directions at 300K.



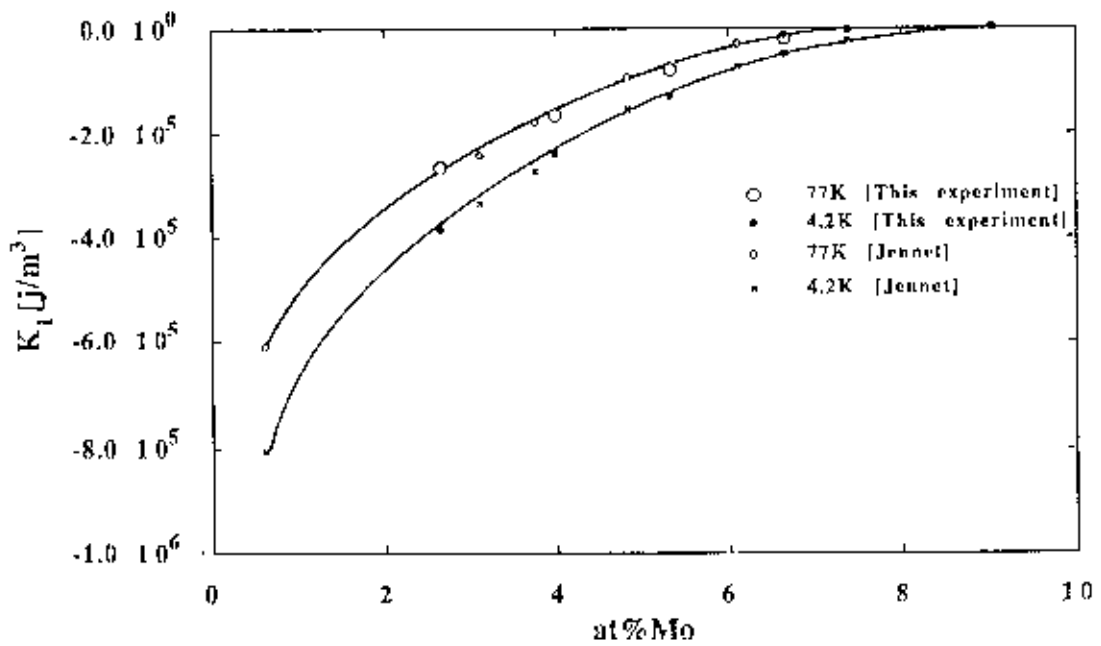


Fig. 4.15 The first anisotropy constants of Nickel-Molybdenum alloy.

From Van Vleck's theory of magnetic anisotropy,  $K_1$  should vary with composition as either  $M(0)$  or as  $M^2(0)$ , depending on the model used. The values of  $K_1$  for Ni-Cu alloys, determined by Williams and Bozorth (1939) are supposed to vary with composition as approximately  $M^2$  (Bozorth 1951) as the values obtained by Puzel (1949) for Ni-Mo and Ni-Cu alloys

$\frac{K_1(c)}{K_1(0)}$  vs  $\frac{M(c)}{M(0)}$  values of Ni-Mo alloys from our experiments are plotted for two temperatures in Fig 4.16. In Fig.4.17  $\ln \left[ \frac{K_1(c)}{K_1(0)} \right]$  vs  $\ln \left[ \frac{M(c)}{M(0)} \right]$  values are plotted for 77K and 4.2K. The slope of both the curves is close to 3

It is found for several ferromagnetic nickel alloys, e.g. Ni-Cu and Ni-Al (Martin, 1958) that the magnetisation and Curie point vary with concentration in such a way that curves of reduced magnetization against  $\frac{T}{T_c}$  show a continuous decrease as the solute concentration increases until a limiting concentration is reached. For alloys containing a greater amount of solute the reduced magnetization curves coincide; and the Law of Corresponding States applies.

The anisotropy constants to be compared with theory are those at constant volume. We shall discuss here, what happens to nickel matrix when molybdenum is added to it. This phenomenon is to be linked with magnetostriction [Asgar 1970]. When molybdenum is added to nickel, the increase in volume  $\delta V(c)$  that occurs will give rise to a magnetostrictive contribution to  $K_1$ , similar to that due to thermal expansion. Therefore the correction that may be done to  $K_1$  is

$$\delta K_1(c) = -h_1(C_{11} + 2C_{12}) \frac{\delta V(c)}{V_0} \dots\dots\dots(4.2)$$

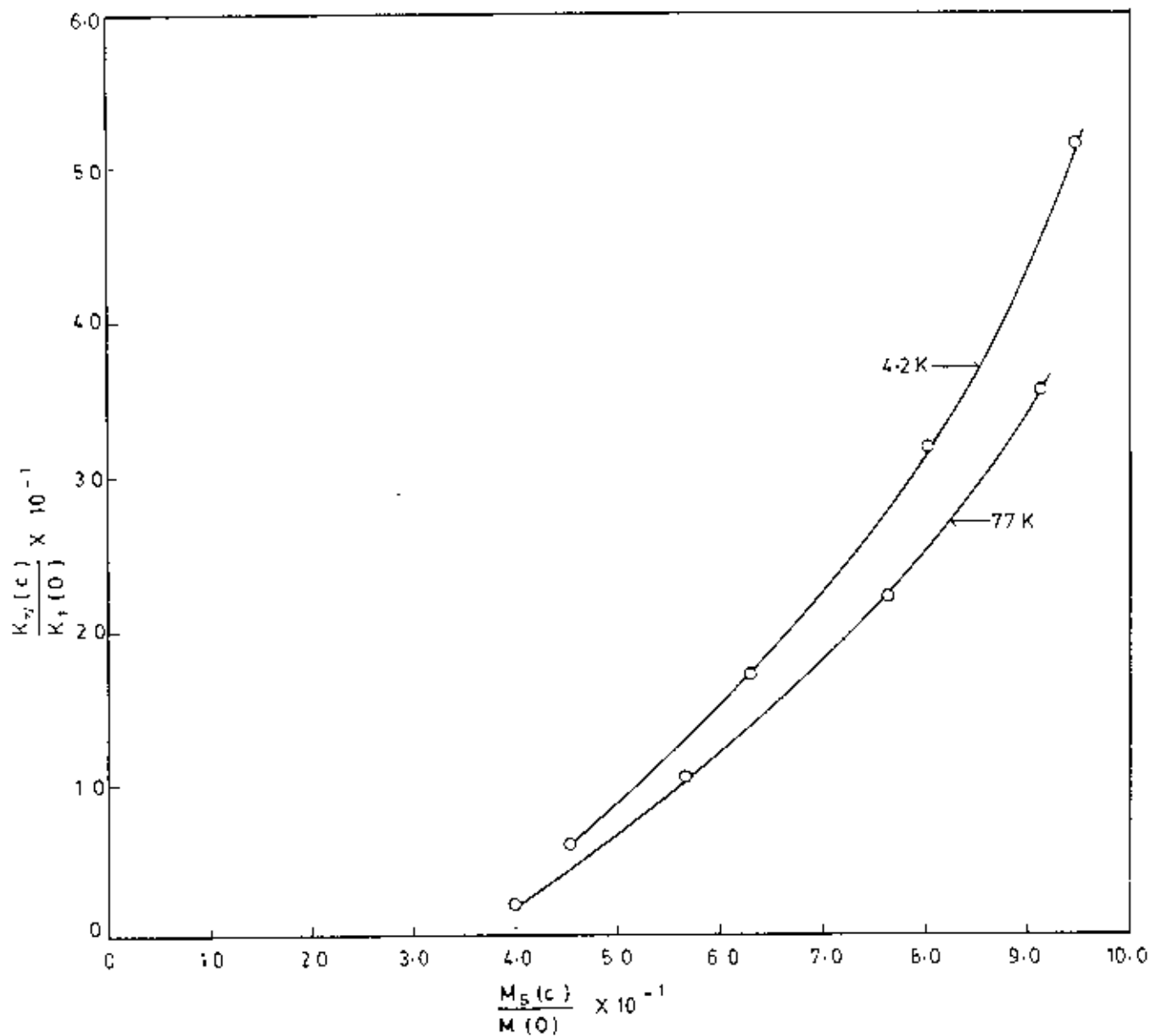


Fig. 4.16  $\frac{K_2(c)}{K_1(0)}$  vs  $\frac{M_2(c)}{M(0)}$  curve of Ni-Mo at 77K and 4.2K

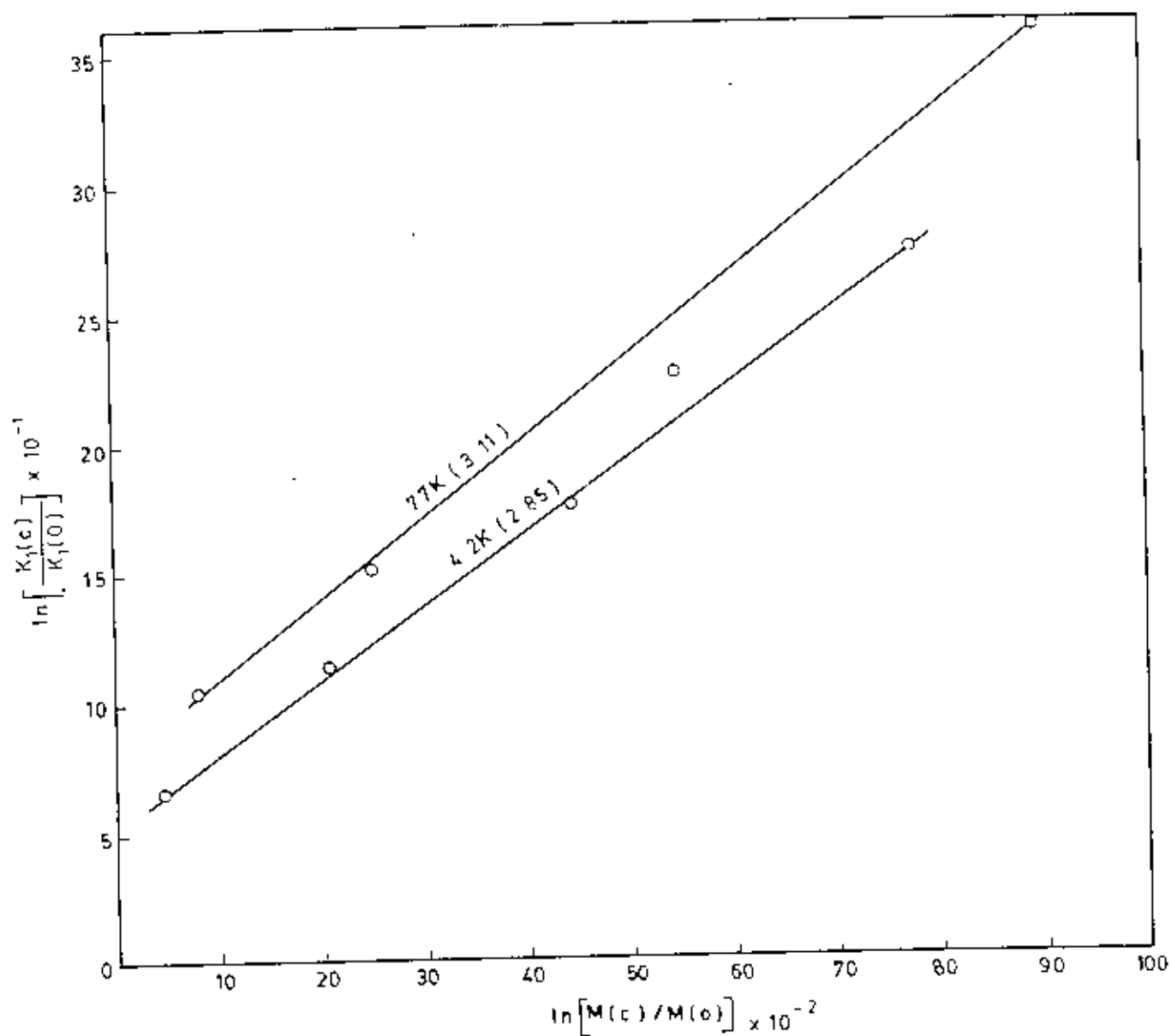


Fig. 4.17  $\ln \left[ \frac{K_1(c)}{K_1(0)} \right]$  vs  $\ln \left[ \frac{M(c)}{M(0)} \right]$  curve of Ni-Mo. at 77K and 4.2K

where  $C_{11}$  and  $C_{12}$  are the elastic constants. From the lattice parameter data for Ni-Mo alloys (Pearson, 1967) it may be found that the greatest increase in volume in the relevant alloy range is 3.5%. Although the elastic constants  $C_{11}$  and  $C_{12}$  have not been determined for Ni-Mo alloys, they do not change much for similar alloys. In a theory of the temperature dependence of magnetoelastic constants of cubic crystals Van Vleck and Kittel (1960) predict that the mechanism causing  $h_1$  is sufficiently closely linked with that of  $K_1$  for  $h_1$  to exhibit a similar variation with temperature. Therefore, it is unreasonable to suppose that the composition dependence of  $h_1(c)$  is also similar to that of  $K_1(c)$ . Thus we assume that  $h_1$  decreases rapidly without change in sign with increasing molybdenum concentration. For nickel at low temperatures,  $h_1 \approx -4.7 \times 10^{-6}$  (Benninger and Pavlovic, 1967). Since the elastic constants are  $10^{12}$ ,  $\delta K_1(c)$  will be positive and small for all the alloys, becoming negligible for the higher Mo alloys. Hence  $\delta K_1(c)$  is ignored. Asgar has determined both the linear magnetostriction constants  $h_1$  and  $h_2$  in the Ni-Mo alloy system. Both the constants are negative as in the case of nickel and decrease monotonically in their absolute values with increasing concentration of molybdenum and increasing temperature.

Magnetisation distribution around a wide variety of impurities in nickel, as studied particularly by neutron diffraction by Low and Collins, Hicks et al, Comly et al and others, has shown that two types of disturbances can be produced by alloying nickel. In one category the magnetic disturbance is confined to the impurity site, for example when Mn, Fe, or Rh is present. And in the second category the magnetic disturbance is wide spread and includes the neighbouring matrix atoms. Ni-Mo alloys belong to the second category. The presence of Mo in Ni matrix has the same effect of moment disturbance in nickel matrix as those of Al, Ga, Si, Ge, Sn, Nb, Cr, W etc except that the

effect of impurity must be weighted by the number of electrons outside the closed shells in the impurity atom.

Friedel has considered that when the difference of valence between the components of an alloy is too large, the rigid band model does not hold. The strong repulsive impurity potential due to a large value of  $\nabla Z$  splits the localized states off the top of the 3d band. However Beeby has shown that the density of states is not altered due to this, unless the localized states remain at the Fermi level. The only effect being to reduce the total number of states available in the band and to reduce the band width. Since the localized states of both spin directions are empty for the alloys we have mentioned, the rigid band model can be used in these nickel alloys when electron concentration is replaced by saturation magnetization. The results of Ni-Mo alloys, therefore, will represent the general behaviour of any nickel alloy of the second category.

Considering the simple mechanism that the decrease in magnetization of the alloys is due to transfer of electrons of Mo atoms outside the inner closed shells of the Ni atoms, we can express the moment per atom using the general relation

$$\mu_{av} = \mu_{magn} - v c \quad \dots\dots\dots(4.3)$$

where  $v$  is the valency, being 6 for Mo and  $c$  is the atomic percentage of impurity on Ni. Our graph of saturation magnetisation supports this showing linear dependence of magnetization with concentration. However, if the equation (4.1) should hold upto the highest concentration of Mo, the magnetisation should vanish around 10 at% of Mo in Ni.

**Chapter 5**  
**Measurements on Iron Phosphide (Fe<sub>2</sub>P)**

### 5.1 Introduction:

The physical properties of iron phosphide ( $\text{Fe}_2\text{P}$ ) have been the subject of many investigations in recent years. Many workers have determined the physical parameters of  $\text{Fe}_2\text{P}$  which both agree and disagree with the earlier results. The most disputed parameters are the ferro-paramagnetic Curie temperature, and the magnetic moment per iron atom. The crystal structure has been determined and refined by Rundqvist and Jellinek. Chiba et. al. has determined from high temperature susceptibility data that  $\text{Fe}_2\text{P}$  is ferromagnetic with a paramagnetic Curie temperature of  $478^\circ\text{K}$ . The ferromagnetic Curie temperature of  $\text{Fe}_2\text{P}$  was reported to be  $353^\circ\text{K}$  by LeChatelier and Wologdine,  $306^\circ\text{K}$  by Chiba,  $266^\circ\text{K}$  by Meyer and Cadeville and  $216^\circ\text{K}$  by Lundgren et.al. The discrepancies in the magnetic properties of  $\text{Fe}_2\text{P}$  have made it difficult to interpret the Mossbauer spectra of this material and hence calls for further studies on this material. Fruchert et. al. reported considerable variation in the magnetic moment with slight variations in the stoichiometry. Meyer and Cadeville and Fruchert et al. were the first to report the existence of a range of stoichiometry for  $\text{Fe}_2\text{P}$ . Bellavance, Mikkelsen and Wold have set the lower limit of stoichiometry for  $\text{Fe}_2\text{P}$  that can be prepared from the electrolysis of fused salts. They have also measured the magnetization as a function of field and temperature for stoichiometric and non-stoichiometric  $\text{Fe}_2\text{P}$ .

The purpose of undertaking this study is to determine mainly the magnetic properties, e.g. the ferro-paramagnetic Curie temperature, the saturation magnetization, the magnetocrystalline anisotropy constant and the temperature dependence of the magnetocrystalline anisotropy constant of  $\text{Fe}_2\text{P}$  with the help of the Super Conducting Quantum Interference Device (SQUID). Besides agreements with previous results, there are also some disagreements in the nature of temperature dependence of



magnetization. Although there is no previous data to compare the temperature dependence of magnetocrystalline anisotropy constant, we have measured the temperature dependence of magnetocrystalline anisotropy constant of  $\text{Fe}_2\text{P}$  and have fitted these data with some power law. Also we have given some degree of interpretation to the persistence of the magneto crystalline anisotropy above the Curie temperature.

### 5.2 $\text{Fe}_2\text{P}$ - alloy:

$\text{Fe}_2\text{P}$  is a ferromagnet which shows a first order ferromagnetic to paramagnetic transition at  $T_c=216$  K. It has a large magnetocrystalline anisotropy with the easy axis along the c-axis. The magnetic moments are directed along the c-axis with an extremely high uniaxial anisotropy of  $K_1 = 2.3 \times 10^6 \text{ joules / m}^3$  at 4.2K. The saturation moment is  $1.46\mu_B$  per Fe atom at 4.2K. The crystal structure is C22 which belongs to the hexagonal structure having two crystallographically different Fe sites,  $\text{Fe}_I$  and  $\text{Fe}_{II}$ .

The crystal structure of  $\text{Fe}_2\text{P}$  was first determined by Rundqvist and Jellinek(1959) and accurately refined by Carlsson et al (1973). At 297 K the unit cell dimensions are  $a=5.8675(2) \text{ \AA}$  ;  $c = 3.4581(2) \text{ \AA}$ .

$\text{Fe}_2\text{P}$  displays rich magnetic properties. A critical balance between ferro- and antiferromagnetic interaction in this compound results in a great sensitivity of the magnetic properties to the external parameters e.g. pressure, concentration of alloying additions, temperature and magnetic field.  $\text{Fe}_2\text{P}$  is basically ferromagnetic but, due to the extreme sensitivity of the phase transition to the presence of vacancies and impurity

atoms, early reports showed large discrepancies as regards transition temperature and the nature of transition. Furthermore the large magnetocrystalline anisotropy prevented an accurate determination of the saturation moment from measurements on polycrystalline samples. The saturation moment is otherwise not sensitive to small deviations from the ideal  $Fe_2P$  formula. The main properties of pure  $Fe_2P$  of ideal stoichiometry can be summarised as follows:

Mossbauer spectroscopic studies (Wappling et al. 1974,1975) as well as magnetic measurements on single crystals (Fujii et al.1977, Lundgren et al.1978, Andersson et al.1978) showed a first order ferro/paramagnetic transition at 216K. with a thermal hysteresis of the transition of about 0.7K. At the transition the hyperfine fields drop from about half of their saturation values ( 11.4T for  $Fe_I$  and 18.0T for  $Fe_{II}$  ) to zero.

The transition is accompanied by a discontinuous change in the dimensions of the hexagonal unit cell with a decrease in the a-axis of 0.06 - 0.07% and an increase of the c-axis of 0.08% for increasing temperatures (i.e. a volume change of  $\frac{\Delta V}{V} = -0.05\%$ ).

The magnetoelastic effects are suppressed if sufficient amount of Ni or Mn are substituted in  $Fe_2P$ . Substitution of Ni results in 'stable' ferromagnetic properties, whereas substitution of Mn gives antiferromagnetism at low temperature.

The pressure ( $p$ ) dependence of the transition is  $\frac{\Delta T}{\Delta p} = -5K / kbar$ . The transition changes from first to second order in applied fields ( $B$ ) above 0.07T and increases by about  $\frac{\Delta T}{\Delta B} = 25K / T$  in fields upto 4T. Specific heat measurements (Beckman et

al.1982) gave an entropy change at the transition of  $\Delta S = 0.02R$ , which is in agreement with Clapeyrons equation:  $\frac{\Delta T}{\Delta p} = \frac{\Delta V}{\Delta S}$ . The very small entropy change at the

transition as well as no indication of magnetic excitations in the specific heat are characteristic for delocalized d-electrons and an itinerant electron model should be

used (Moriya and Usami 1977, Moriya 1985, Wohlfarth 1979, 1986). The low temperature specific heat measurements gives an electronic part of  $\gamma = 24 \text{ mJ} / \text{K}^2 \text{ mole}$ . Magnetization measurements on single crystals (Fujii et al. 1977, Lundgren et al. 1978) show that the spins are directed along the hexagonal c-axis with an exceedingly high uniaxial anisotropy. The saturation moment is  $2.92 \mu_B$  per formula unit and the anisotropy field is  $6.5T$ , equivalent to a uniaxial anisotropy energy of  $2.3 \times 10^6 \text{ J} / \text{m}^3$ . Neutron diffraction results on powdered samples at 77K (Scheerlinck and Legrand 1978) gave moments of  $0.69 \mu_B$  and  $2.31 \mu_B$  for  $\text{Fe}_I$  and  $\text{Fe}_{II}$ , respectively. In contrast, a single crystal polarised neutron diffraction study (Fujii et al 1979), at the same temperature, gave  $0.92 \mu_B$  and  $1.70 \mu_B$ . The magnetic form factor of  $\text{Fe}_I$  was found to be close to that of a free iron atom, while that of  $\text{Fe}_{II}$  was found to be close to that of  $\text{Fe}^{4+}$  ion. The total magnetic moment determined from this single crystal measurement is about 10% smaller than the value obtained from magnetization measurements.

The electronic structure of  $\text{Fe}_2\text{P}$  has been calculated by Ishida et. al (1987) using the KKR and LMTO methods within the framework of LSD approximation. The calculations indicate that  $\text{Fe}_2\text{P}$  is ferromagnetic and the values of the magnetic moment for  $\text{Fe}_I$ ,  $\text{Fe}_{II}$ ,  $\text{P}_I$  and  $\text{P}_{II}$  found to be 0.89, 2.24, -0.07 and -0.06  $\mu_B$  by the KKR method and 0.76, 2.31, -0.09 and -0.08  $\mu_B$  by the LMTO method. This result agrees well with self-consistent spin-polarised electronic structure calculations by Eriksson et al (1988), using the LMTO method, where 0.92 and  $2.03 \mu_B$  are found for the two iron sites.

$\text{Fe}_2\text{P}$  has an orthorhombic structure at high temperatures (900°C, 80kbar, Senateur et al 1976). Electronic structure calculations of orthorhombic ferromagnetic  $\text{Fe}_2\text{P}$  by

S. Fujii et al (1988) gave  $3.02\mu_B$  per formula unit and 0.86, 2.19 and  $-0.03\mu_B$  for Fe<sub>I</sub>, Fe<sub>II</sub> and P, respectively

At temperatures above  $T_C$  the susceptibility deviates markedly from Curie-Weiss behaviour and high temperature measurements (Krumbugel-Nylund 1974, Krumbugel Nylund et al. 1974, Wappling et. al. 1985, Chenevier et al. 1989) gave a paramagnetic Curie temperature of about 470K i.e., more than twice the value of the transition temperature, which implies strong short range order above  $T_C$ . Kómura et al.(1980, 1983) have studied the magnetic excitations at temperatures above 77K. They found that the spin wave energies of magnons propagating along  $\langle 001 \rangle$  are much larger than those in the basal plane. It was inferred that one dimensional ferromagnetic chains along  $\langle 001 \rangle$  persist well above the transition temperature. From elastic and inelastic neutron scattering (Fujii et al. 1988) it was shown that giant short range order exists at temperatures upto  $T \approx 3T_C$ . Polarised neutron scattering investigations by Wilkinson et. al.(1989) revealed spin correlations upto a distance of 12Å at temperatures upto atleast  $T \approx 3.7T_C$ . However, from transverse field  $\mu SR$  measurements (Wappling et al.1985) no magnetic correlations could be found at life time larger than  $10^{-10}$ sec

The magnetic properties of Fe<sub>2</sub>P are sensitive to pressure, with pronounced anisotropy. The transition temperature  $T_C$  decreases with hydrostatic pressure, but deviates at about 5kbar. In the limit of zero pressure  $\frac{\nabla T}{\nabla p}$  has been reported to be

$-3.5K/kbar$  (Fujii et al. 1977)  $-4.0K/kbar$  (Goodenough et al. 1973) and

$-5.4K/kbar$  (Fujiwara et al. 1980). Due to an anisotropic compressibility ( $\frac{\nabla a}{a} = -2.5 \times 10^{-4}/kbar$  and  $\frac{\nabla c}{c} = -1.5 \times 10^{-4}$ ) at room temperature (S.Rundqvist,

unpublished) the  $\frac{c}{a}$  ratio increases with hydrostatic pressure.

Uniaxial stress experiments by Fujiwara et. al.(1982) revealed anisotropic effects. Pressure applied along the a-axis gives  $\frac{\nabla T}{\nabla p} = -6.4K / kbar$ , whereas pressure applied along the c-axis gives  $\frac{\nabla T}{\nabla p} = 7.8K / kbar$ , which is in accordance with results by Lundgren et. al.(1977, 78), who found that a tensile stress of  $10^8 \text{ N/m}^2$ , along the c-axis decreases the transition temperature by 8K. Fujiwara et al. measured the weak field a.c. susceptibility and the resistivity of Fe<sub>2</sub>P single crystals as a function of temperature from 4.2 K -300 K and as functions of hydrostatic pressures upto 20 kbar. The Curie temperature, and the first-order transition temperature decreased rapidly with increasing pressure, and ferromagnetism vanished at about 13 kbar at 0 K. Small substitutions of B, Si or As results in an increase of the a-parameter and a decrease in the c-parameter. The transition temperature increases rapidly with non-metal substitution. A crystallographic hexagonal/orthorhombic transformation occurs for both Si and As substitutions (Jernberg et al. 1984, Lundgren et al 1977, 78).

The pressure effects have been discussed on the basis of a pair interaction model (Kadomatsu et al.1985) It was argued that the exchange interactions between the iron sites I and I, sites I and II, and sites II and II are strongly antiferromagnetic, strongly ferromagnetic and weakly antiferromagnetic. With an increase of the  $\frac{c}{a}$  ratio the antiferromagnetic I-I interaction in the basal plane becomes stronger than the ferromagnetic I-II interaction, which runs zigzag along the c-axis. This results in decrease of T<sub>c</sub> in agreement with pressure data. From a somewhat modified viewpoint (Lundgren et al 1980), it appears that an increase of the a-parameter and / or decrease of the c-parameter gives rise to an increase of T<sub>c</sub>. A larger emphasis is put on variation of the a-parameter since both the a-parameter and the volume show a similar change at the transition. It is found that the variation of T<sub>c</sub> with pressure, stress and non-metal

substitutions is well correlated to the parameter  $(\frac{\nabla a}{a} = \frac{\nabla c}{2c})$ . The good correlation between  $T_C$  and lattice parameters indicate that the change in electron concentration with non-metal atom (X) substitutions only has a minor influence on the ordering temperature

### 5.3 Magnetocrystalline anisotropy in Fe<sub>2</sub>P:

Although there are anomalous results on the determination of  $K_1$  for Fe<sub>2</sub>P calculated by different authors, our results seem to be quite consistent with Hironobu Fuji et. al. The two methods employed for the determination of  $K_1$  gave identical results which is about  $2.3 \times 10^6 \text{ joules / m}^3$ . This large uni-axial anisotropy is due to the strong spin-orbit coupling as its moments prefer to point along the c-axis and the orbit-lattice coupling is also very strong. For systems that exhibit itinerant ferromagnetism like Fe<sub>2</sub>P, correlations between magnetic spins have been detected at temperatures significantly above the Curie temperature. This is one of the reasons behind the persistence of magnetic anisotropy above the Curie temperature. There are many striking features observed in Fe<sub>2</sub>P in terms of its sensitivity to external pressure, or some substitutions etc. But there is no data on the change in magnetic anisotropy when Fe<sub>2</sub>P is subjected to these changes. However, we have analysed the temperature dependence of the magnetocrystalline anisotropy of Fe<sub>2</sub>P which we claim to be a new work on this line.

#### **5.4 Super Conducting Quantum Interference Device (SQUID):**

The Super Conducting Quantum Interference Device(SQUID) provides the ultimate in resolution for field measurements. The SQUID consists of a superconducting ring with a small insulating layer known as the 'weak link' as shown in Fig.5.2 a. The weak link is also known as a Josephson junction. The resolution of this device is of the order of  $10^{-14}$  tesla( $10^{-10}$  gauss). The flux passing through the ring is quantized once the ring has gone superconducting. But the weak link enables the flux trapped in the ring to change by discrete amounts. Changes in the pick-up voltage occur as the flux is incremented in amounts of  $\nabla\phi = 2.067 \times 10^{-15}$  *Wb*. The device can thereby be used to measure very small changes in flux. In fact it can be used to count the changes in flux quanta in the ring.

With no 'weak link' the flux cannot enter the ring as we know from the property of a superconductor, and thus the field passing through the ring remains at the value it was at when the ring became superconducting. The presence of the weak link typically restricts the value of the super current flowing in the ring to less than  $10^{-1}$  *A*. Therefore with a weak link the magnetic flux can enter the ring. The supercurrent in the weak link tries to oppose the entry of the flux but because it is limited by the weak link it cannot achieve this entirely as the flux is increased. It therefore becomes a periodic function of the flux threading the superconducting ring. The relation between the flux density in the ring and the flux density due to the applied field is

$$\phi = \phi_a + LI_s \quad (5.1)$$

where  $\phi$  is the flux density in the ring,  $\phi_a$  is the flux due to the applied field,  $L$  is the inductance of the ring and  $I_s$  is the supercurrent which produces a flux of  $\phi_s = LI_s$ . In the Josephson junction the supercurrent  $I_s$  in the ring is related to the critical current  $I_c$  determined by the properties of the weaklink

$$I_s = I_c \sin \theta \quad (5.2)$$

where  $\theta$  is the phase difference of the electron wave functions across the weak link.

Thus

$$\phi = \phi_a + LI_c \sin \theta \quad (5.3)$$

In a completely superconducting ring the flux is an integral number of flux quanta.

Therefore if  $\phi_0$  is the flux quantum of  $2.067 \times 10^{-15} \text{ Wb}$ ,

$$\phi = N\phi_0 \quad (5.4)$$

With the weak link the phase angle  $\theta$  across the link depends on the flux in the following way

$$\theta = 2\pi N - 2\pi \left( \frac{\phi}{\phi_0} \right) \quad (5.5)$$

since  $N$  is an integer

$$\begin{aligned} \sin \theta &= \sin \left( -2\pi \frac{\phi}{\phi_0} \right) \\ &= -\sin \left( 2\pi \frac{\phi}{\phi_0} \right) \end{aligned} \quad (5.6)$$

and therefore

$$\phi = \phi_a - LI_c \sin \left( 2\pi \frac{\phi}{\phi_0} \right) \quad (5.7)$$

and the relation between  $\phi$  and  $\phi_a$  is given in Fig.5.2 b. From this graph we see that the SQUID counts flux quanta of the applied field in units of  $2.067 \times 10^{-15} \text{ Wb}$ . If a loop of wire or a coil is placed around the superconducting ring then a voltage pulse is induced in the coil at each quantum jump, and this pulse can be used to measure the applied field. The SQUID is clearly a very highly sensitive device and is therefore best suited to measuring very small changes in magnetic field. A schematic diagram of the SQUID magnetometer is shown in Fig.5.1.



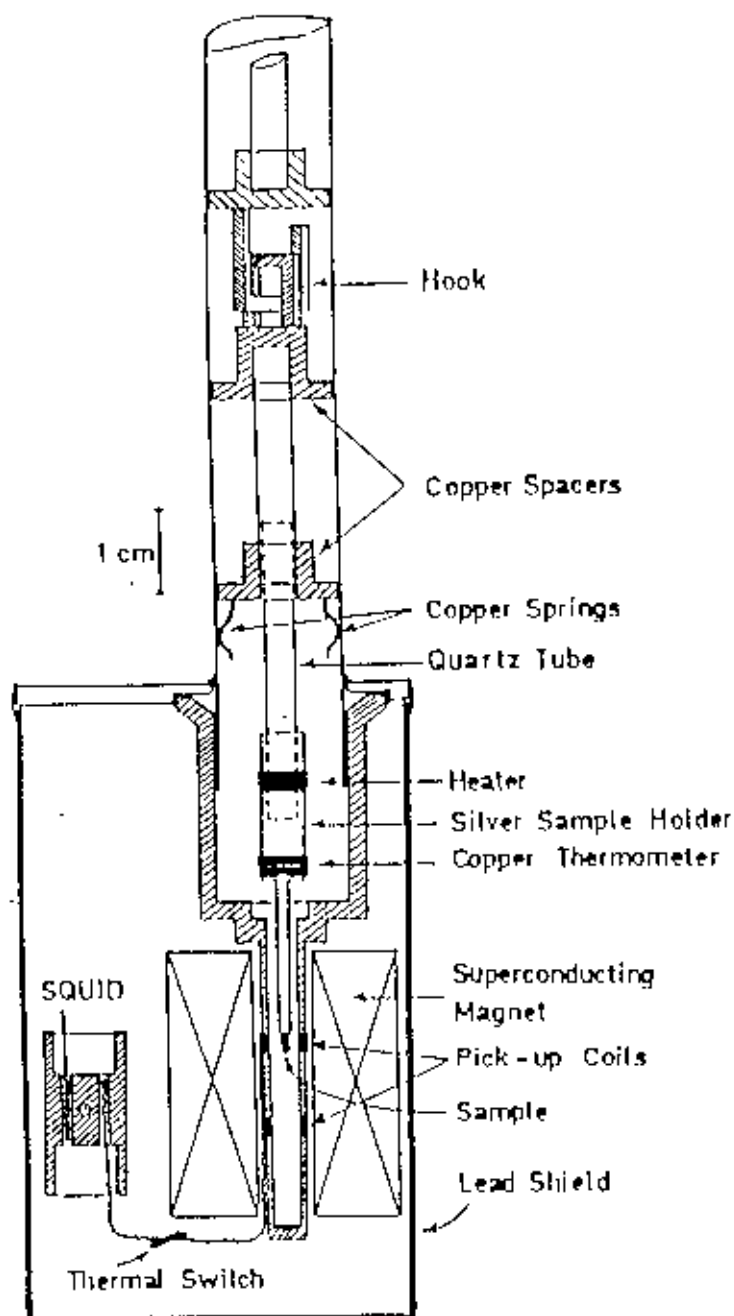


**Fig. 5.1 Schematic drawing of the central part of the SQUID magnetometer.**  
 (All parts not drawn to scale)

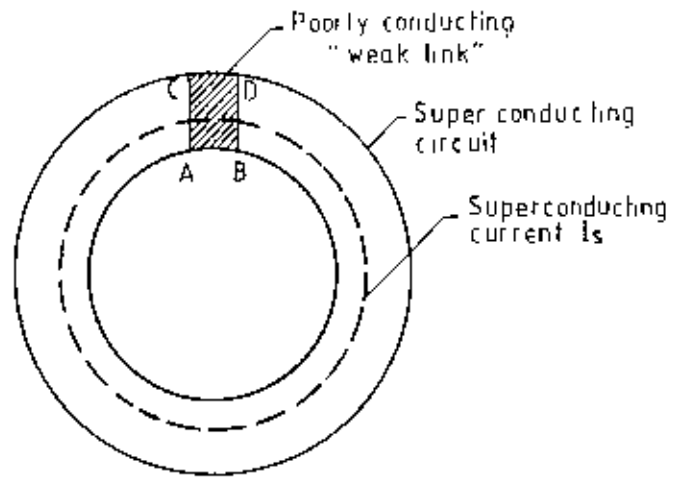


Fig. 5.2.a A Josephson junction device which consists of a superconductor with a poorly conducting "weak link" ABCD

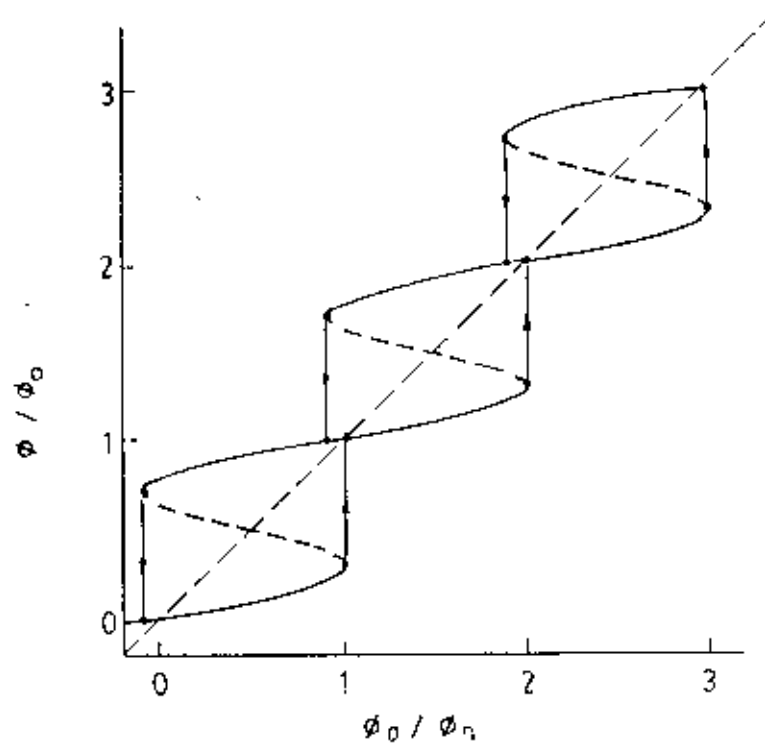


Fig. 5.2.b The relation between  $\phi$ , the flux in the ring and  $\phi_0$ , the flux due to the applied field, in a SQUID magnetometer

### 5.5...Experimental:

The Fe<sub>2</sub>P sample is glued by silver glue in a sample cup of diameter 5mm. The cup is then fixed with the SQUID sample rod. The SQUID Cryostat is then filled with liquid Helium. The sample rod with the sample is then put in the SQUID magnetometer with the data acquisition system for measurements. At first a small probing field of 50 Gauss is applied on the sample. The SQUID response is then recorded. The position of the maximum signal is observed on the SQUID monitor. The position of the sample is then changed using the SQUID command through which the sample position can be raised or lowered by fraction of a millimeter. Thus the signal from the sample is maximised. Once the sample is accurately positioned, the Computer is programmed for executing the measurements. The magnetization of the sample is measured in both the axes e.g. parallel to the c-axis, and perpendicular to the c-axis. In the perpendicular direction to the c-axis, the demagnetising factor is  $\frac{1}{2}$ . The measured data is stored automatically by the Computer for analysis.

### 5.6 Evaluation of the first anisotropy constant $K_1$ :

For the evaluation of the first anisotropy constant  $K_1$ , two methods are employed. One is the slope method, the other is the calculation of the area under the M-H curve. In the slope method the initial slope of the linear portion of the M-H curve is accurately measured and tabulated. The saturation magnetization  $M_S$  at 4.2K is estimated by extrapolating the M-H curve to very high magnetic field where the sample is assumed to have been saturated as we know that the saturation field of Fe<sub>2</sub>P is very high due to

its large uniaxial anisotropy. The anisotropy constant is then calculated by using equation(5.3).

In another method the anisotropy constants are calculated by integrating the area under the M-H curve. Both the methods agree very nicely with each other.

**Table. 5.1. ( $K_1$  calculated from area under the M vs H curve)**

| Temperature (K) | $K_1$ (Joule/m <sup>3</sup> )                | $M_s$ (Ampere/m)                             |
|-----------------|--|--|
| 0               | $2.32 \times 10^6$ <sub>(extrapolated)</sub> | $6.80 \times 10^5$ <sub>(extrapolated)</sub> |
| 5               | $2.30 \times 10^6$                           | $6.66 \times 10^5$                           |
| 30              | $2.23 \times 10^6$                           | $6.60 \times 10^5$                           |
| 50              | $2.16 \times 10^6$                           | $6.50 \times 10^5$                           |
| 75              | $1.88 \times 10^6$                           | $6.38 \times 10^5$                           |
| 100             | $1.54 \times 10^6$                           | $6.14 \times 10^5$                           |
| 150             | $0.92 \times 10^6$                           | $5.53 \times 10^5$                           |
| 180             | $0.41 \times 10^6$                           | $4.10 \times 10^5$                           |
| 200             | $0.35 \times 10^6$                           | $3.83 \times 10^5$                           |
| 210             | $0.33 \times 10^6$                           | $3.63 \times 10^5$                           |

**Table .5.2 ( $K_1$  calculated from the slope of M vs H curve)**

| Temperature (K) | $K_1$ (Joule/m <sup>3</sup> )     | $M_s$ (Ampere/m)                  |
|-----------------|-----------------------------------|-----------------------------------|
| 0               | $2.31 \times 10^6$ (extrapolated) | $6.79 \times 10^5$ (extrapolated) |
| 5               | $2.28 \times 10^6$                | $6.77 \times 10^5$                |
| 30              | $2.22 \times 10^6$                | $6.68 \times 10^5$                |
| 50              | $2.04 \times 10^6$                | $6.52 \times 10^5$                |
| 75              | $1.77 \times 10^6$                | $6.36 \times 10^5$                |
| 100             | $1.52 \times 10^6$                | $6.14 \times 10^5$                |
| 150             | $0.92 \times 10^6$                | $5.49 \times 10^5$                |
| 180             | $3.84 \times 10^5$                | $4.19 \times 10^5$                |
| 200             | $2.71 \times 10^5$                | $3.82 \times 10^5$                |
| 210             | $2.14 \times 10^5$                | $3.51 \times 10^5$                |

## 5.7 Results and Discussion:

Fig.5.3 shows the M vs H curve at 5K for Fe<sub>2</sub>P. The saturation field is very high due to large uniaxial anisotropy. The saturation field is estimated by extrapolating the M vs H curve using a linear equation of the form  $ax+bx^2+cx^3+\dots$ . The estimated saturation field is about 9 tesla. This large saturation field perpendicular to the c-axis is a characteristic of Fe<sub>2</sub>P. The initial slope of the M vs H curve is used to calculate the first anisotropy constant  $K_1$ . Fig.5.4 shows the magnetization curve of Fe<sub>2</sub>P obtained by applying the magnetic field parallel to the c-axis. The saturation magnetization  $M_S$  is obtained by extrapolating high field magnetization along the c-axis to  $H = 0$ . The same figure also shows the M vs H curve perpendicular to the c-axis at 150K. This curve shows a continuous increase of magnetization with the applied magnetic field. The calculated saturation moment of Fe<sub>2</sub>P is  $2.48\mu_B$  per formula unit. Fig.5.5 shows the M vs T curve for different applied fields. All the curves show a remarkable jump in and around  $T_C$ . The reason of these jumps in magnetization is the possible magnetic scattering (S.Komura et.al.) which increases around the Curie temperature and goes through a maximum at  $T_C$  before decreasing sharply. Another possible reason for these jumps is the change in lattice parameter which takes place at  $T_C$ . Fig.5.6 shows the M vs H curve of Fe<sub>2</sub>P above the ferromagnetic Curie temperature. Fig.5.7 shows the M vs H curve for two different temperature 30K and 100K. Fig.5.8 shows the M vs H curve at 230K and 250K. Fig.5.9 shows the  $\frac{1}{\chi}$  vs temperature plot of Fe<sub>2</sub>P. The extrapolation of the slope of the curve intercepts at  $T_C$ . Fig.5.10 shows a plot of the temperature derivative of magnetization  $\frac{dM}{dT}$  against temperature for different applied fields. The function  $\frac{dM}{dT} = 0$  is a measure of the Curie temperature  $T_C$ . Fig.5.11-5.14 are the plots of parallel and perpendicular susceptibility data of Fe<sub>2</sub>P. The difference in

susceptibility is a measure of the magnetocrystalline anisotropy above  $T_c$ . Usually for all the 3d elements the anisotropy vanishes at  $T_c$ . But in  $Fe_2P$  the high uniaxial anisotropy seem to persist well above the Curie temperature. This phenomenon supports R.Wappling et al(1985). It may be argued that although the spin-spin interactions cease to take place above  $T_c$ , there may still be some interactions between the spins and the orbits above  $T_c$  which in turn gives rise to some preferred orientations of the spins. This may be the possible reason for the persisting anisotropy above  $T_c$ . Fig.5.15 shows a curve of the susceptibility versus temperature. This curve shows a hump at the Curie point confirming further a first order transition accompanied by a sudden change in lattice parameter at  $T_c$ . Fig.5.16 shows the temperature dependence of the saturation magnetization. The change in saturation magnetization is linear at low temperature but falls sharply at higher temperature and goes to zero at  $T_c$ . Fig.5.17 shows the  $M$  vs  $T$  curve of  $Fe_2P$  for different applied fields parallel to the  $c$ -axis. Fig.5.18 shows the  $M$  vs  $T$  curve at low applied field close to  $T_c$ . Fig.5.19 shows the hysteresis curve of  $Fe_2P$  at 35K. Fig.5.20 shows the reduced magnetization versus reduced temperature. Fig.5.21 shows the temperature dependence of the magnetocrystalline anisotropy constant  $K_1$  calculated from the slope of the  $M$  vs  $H$  curve and the saturation magnetization  $M_s$ .

The anisotropy energy of a hexagonal crystal may be written as

$$E_a = K_0 + K_1 \sin^2 \theta + K_2 \sin^4 \theta \quad \dots\dots\dots(5.1)$$

where  $K_1$  and  $K_2$  are first and second anisotropy constants respectively. From the minimum condition of the free energy containing Zeeman energy, we can use the relation

$$\frac{H}{M} = \frac{2K_1}{M_s^2} + \frac{(4K_2)M^2}{M_s^4} \quad \dots\dots\dots(5.2)$$

For all most all hexagonal crystals  $K_1 \gg K_2$  ( $K_2$  is negligible) In that case we can write

$$\frac{H}{M} = \frac{2K_1}{M_s^2} \quad \dots\dots\dots(5.3)$$

Thus by measuring the slope of the M vs H curve and the saturation magnetization, the first anisotropy constant  $K_1$  can be calculated. Fig 5.22 shows the temperature dependence of  $K_1$  calculated from the area under the M vs H curve  $K_1$  calculated by this method agrees favourably with that calculated by the slope method. The temperature dependence of the magnetocrystalline anisotropy constant for hexagonal crystal follows the 3rd power law as can be seen in Fig.5.23. The dotted curve is plotted taking the exponent  $n$  of the equation

$$\frac{K_1(T)}{K_1(0)} = \left[ \frac{M(T)}{M(0)} \right]^n \quad \dots\dots\dots (5.4)$$

to be equal to 3. Thus our results follow the 3rd power law. This confirms that the temperature dependence of the magnetocrystalline anisotropy constant  $K_1$  for  $Fe_2P$  follows the 3rd power law.



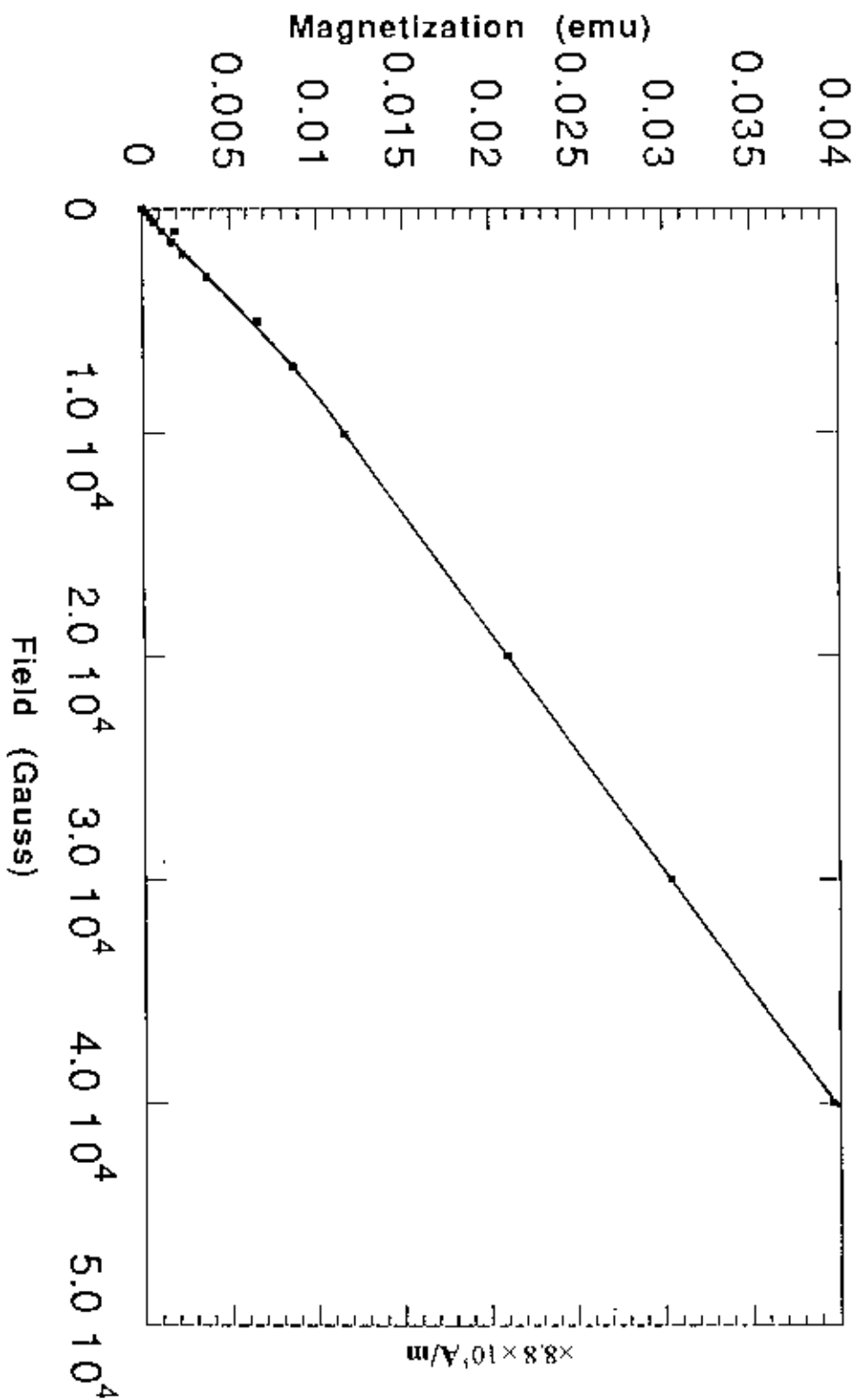


Fig. 5.3 Magnetisation vs field curves of Fe<sub>2</sub>P at 5K

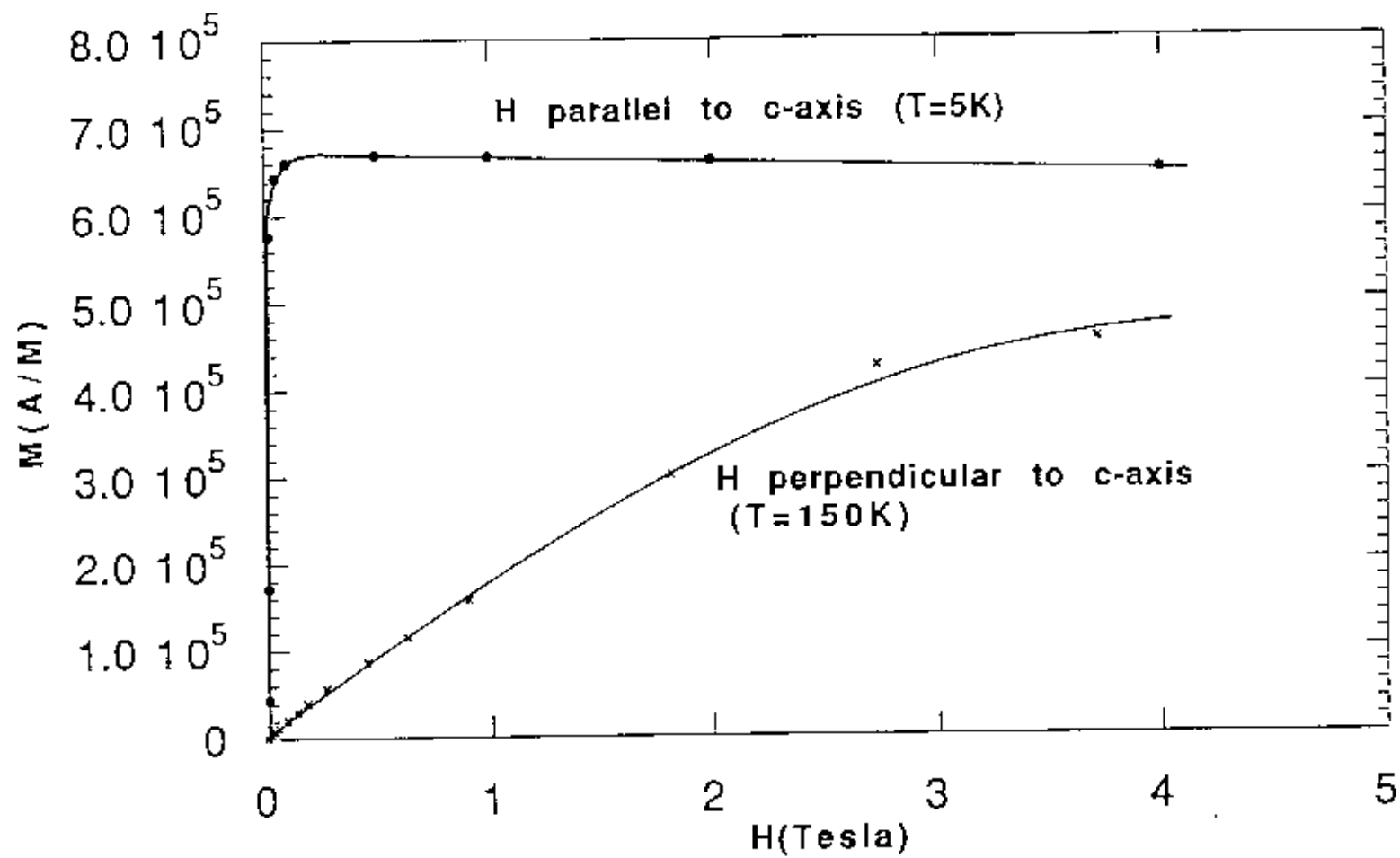


Fig. 5.4 Magnetisation vs field curves of  $\text{Fe}_2\text{P}$

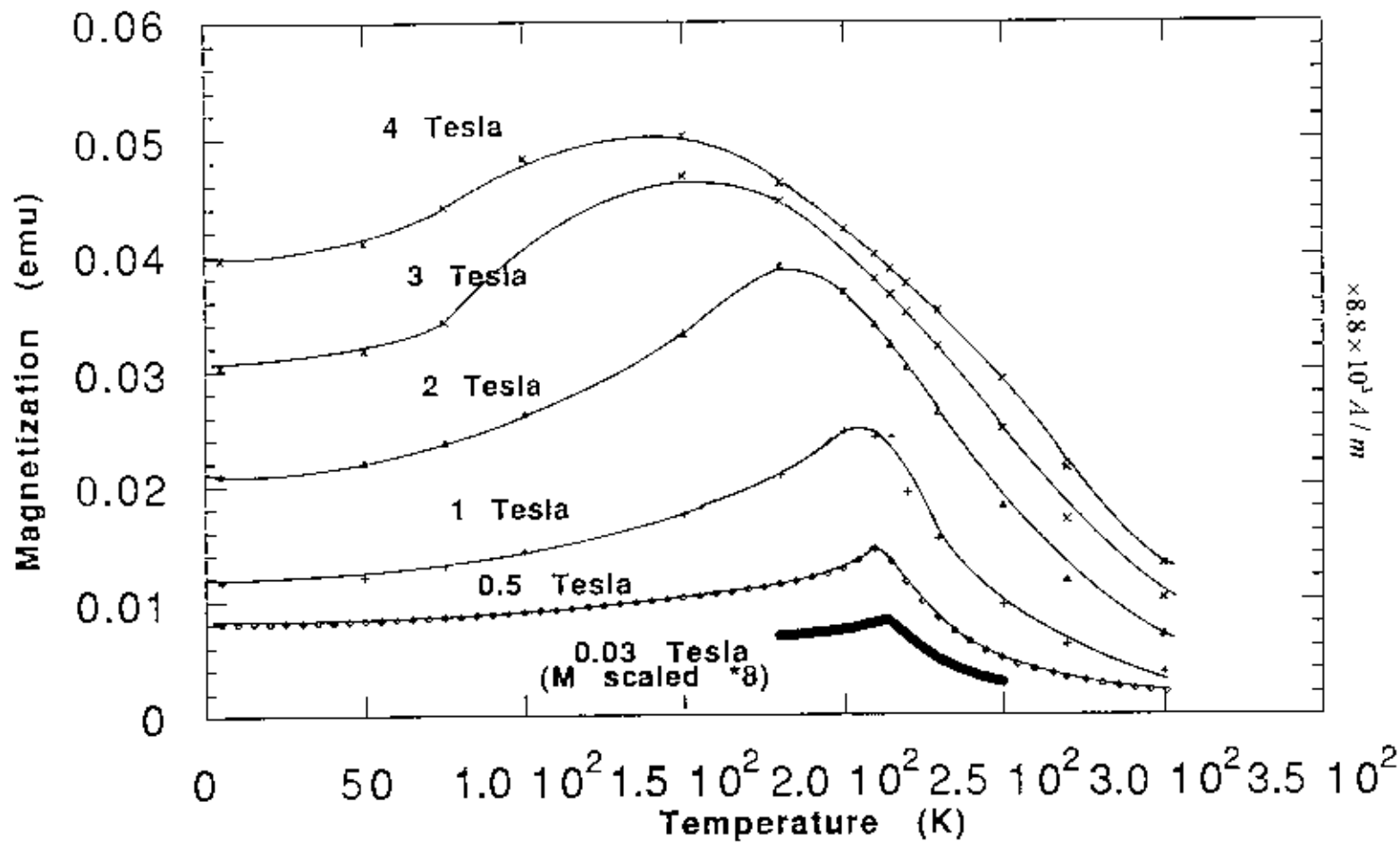


Fig. 5.5 Magnetisation vs temperature curve of  $\text{Fe}_2\text{P}$  at different applied fields

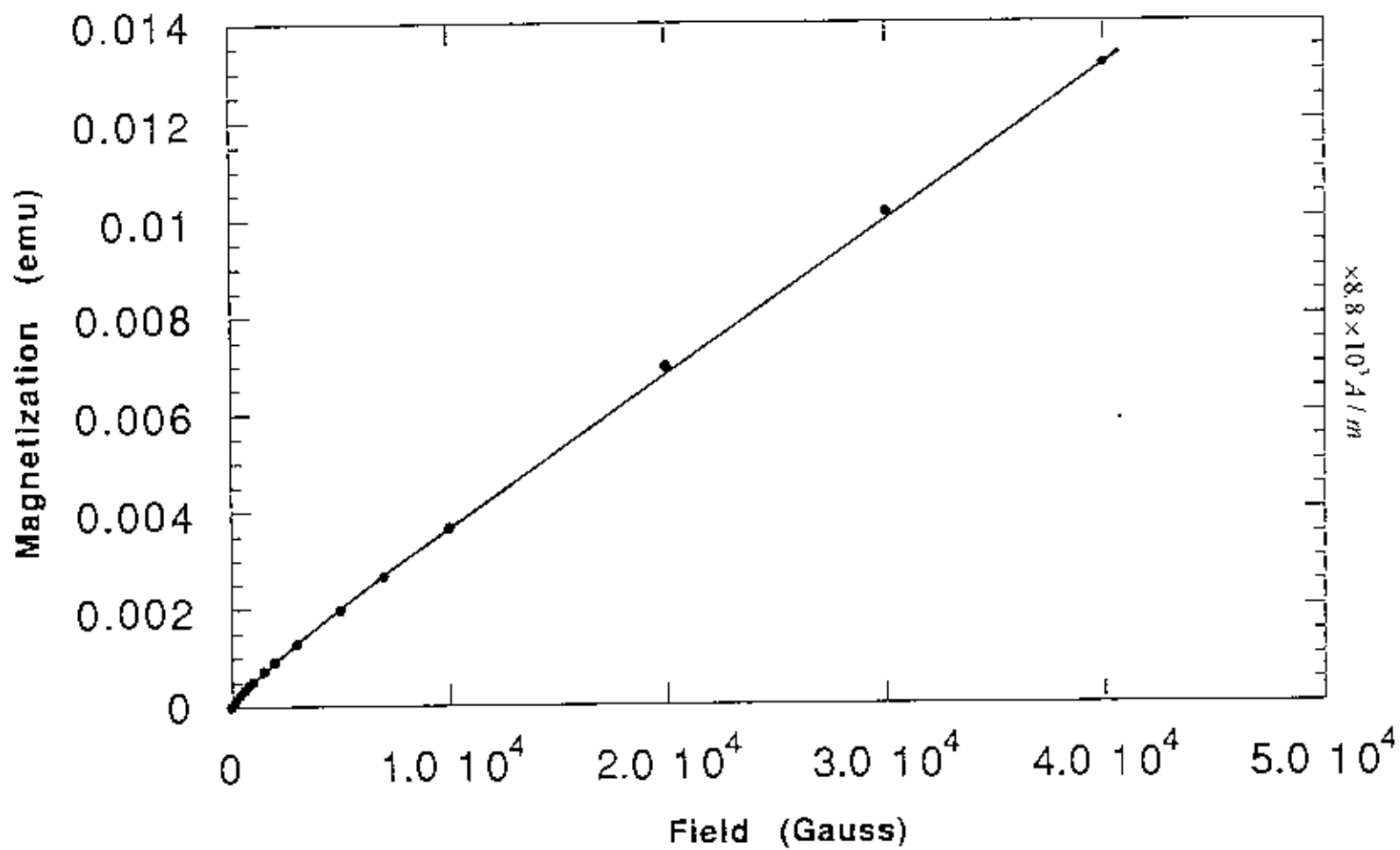


Fig. 5.6 Magnetisation vs field curves of Fe<sub>2</sub>P at 300K

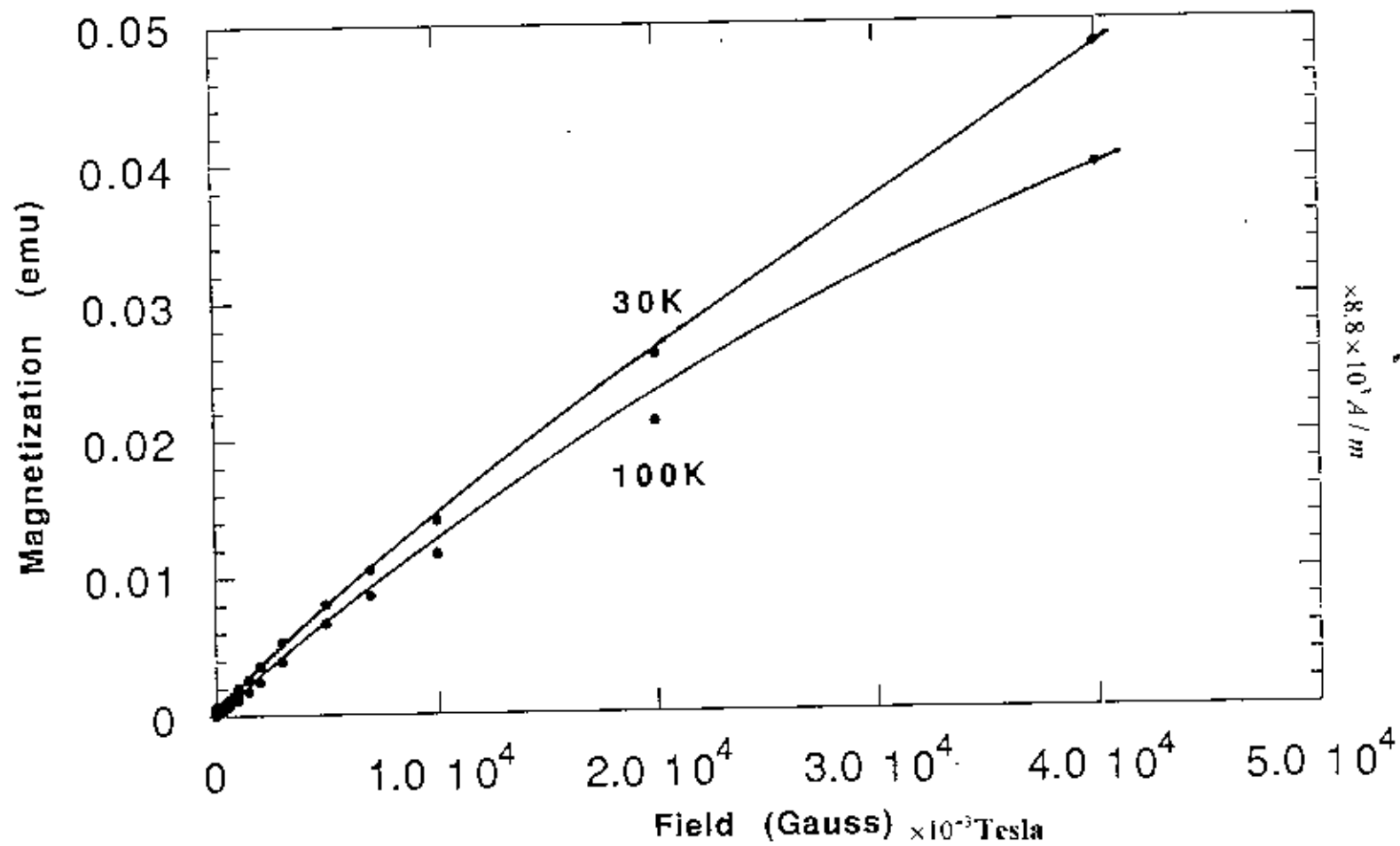


Fig. 5.7 Magnetisation vs field curves of  $\text{Fe}_2\text{P}$

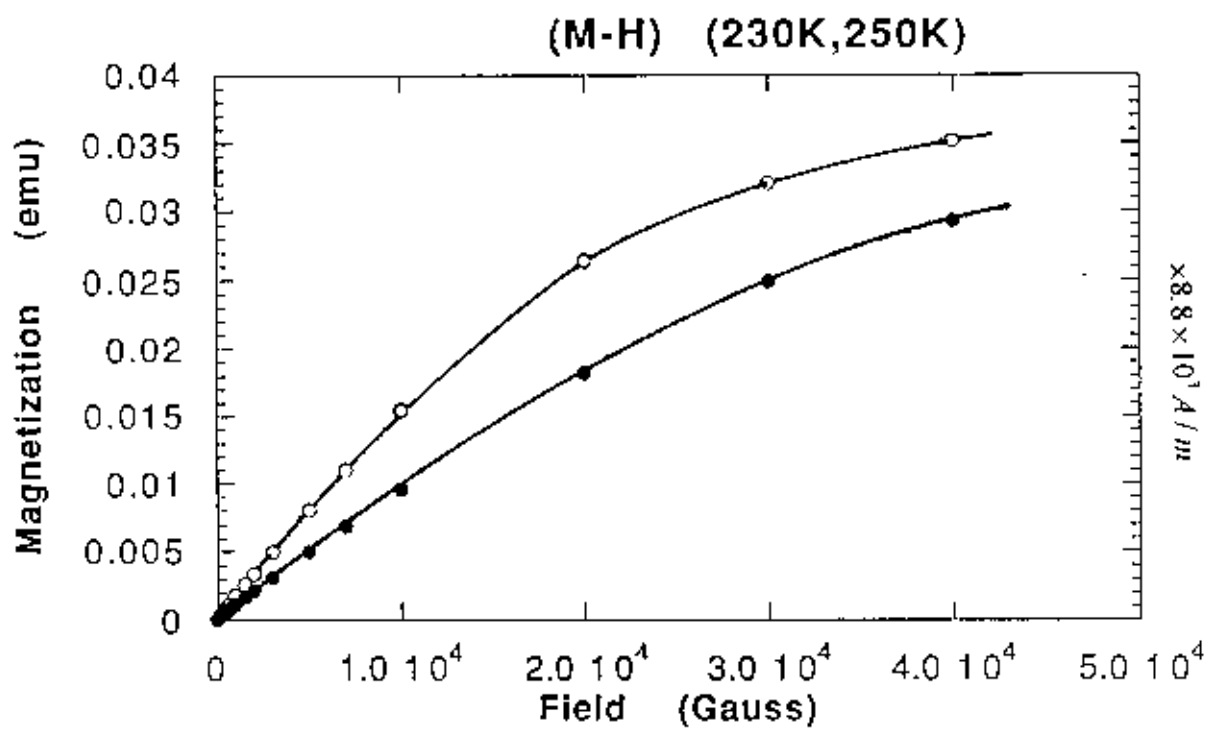


Fig. 5.8 Magnetisation vs field curves of  $Fe_2P$

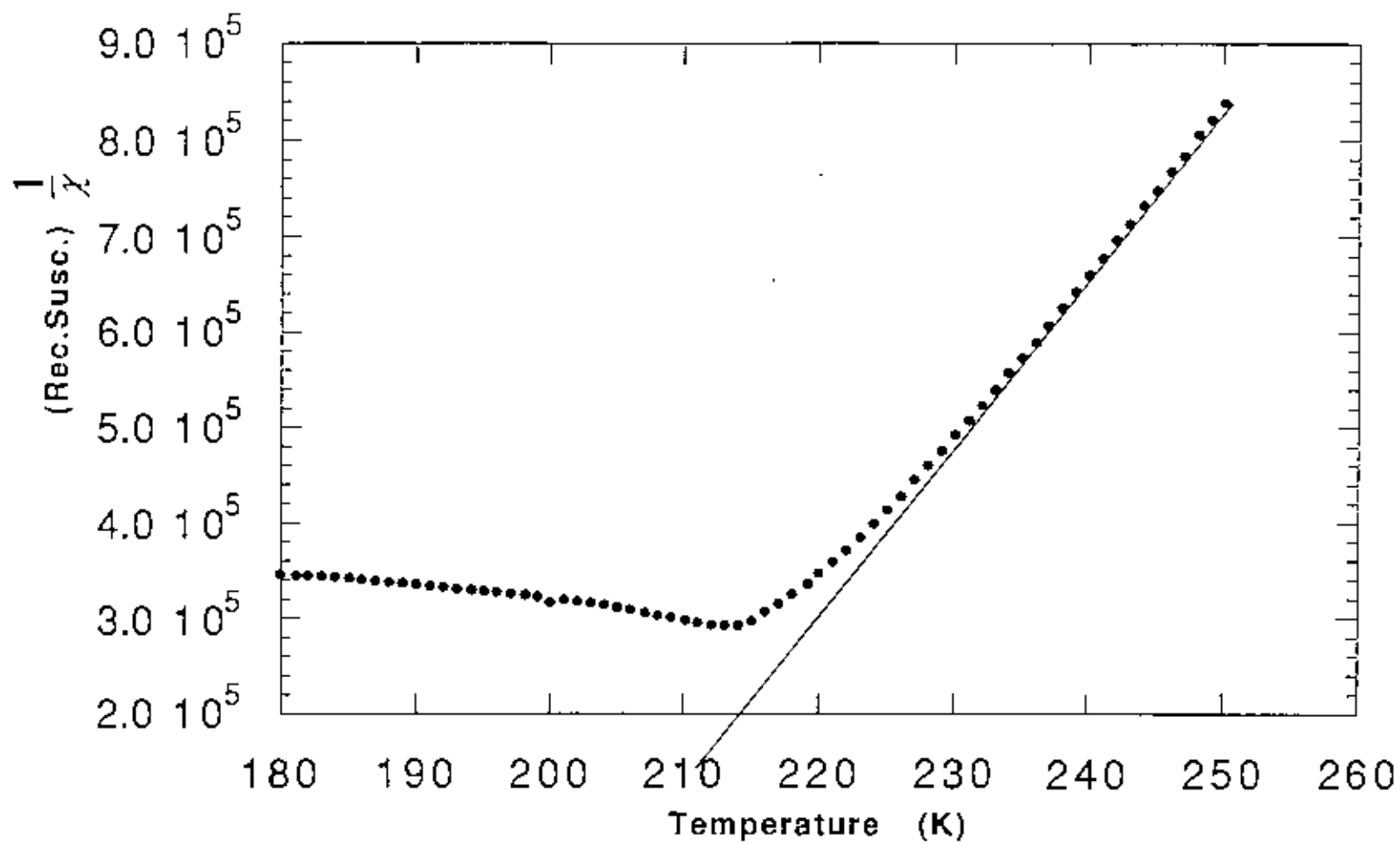


Fig. 5.9 Reciprocal susceptibility vs temperature curve of Fe<sub>2</sub>P

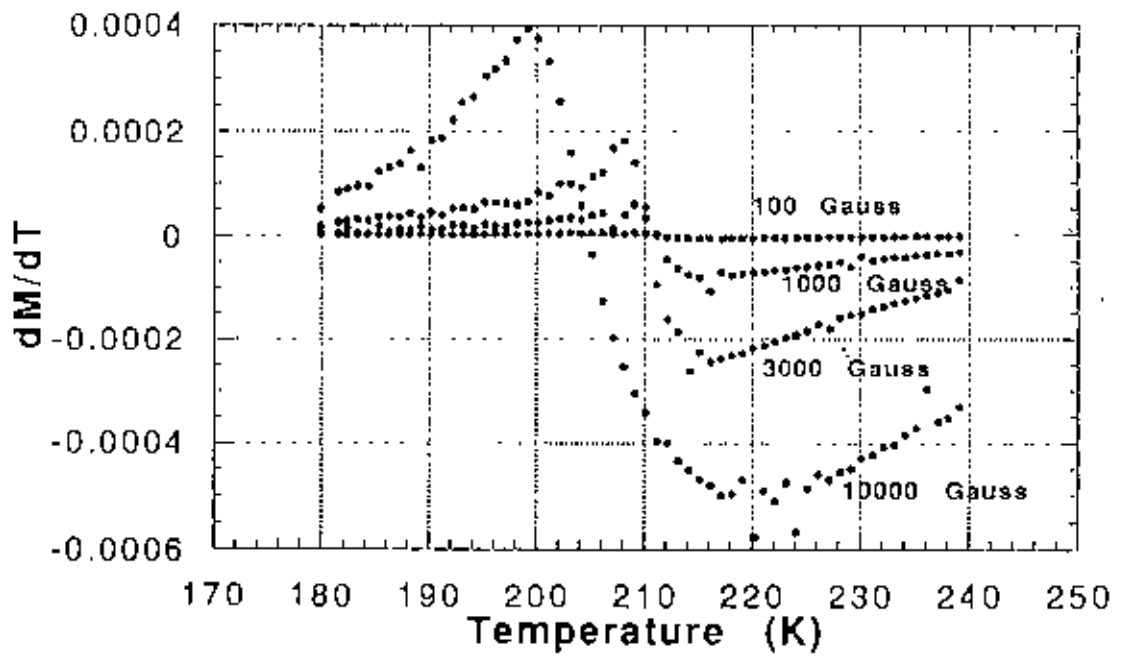


Fig. 5.10 Temperature derivative of magnetisation curves of  $Fe_2P$



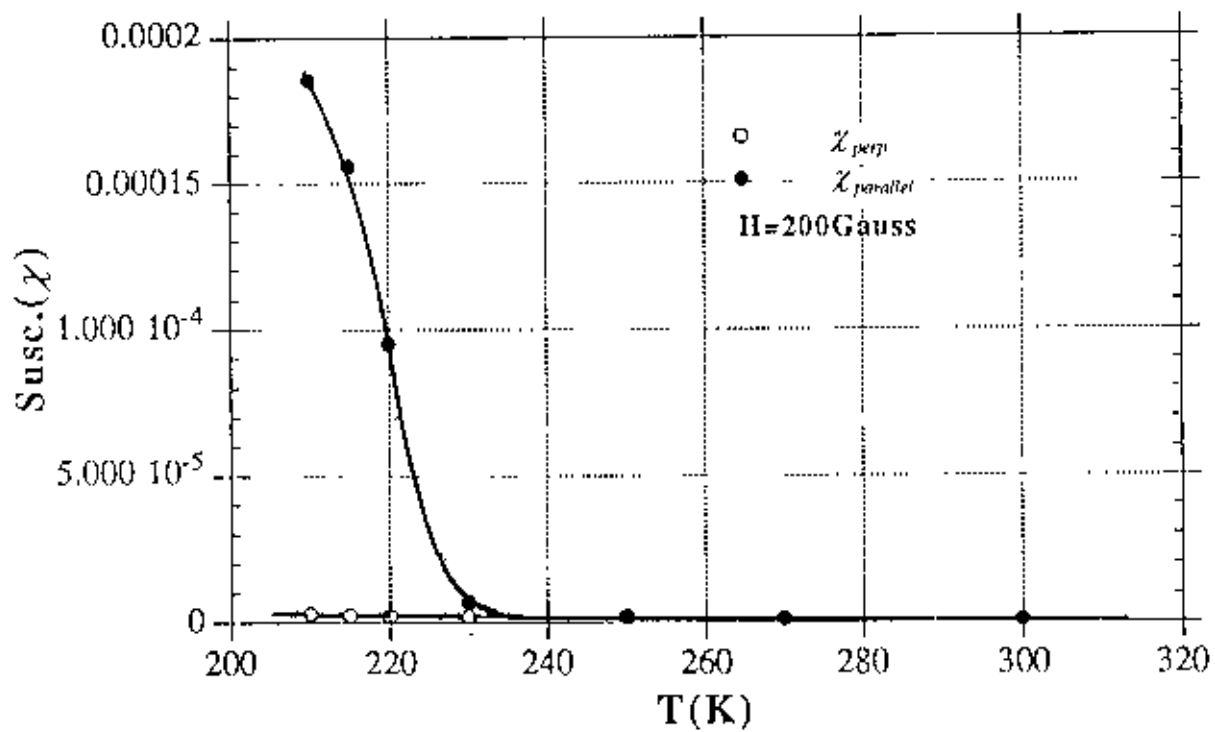


Fig. 5.11 Susceptibility vs temperature curve of  $\text{Fe}_2\text{P}$

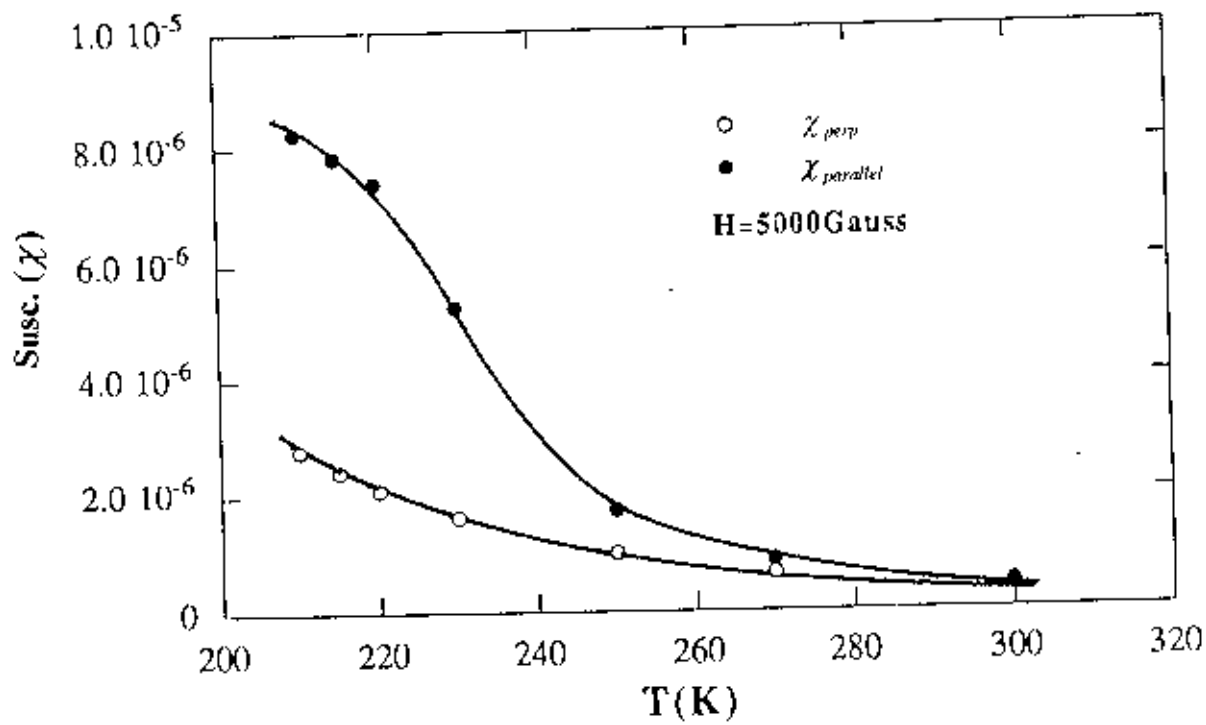


Fig. 5.12 Susceptibility vs temperature curve of Fe<sub>2</sub>P

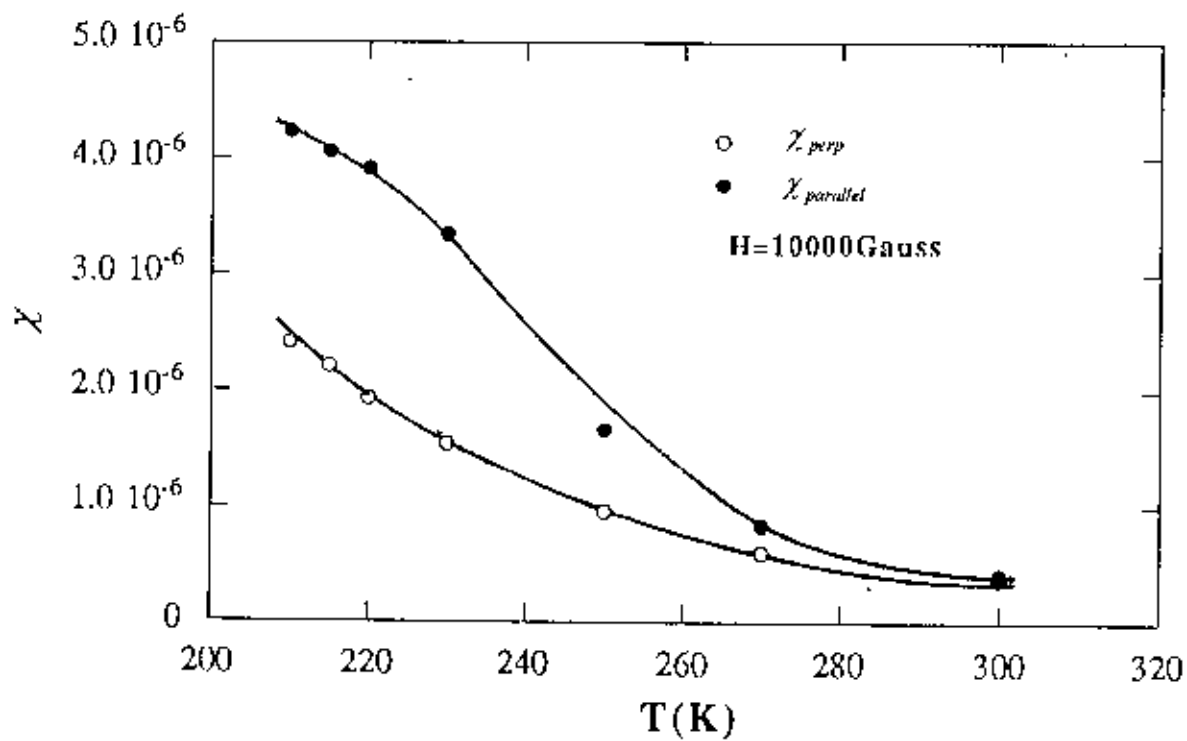


Fig. 5.13 Susceptibility vs temperature curve of  $\text{Fe}_2\text{P}$

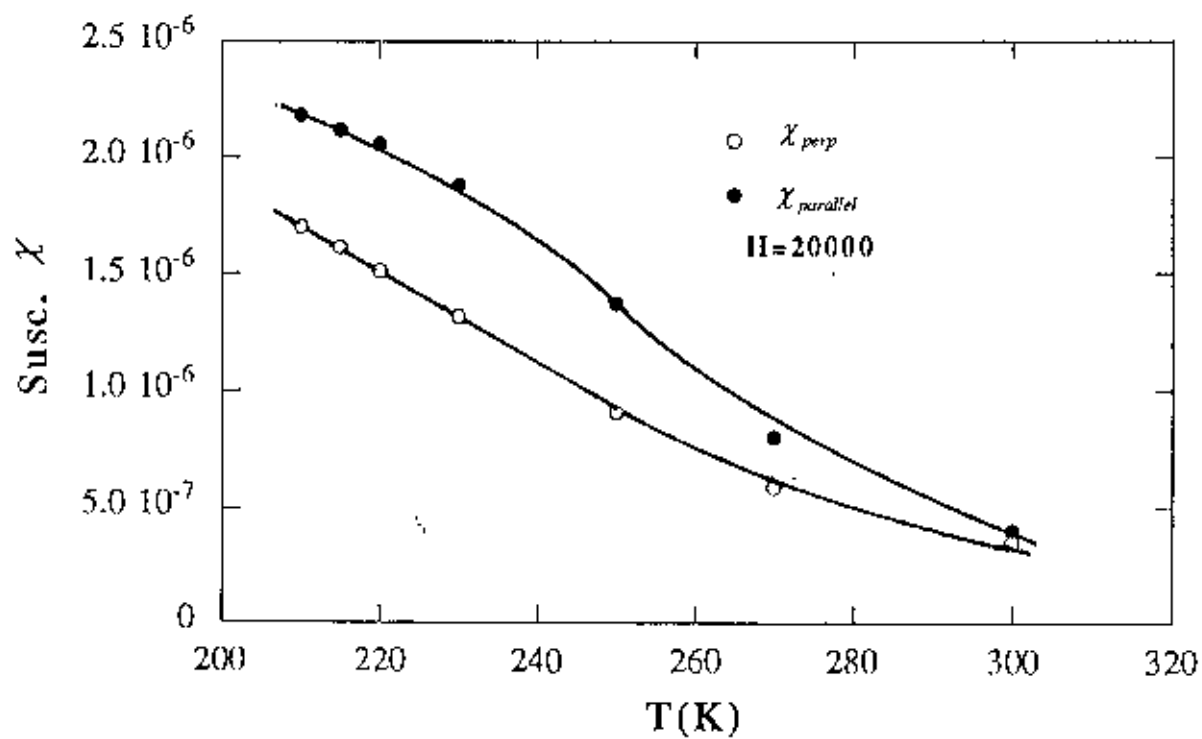
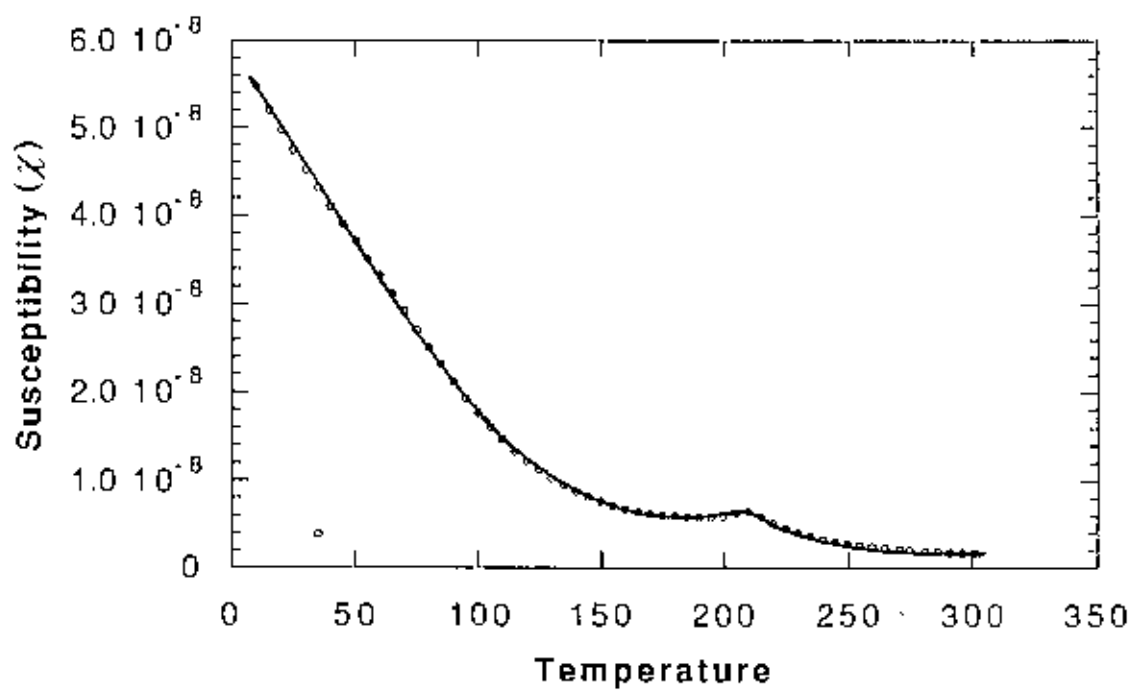


Fig. 5.14 Susceptibility vs Temperature curve of  $Fe_2P$



**Fig. 5.15** Susceptibility vs Temperature curve of  $\text{Fe}_2\text{P}$

(M vs T)

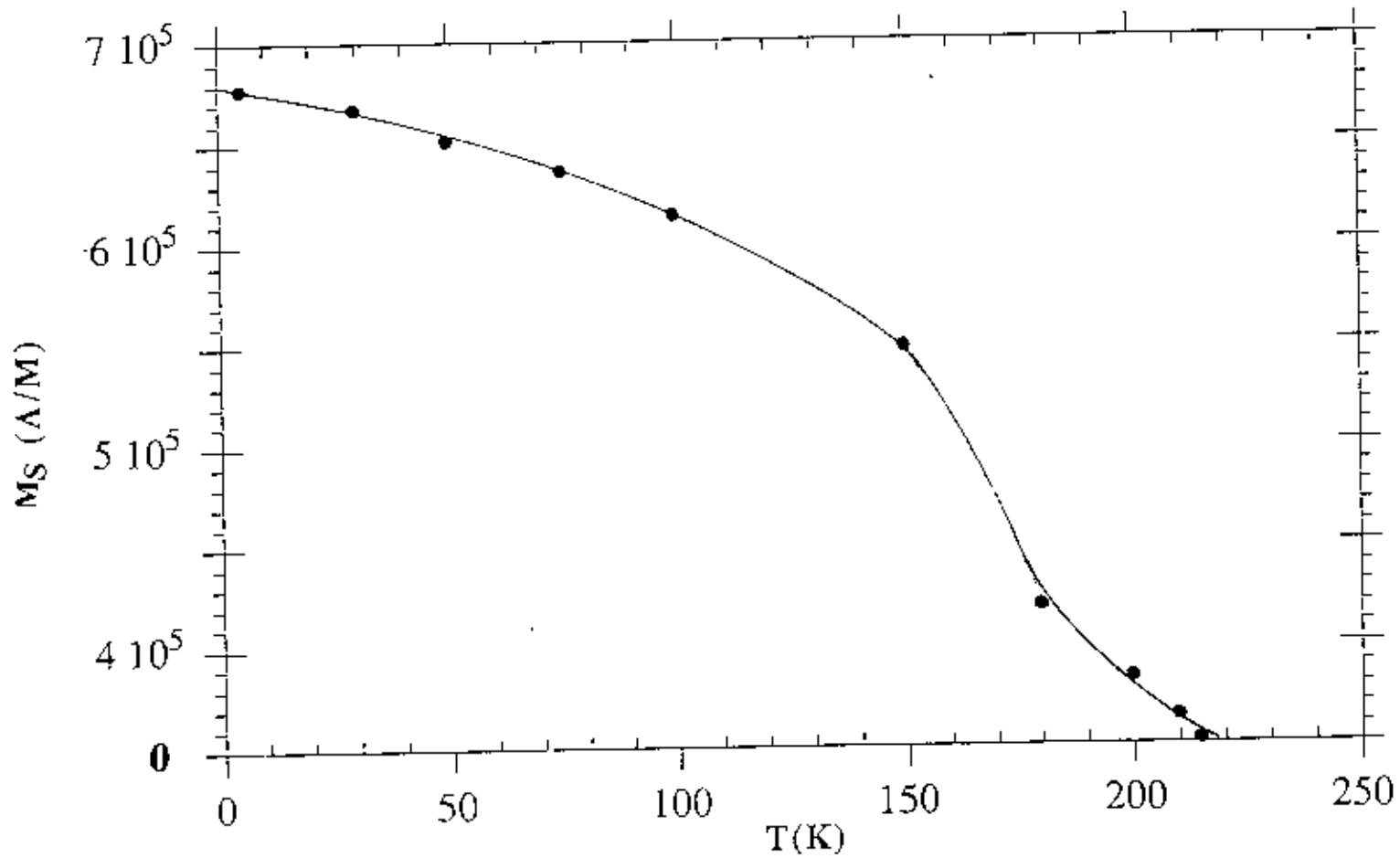


Fig. 5.16 Temperature dependence of saturation magnetization of  $\text{Fe}_2\text{P}$

(M vs T) Field parallel to c-axis

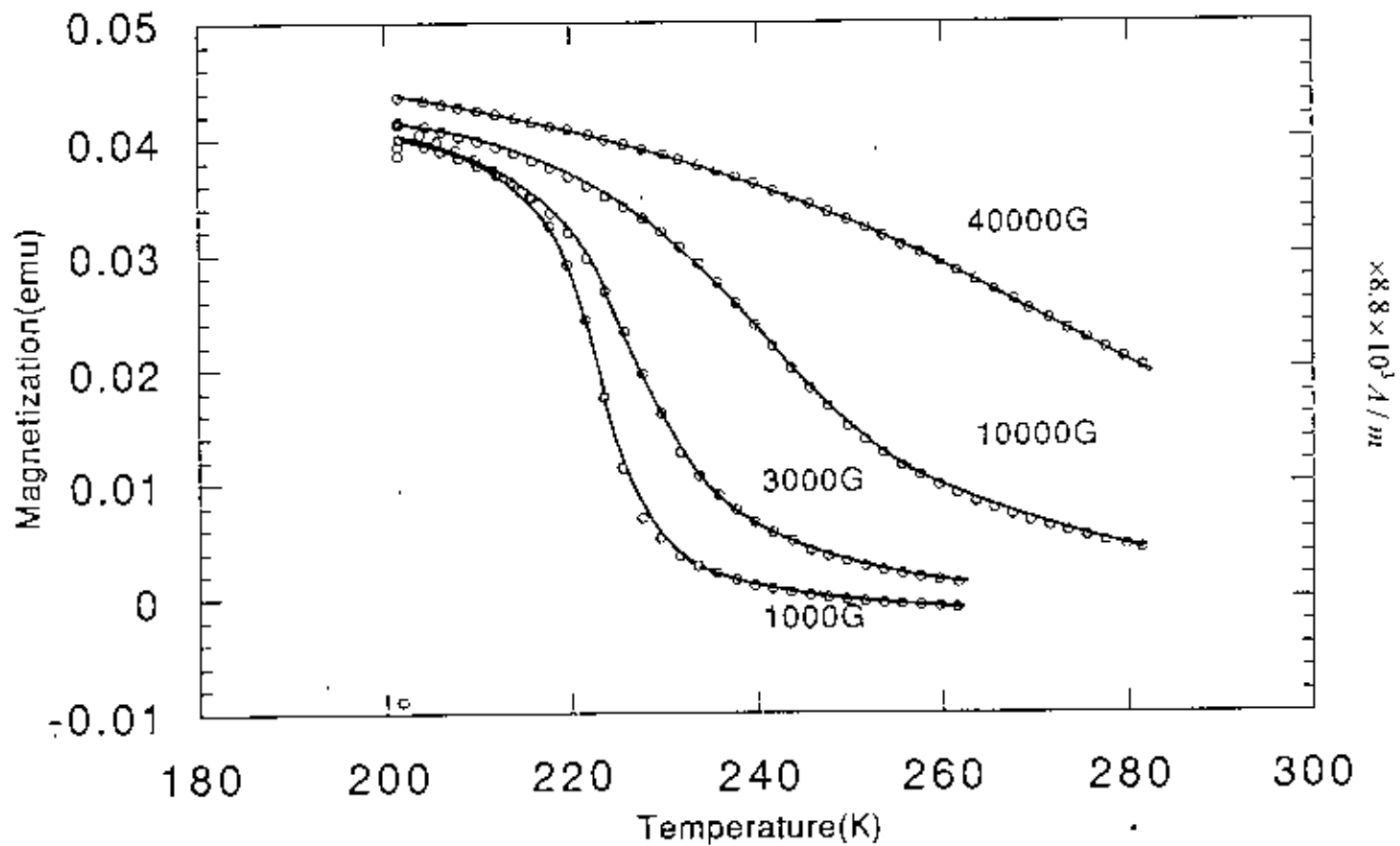
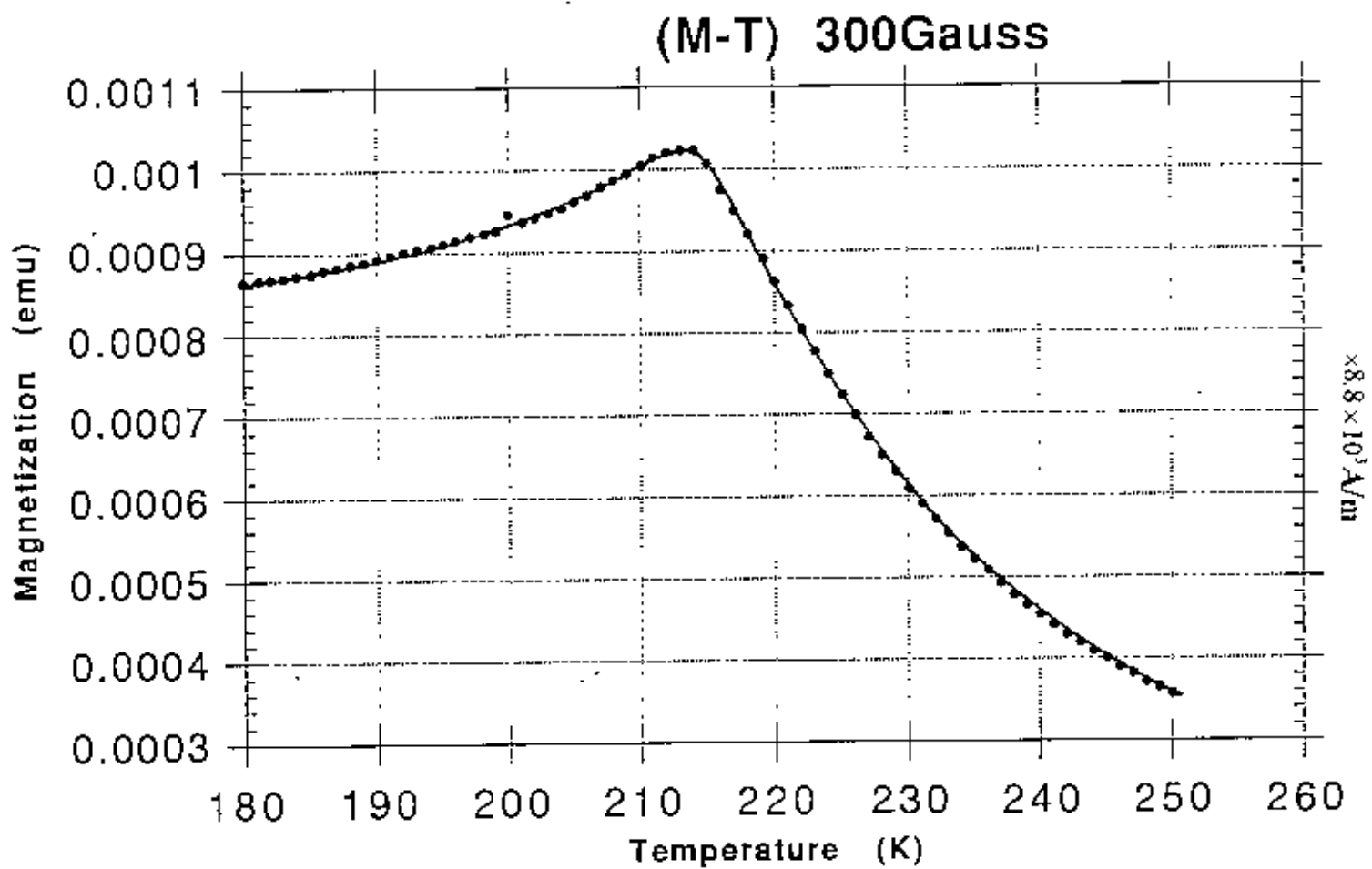


Fig. 5.17 Temperature dependence of magnetization of Fe<sub>2</sub>P



**Fig. 5.18** Temperature dependence of magnetization of  $\text{Fe}_2\text{P}$



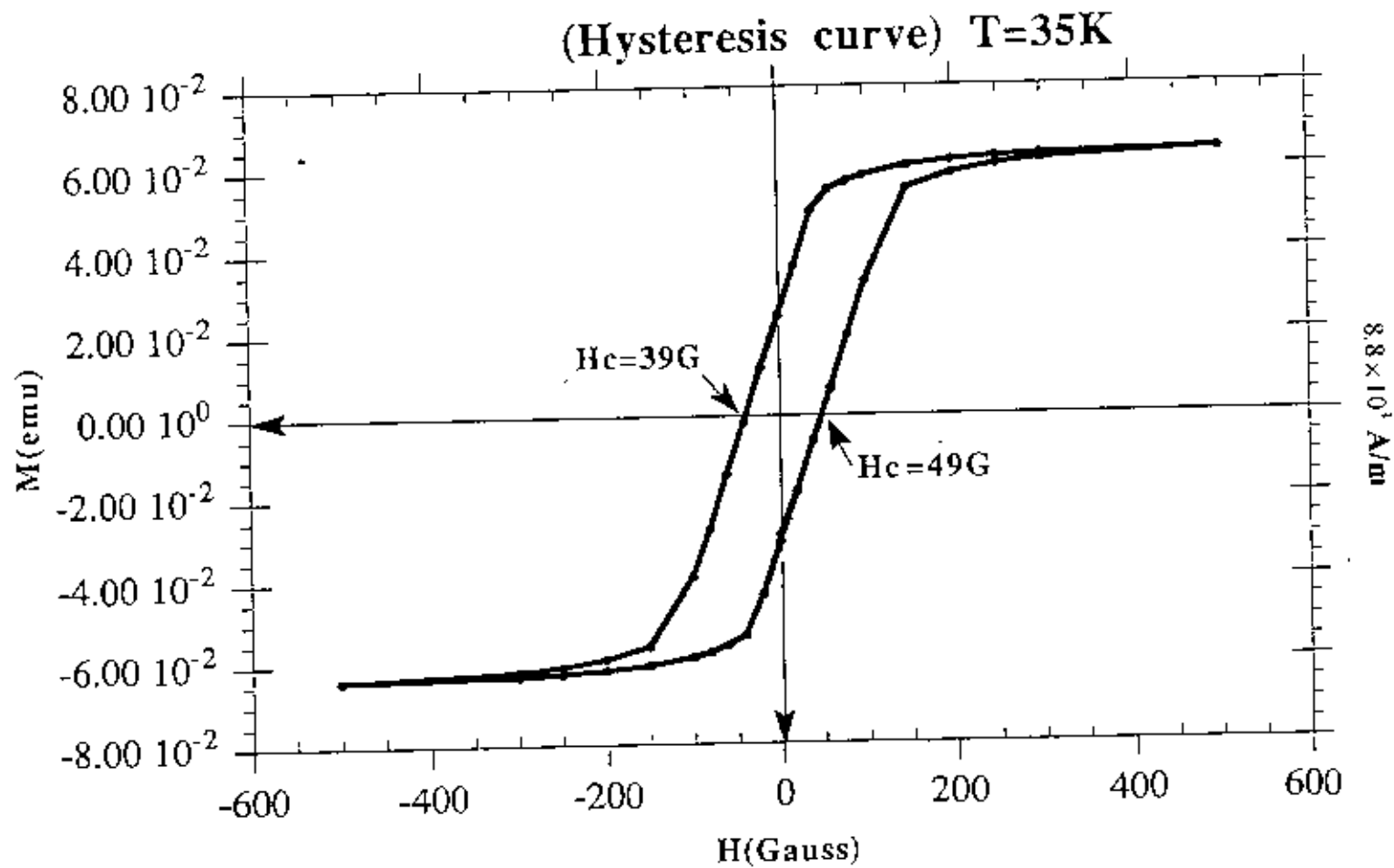


Fig. 5.19 Hysteresis curve of  $Fe_2P$

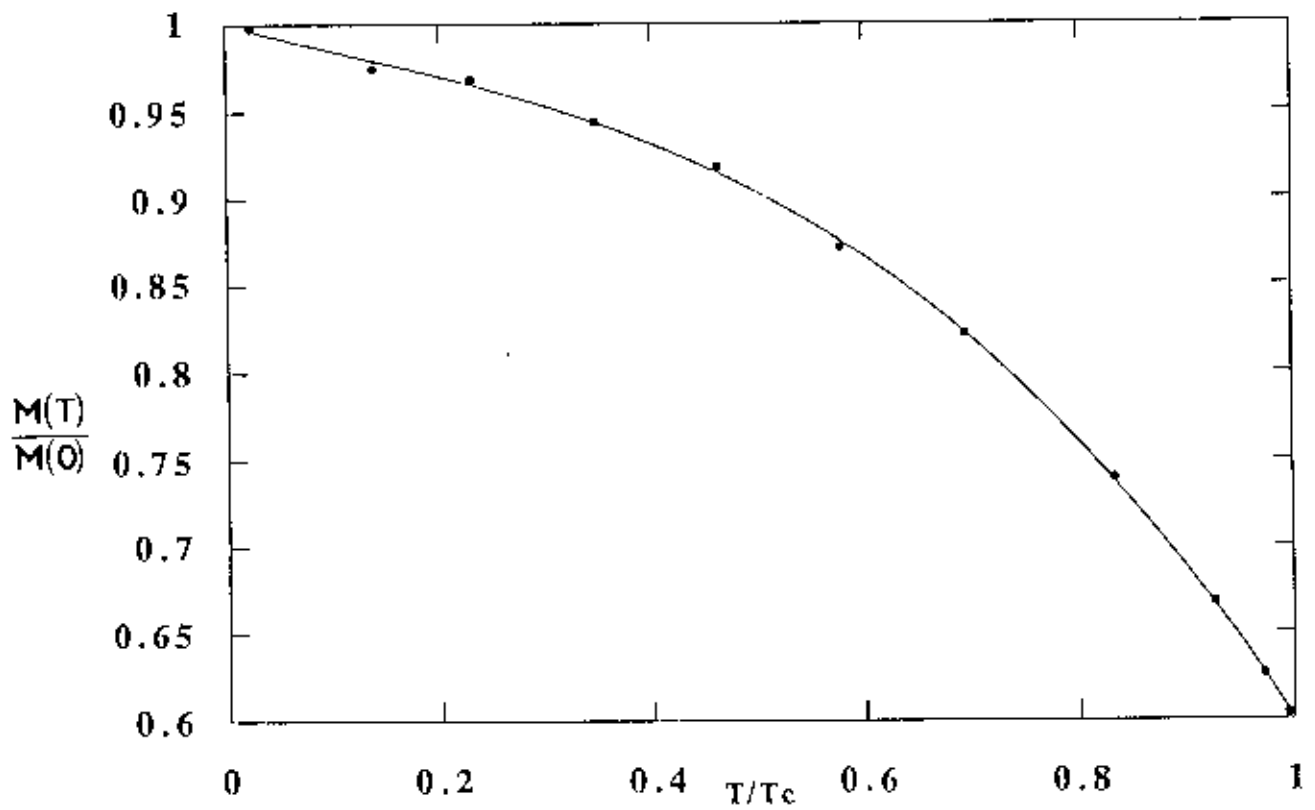


Fig. 5.20 Reduced magnetization versus reduced temperature for  $\text{Fe}_2\text{P}$  single crystal:

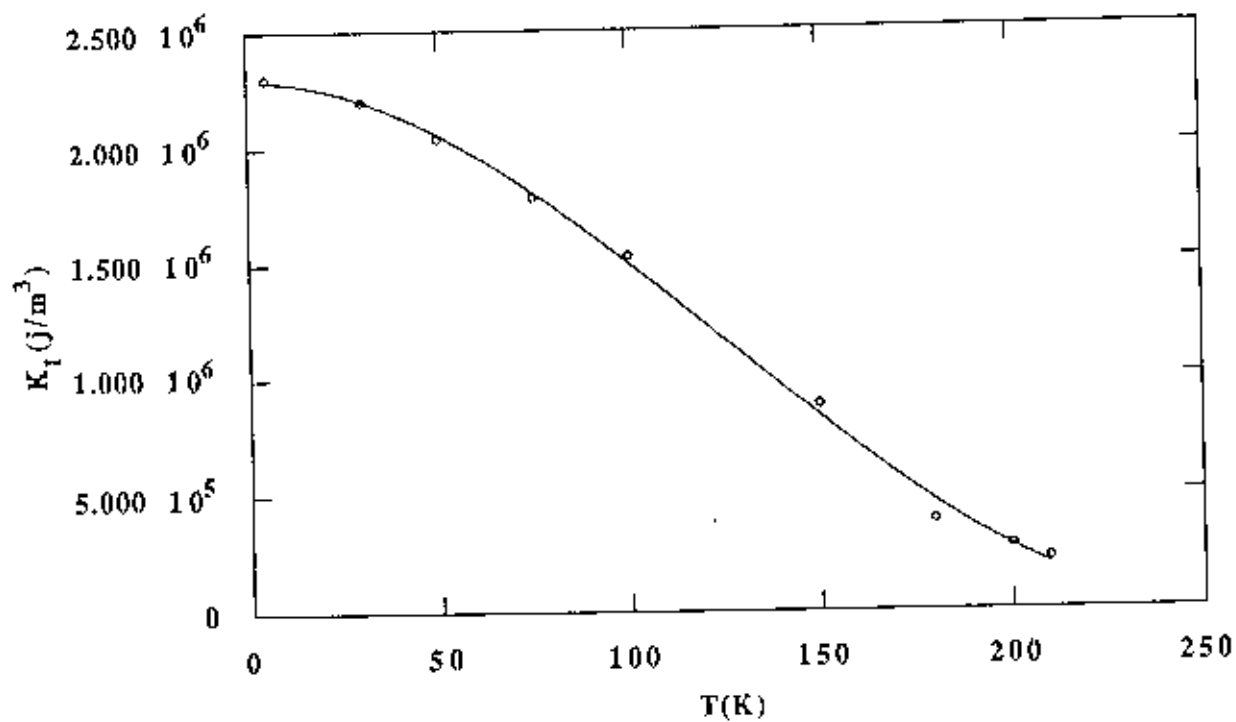


Fig. 5.21 First anisotropy constant of Fe<sub>2</sub>P as function of temperature [ $K_1$  calculated from slope of M vs H curve]

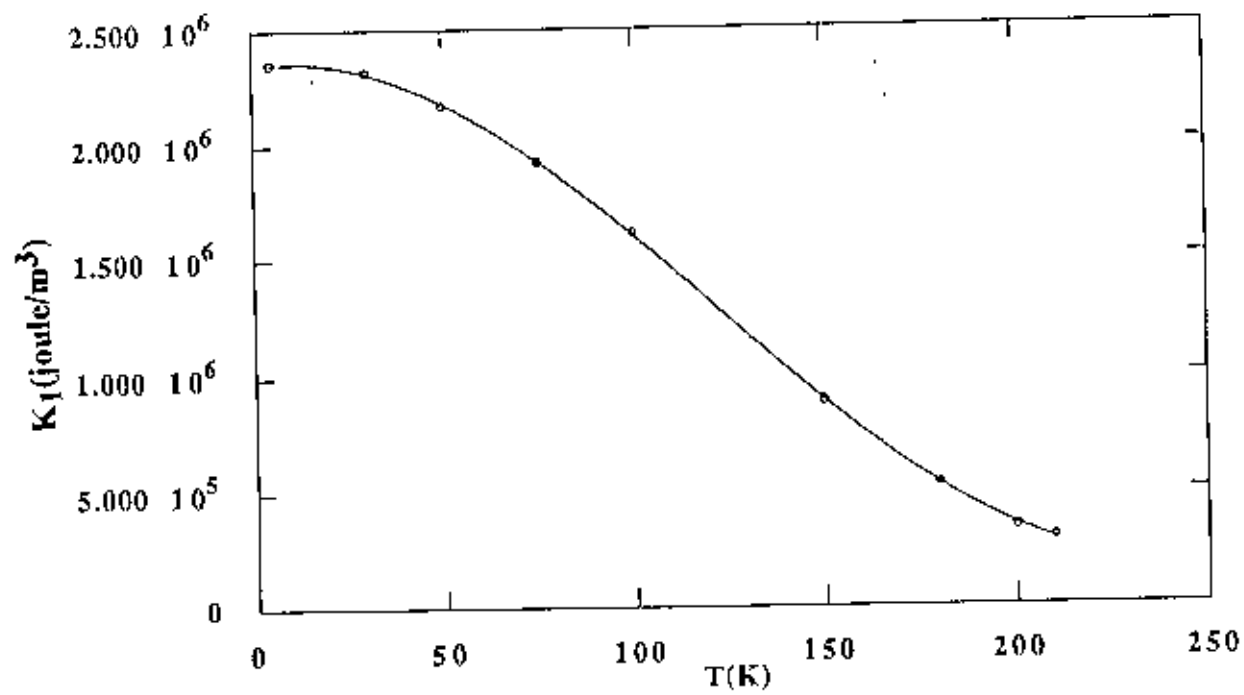


Fig. 5.22 First anisotropy constant of  $\text{Fe}_2\text{P}$  as function of temperature [ $K_1$  calculated from area under  $M$  vs  $H$  curve]

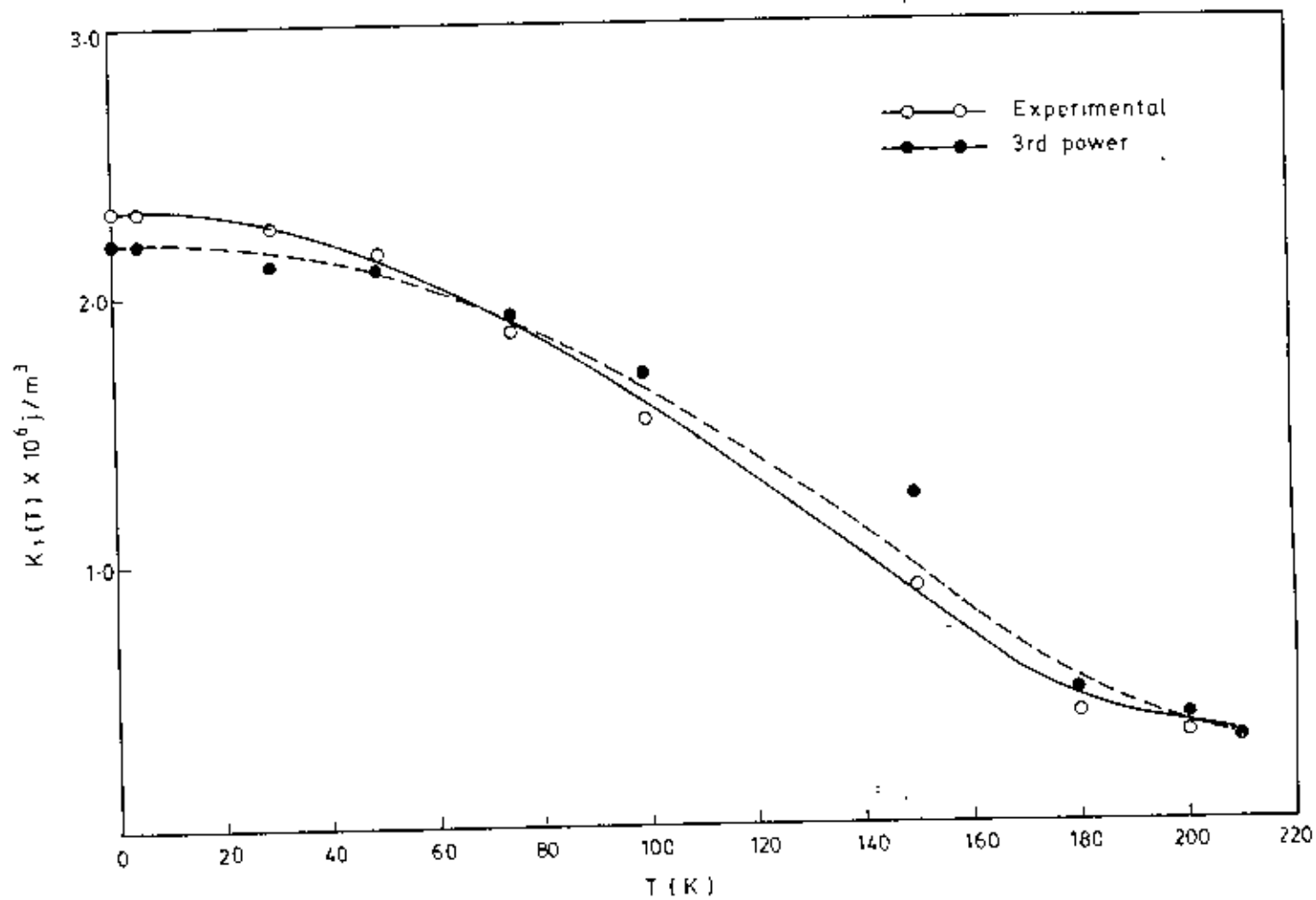


Fig. 5.23 Temperature dependence of the first anisotropy constant  $K_1$  of  $\text{Fe}_2\text{P}$

**Chapter 6**  
**Measurements on Ferrofluid ( $\text{Fe}_3\text{O}_4$ )**

### **6.1 Introduction:**

A magnetic liquid or a ferrofluid contains fine magnetic particles with sizes in the nanometer range, which are suspended in a suitable carrier liquid e.g. hydrocarbon oil. To prevent agglomeration, the particles are coated with long chained organic molecules or polymers to achieve sterical repulsion. The magnetic liquids are used in seals, as lubricating or damping medium. The first stable magnetic liquid was produced in the year 1963. In order to get a stable magnetic liquid of iron oxide, the particle diameters have to be smaller than 10 nm. Magnetic particles with sizes in the 10 nm range are monodomains. When a magnetic field is applied on the particles a complete monodomain particle with coherent magnetization reversal is maintained only for iron particles with diameters smaller than 20 nm [Cullity & Kneller]. The thermal relaxation time in magnetization reversal for monodomain particles was first calculated by Neel in 1949. He pointed out that the magnetization fluctuations for fine magnetic particles undergo a sort of Brownian rotation. At some temperature, the so called blocking temperature  $T_B$ , the relaxation time may be the same as the time scale of the measuring technique. This kind of behaviour leads directly to the concept of superparamagnetism. At temperatures below  $T_B$  the intrinsic magnetization in the particles is thermally blocked, while at temperatures above  $T_B$  the intrinsic magnetization follows superparamagnetism.

## 6.2 Review of previous works :

Brown(1963) and Aharoni(1969) calculated the dependence of superparamagnetic relaxation time on the magnetic field. They considered the case when the applied field was parallel to the easy axis of the particles. Both Brown and Aharoni found that the relaxation time decreases with increasing magnetic field, which yields a decrease in  $T_B$ . Later calculations confirmed their results, and showed that in low fields  $T_B$  is practically independent of the angle between the field and the easy axis of the particle. Shtrikman and Wohlfarth also Chantrell and Wohlfarth considered the interactions between the particles in the superparamagnetic relaxation models. They found that when the magnetic interparticle interactions are considered, the superparamagnetic relaxation time increases and so does  $T_B$ . The cusp in the zero field cooled magnetization represents the blocking temperature. When there is a particle size distribution, the cusp in the zero field cooled magnetization is shifted towards the high temperature[Gittleman et al.]. By using the *Mössbauer* technique  $T_B$  can also be identified. The experiments confirm the calculated field and concentration dependence of  $T_B$ . The concentration dependence of  $T_B$ , which is determined experimentally is well described by a power law.

In the superparamagnetic regime the magnetisation of an ensemble of fine magnetic particles can be expressed by the Langevin function. The initial magnetic susceptibility for superparamagnetic non-interacting particles, can be described by a Curie law. As in the case of superparamagnetic relaxation time, the magnetic interparticle interactions will also influence the initial susceptibility. It has been theoretically and experimentally found that the initial susceptibility can be expressed by a Curie-Weiss law. The Curie-Weiss temperature which reflects the interactions between the particles is defined as the intercept at the temperature axis of the extrapolated linear portion of the reciprocal



susceptibility versus temperature plot. The Curie-Weiss temperature has been experimentally determined to be both positive and negative for magnetic liquids. The positive Curie-Weiss temperatures were obtained from measurements above the melting point of the magnetic liquid where the particles are mobile, and yield the negative temperatures below the melting point.

The magnetization in high fields of a magnetic liquid containing fine magnetic particles should saturate according to the Langevin expression. The non-saturated magnetization is mainly due to the intrinsic spin structure in the particles. The ions in the carrier liquid are responsible for some part of the magnetization increase in high fields. From *Mossbauer* experiments it has been concluded that the ferrimagnetic oxide particles for instance  $\gamma\text{-Fe}_2\text{O}_3$  have got its magnetic moments neither parallel nor anti-parallel within such small particles. The non-collinear magnetic moment structure has been explained as a surface effect.  $\text{Fe}_3\text{O}_4$  does not have such spin structure. In magnetic measurements this phenomenon can be seen as a linear magnetization increase with the increasing field. The differential high field susceptibility is defined as the slope of the linear portion of the magnetization versus field curve in high fields.

### 6.3 Magnetism of ferrofluid:

The magnetic liquids studied in this work contain ferrimagnetic fine particles of  $Fe_3O_4$ . When the magnetization in the particle changes direction two rotational processes may occur, the coherent process and the curling process. In the coherent process all the spins are parallel during the whole reversal of the magnetization. In the curling process the rotation of the magnetization is incoherent. In this process the angles between the spins change gradually. It has been revealed through calculations that the particles with diameter smaller than about 20 nm will reverse their spins by the coherent process, and the larger particles will reverse their spin by curling process. The particles in the magnetic liquids have diameters of the order of 10 nm or below, therefore the magnetization reversal is considered to occur by the coherent process.

### 6.4 Static magnetization of ferrofluid:

#### **The Langevin function**

Neglecting the magnetic anisotropy the energy of a fine magnetic particle with volume  $V$  in a magnetic field  $\mathbf{B}$ , can be written as :

$$E = -\mathbf{m} \cdot \mathbf{B} = -M_s V B \cos \alpha \quad \dots\dots\dots(6.1)$$

where  $\mathbf{m}$  is the magnetic moment of the particle,  $M_s$  is the intrinsic magnetization and  $\alpha$  the angle between the field and the magnetic moment. When non interacting monodisperse single domain particles have attained thermodynamic equilibrium, the magnetization  $M$ , of the particle ensemble, in the direction of the field is given by

$$M = nM_s V \frac{\int_0^\pi \cos \alpha \exp\left(\frac{E}{kT}\right) d\alpha}{\int_0^\pi \exp\left(\frac{E}{kT}\right) d\alpha} \quad \dots\dots\dots (6.2)$$

$$= nM_s V \frac{\int_0^\pi \cos \alpha \exp\left(\frac{M_s V B \cos \alpha}{kT}\right) d\alpha}{\int_0^\pi \exp\left(\frac{M_s V B \cos \alpha}{kT}\right) d\alpha} \quad \dots\dots\dots (6.3)$$

putting  $x = \frac{M_s V B}{kT}$  yields

$$M = nM_s V \left\{ \coth(x) - \frac{1}{x} \right\} = M_0 L(x) \quad \dots\dots\dots (6.4)$$

Here  $n$  is the number of particles per unit volume,  $M_0$  the saturation magnetization given by  $nM_s V$ ,  $k$  the Boltzmann constant,  $T$  the temperature and  $L(x)$  is the Langevin function.

The magnetization of the ensemble of single domain particles is identical to that of paramagnetic substances except for the fact that magnetic saturation for single domain particles may be attained even in low magnetic fields and high temperatures. The particle ensemble can then be represented as a paramagnetic gas with giant magnetic moments

In low fields or high temperatures when  $\frac{M_s V B}{kT} \ll 1$  equation (6.4) changes into

$$M = nM_s V \frac{x}{3} = \frac{nM_s^2 V^2 B}{3kT} \quad \dots\dots\dots (6.5)$$

The initial magnetic susceptibility,  $\chi_i$ , is defined as

$$\chi_i = \mu_0 \lim_{B \rightarrow 0} \frac{dM}{dB} = \mu_0 \frac{nM_s^2 V^2}{3kT} = \frac{C}{T} \quad \dots\dots\dots (6.6)$$

where  $\mu_0$  is the permeability of vacuum and  $C$  is the Curie constant

In the case of high fields or low temperatures when  $\frac{M_s VB}{kT} \gg 1$ , equation (6.4)

changes to

$$M = nM_s V \left\{ 1 - \frac{1}{x} \right\} = nM_s V \left\{ 1 - \frac{kT}{M_s VB} \right\} \dots\dots\dots(6.7)$$

### 6.5 The effect of particle size distribution on the magnetization:

In a real ensemble of fine magnetic particles there is always to some degree a particle size distribution. According to the ideas of Chantrell et.al. if the particle size distribution is known to be  $f(V)$ , then the magnetization can be obtained by integrating the Langevin function weighted by  $f(V)$  :

$$M = nM_s \int_{V_{\min}}^{V_{\max}} f(V) VL \left( \frac{M_s VB}{kT} \right) dV \dots\dots\dots(6.8)$$

where  $V_{\min}$  and  $V_{\max}$  are the minimum and maximum particle volume in the ensemble. The particle size usually follows a log-normal distribution. Taking the particle size distribution into consideration gives higher values of the calculated magnetization in low and intermediate fields.

### 6.6 The effect of magnetic anisotropy on magnetization:

Magnetic anisotropy means that the magnetization depends on the direction in which it is measured. At very low temperatures the magnetization of a fine magnetic particle is oriented in the easy axis. The anisotropy energy is the energy required to turn the magnetization out from the easy direction. For a particle with uniaxial anisotropy, the anisotropy energy can be written as

$$E = KV \sin^2 \beta \quad \dots\dots\dots(6.9)$$

where  $\beta$  is the angle between the direction of magnetization and the easy axis, and  $K$  is the anisotropy constant.

A fine magnetic particle may have anisotropy of different origins:

#### **Magnetocrystalline anisotropy -**

The magnetocrystalline anisotropy is originated from the spin-orbit coupling. Thus the energy required to overcome this coupling is magnetocrystalline anisotropy energy.

#### **Shape anisotropy:**

When a magnetic field is applied to a magnetic material, there is a demagnetising field opposite to the direction of magnetization, this happens due to the free magnetic poles at the particle surface. For a non-spherical particle the demagnetising field depends on the direction of magnetization giving a direction dependent magnetostatic energy which is the origin of shape anisotropy.

### Surface anisotropy:

The surface anisotropy is due to the low symmetry of the surface atoms compared to the bulk of the crystal. The surface anisotropy is large for small particles as the area to volume ratio is large.

### Anisotropy due to mechanical stress:

When a particle is subjected to mechanical stress, the magnetic anisotropy can be introduced into the particle. This is due to the magnetostriction effect.

In the derivation of the Langevin relation the magnetic anisotropy has been neglected. Thus taking the magnetic anisotropy into account we can calculate the total magnetization according to the expression

$$E = -M_s V B \cos \alpha + KV \sin^2 \beta \quad \dots \dots \dots (6.10)$$

The corresponding integration is then carried out essentially over  $\alpha$  and  $\beta$  for a fixed direction of the easy axis of the particle. The final magnetization is then obtained by integrating over a specific orientation distribution of the easy axis direction relative to the applied field.

In high magnetic fields the magnetic dipole energy is much larger than the magnetic anisotropy energy. Therefore, the magnetization including the anisotropy energy coincides with Langevin function.

### 6.7 Magnetic dipole-dipole interaction:

The most important inter-particle interaction which influences the magnetic properties of an ensemble of fine magnetic particles is the dipole-dipole interaction. The interaction strength is large and is almost independent of the distance. Between the two magnetic dipoles with magnetic moments  $m_i$  and  $m_j$ , the interaction energy  $E_{int}$  is given by the relation

$$E_{int} = \frac{\mu_0}{4\pi} \left\{ \frac{m_i \cdot m_j}{r_{ij}^3} - \frac{3(m_i \cdot r_{ij})(m_j \cdot r_{ij})}{r_{ij}^5} \right\} \dots \dots \dots (6.11)$$

where  $r_{ij}$  is the vector from dipole  $i$  and dipole  $j$ . The relation (6.11) holds good for more or less spherical particles. Thus the magnetic moment of each particle is equal to  $M_s V$  and  $r_{ij}$  is the vector joining the centre of two particles. The interaction energy varies in a complex manner due to its distance and orientation dependence. It can be both attractive and repulsive depending on the relative orientation of the magnetic moments.

The magnetization of an ensemble of fine magnetic particles depends on the magnetic dipole-dipole interaction between the particles. The interaction effect is most pronounced at low magnetic field and decreases as the field is increased. The interaction effect vanishes at high magnetic field. The initial magnetic susceptibility for a system of interacting particles can be described by the Curie-Weiss law given by

$$\chi_i = \frac{C}{T - \theta} \dots \dots \dots (6.12)$$

where  $\theta$  is an interaction parameter which depends on the particle concentration and particle volume.  $\theta$  is usually called as the Curie-Weiss temperature. This relation holds good for  $T \gg \theta$ .

### 6.8 The superparamagnetic relaxation:

The energy of a particle with uniaxial anisotropy has two energy minima separated by an energy barrier  $E_B$ . The intrinsic magnetization of a particle can be reversed either thermally over the barrier or by quantum tunnelling. Thermal activation of the magnetization over the energy barrier is known as the Neel relaxation process. At temperatures when the viscosity of the carrier liquid is low and the particles are free to rotate, both Neel and the Brownian relaxation process may be present. The Brownian relaxation process is the rotation of the particle magnetic moment and the particle as a whole. Shliomis concluded that iron particles larger than about 8.5 nm will relax by the Brownian process.

### 6.9 The Neel relaxation of interacting and non-interacting particles:

There are several models to include the magnetic interparticle interaction in the calculation of the superparamagnetic relaxation time. When the interaction field at a magnetic particle is considered to be unidirectional, the relaxation time is found to resemble a Vogel-Fulcher type law according to Shtrikman and Wohlfarth,

$$\tau = \tau_0 \exp\left(\frac{KV}{k(T - T_0)}\right) \dots\dots\dots(6.13)$$

where  $T_0$  is a measure of the interaction strength. The above relation is only valid in the weak interaction regime,  $T_0 \ll \frac{KV}{k}$  and  $T \gg T_0$ . While in the strong interaction



regime,  $T_0 \gg \frac{KV}{k}$  the anisotropy constant and the particle volume are replaced by temperature dependent effective values

For a non-interacting particle system let us consider a particle with the magnetic energy given by equation (6.10). In zero magnetic field there are two equal minima separated by a maximum. The magnetization reversal takes place over the energy barrier  $E_B = KV$  between the magnetic states  $\beta = 0$  and  $\beta = \pi$ . Then the relaxation time,  $\tau$  for magnetization reversal can be expressed by the Neel relation,

$$\tau = \tau_0 \exp\left(\frac{E_B}{kT}\right) = \tau_0 \exp\left(\frac{KV}{kT}\right) \quad \dots\dots\dots (6.14)$$

where  $\tau_0$  is the characteristic relaxation time of the order of  $10^{-10}$  sec.

#### 6.10 Dynamic magnetization of ferrofluid:

When a magnetic field is applied to or removed from an ensemble of magnetic particle, the system will not attain its equilibrium value instantaneously. The magnetization will attain its equilibrium value exponentially in the first approximation. Similarly when an alternating magnetic field is applied to the system, there will be a phase lag between the magnetization and the field. The phase lag can be expressed by the angle  $\psi$ , which is given by,

$$\tan \psi = \frac{\chi''(\omega)}{\chi'(\omega)} \quad \dots\dots\dots (6.15)$$

where  $\omega = 2\pi\nu$ ,  $\chi'(\omega)$  and  $\chi''(\omega)$  are the real and imaginary parts of the complex susceptibility  $\chi(\omega) = \chi'(\omega) - i\chi''(\omega)$ .  $\chi'(\omega)$  and  $\chi''(\omega)$  may be expressed by the Debye relations,

$$\chi'(\omega) = \frac{\chi_0}{(1 + (\omega\tau)^2)} \quad \dots\dots\dots(6.16)$$

$$\chi''(\omega) = \frac{\chi_0(\omega\tau)}{(1 + (\omega\tau)^2)} \quad \dots\dots\dots(6.17)$$

Where  $\chi_0$  is the static initial susceptibility and  $\tau$  is the relaxation time for the Neel or Brownian process.

### 6.11 Superparamagnetism:

The decay of the magnetization of an ensemble of fine magnetic particles which are initially magnetised follows in the first approximation an exponential law,

$$M = M(0)\exp\left(-\frac{t}{\tau}\right) \quad \dots\dots\dots(6.18)$$

where  $M(0)$  is the magnetization at time  $t = 0$  and  $\tau$  is the Neel relaxation time. In Fig.6.1 the decay in magnetization after 10 sec and 1 year have been plotted as a function of  $\frac{KV}{kT}$ . From the figure it is evident that there exists a narrow region of  $\frac{KV}{kT}$  which separates the particles that have relaxed almost immediately,

(superparamagnetic particles) from the particles with a remanent

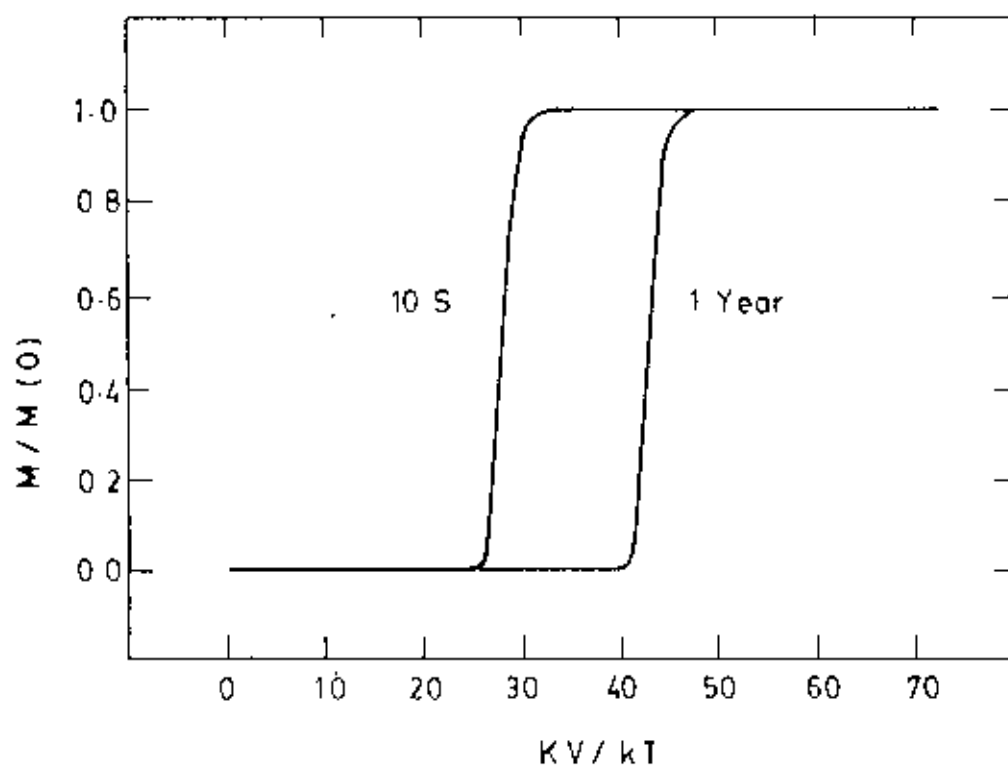


Fig. 6.1 The magnetization decay as a function of  $KV/kT$ , with  $\tau_0 = 10^{-11}$  S.

magnetization(blocked particles). The definition of superparamagnetism is that there is no remanent magnetization, and the particles relax almost immediately. Thus it is possible to define a blocking volume  $V_B$  and a blocking temperature  $T_B$  for blocked particles that separate from superparamagnetism. the expressions are given as,

$$V_B = \frac{kT}{K} \ln \left( \frac{t_m}{\tau_0} \right) \dots\dots\dots(6.19)$$

$$T_B = \frac{KV}{k \ln \left( \frac{t_m}{\tau_0} \right)} \dots\dots\dots(6.20)$$

where  $t_m$  is the characteristic measuring time.

**6.12 Experimentals:**

The ferrofluid samples are supplied by Ferrofluidics Inc. Two different size distribution of particles are measured. Both are lognormal distributed with mean particle diameters of 45Å(sample A) and 60Å(sample B) with FWHM of 23Å and 31Å respectively. The volume fraction of particles in the solvent have been 1.7%, 0.17% and 0.017% for both the samples and also 10.6% for sample A. The samples are sealed in small cups made of sapphire and is fixed in a thin sapphire rod. The sample is put in the a.c Susceptometer with the Computer controlled data acquisition system to perform a.c.susceptibility measurements. The Computer is programmed for different a.c. and d.c.fields and different probing frequencies.

For the d.c.relaxation measurements the sample is put in a Computer controlled r.f.SQUID. This SQUID is very sensitive for d.c.relaxation measurements. The samples are cooled in zero magnetic field (ZFC) to the measuring temperature  $T_m$ , then

equilibrated for a time  $t_n$  and then probed by applying a magnetic field. The applied magnetic field is  $h = 3\text{Gauss}$  which is low enough to be in the linear response regime. When the solvent freezes at  $T \rightarrow 177\text{K}$ , the particles are fixed with their easy axes randomly distributed. The field cooled (FC) measurements are also performed.

### 6.13 Results and Discussion:

The relaxation time of a single domain particle is given by

$$\tau = \tau_0 \exp \frac{E_b}{k_B T} \dots\dots\dots (6.21)$$

where  $\tau_0$  is a microscopic time and  $E_b$  is the energy barrier which for sufficiently dilute samples equals  $\langle KV \rangle$ . Due to volume distribution of particles,  $\langle KV \rangle$  indicates an effective anisotropy energy for the whole sample.

Fig 6.2 shows the block diagram of the a.c.Susceptometer. Fig.6.3.a and 6.3.b show the in-phase component  $\chi'(T)$  of the complex a.c.susceptibility at the probing frequency  $\frac{\omega}{2\pi} = 125\text{Hz}$  for different concentrations of samples A and B. The inset shows the field cooled (FC) and the zero field cooled (ZFC) magnetization for 10.6% concentration particles. Fig 6.4.a and 6.4.b show the in and out of phase components  $\chi'(T)$  and  $\chi''(T)$  for both the samples A and B at different probing frequencies. It is checked that the a.c.field amplitude is in the regime giving linear response. The position of the cusp in  $\chi'(T)$  and  $\chi''(T)$  is shifted to lower temperatures as the concentration decreases and only a small difference can be seen between the two most diluted samples, indicating that  $E_{im}$  is negligible for the least concentrated sample. The

inflection point in  $\chi''$  gives the blocking temperature  $T_b$ , where the relaxation time equals the probing a.c. field time  $\tau = \frac{1}{2\pi f}$ . In a sample with negligible interaction between the dipoles, eq(6.21) should hold with  $E_b = \langle KV \rangle$ . In this case the anisotropy energy  $\langle KV \rangle$  and the time constant  $\tau_0$ , can be determined by plotting  $\log \tau$  vs  $\frac{1}{T_b}$ . This analysis is performed for the most diluted samples. The calculated values of  $\tau_0$  are respectively  $\tau = 2.0 \times 10^{-10}$  sec and  $4.0 \times 10^{-10}$  sec for samples A and B. The calculated anisotropy constants for both the samples are  $K = 80 \text{ kJ} / \text{m}^3$ .

To investigate the interaction effects the magnetic relaxation measurements are done. Simulation have shown that dipole-dipole interaction can cause typical spin glass (SG) behaviour. In a spin glass, the ground state is different for different temperatures implying that the domains of spins in equilibrium can grow only when the temperature is kept constant. If a magnetic field  $h$  is applied after waiting time  $t_w$ , the rate of relaxation will depend on the size of the quasi equilibrated domains. This measurement is performed for sample A using a volume concentration of magnetic particles of 1.7% in which the dipole-dipole interaction is strongest. Three relaxation rate curves are obtained at  $T = 12.5\text{K}$  with  $T_w = 10^3; 10^4$  and  $10^5$  sec and are plotted as a function of time in Fig.6.5. Fig.6.6 a, 6.6.b and 6.6.c show the relaxation rate curves for sample B at  $T_m = 15\text{K}, 25\text{K}$  and  $35\text{K}$  and for three different waiting times. There is a clear difference in relaxation rates between curves corresponding to different waiting times  $t_w$ . This is an indication that the system behaves more like a spin glass.

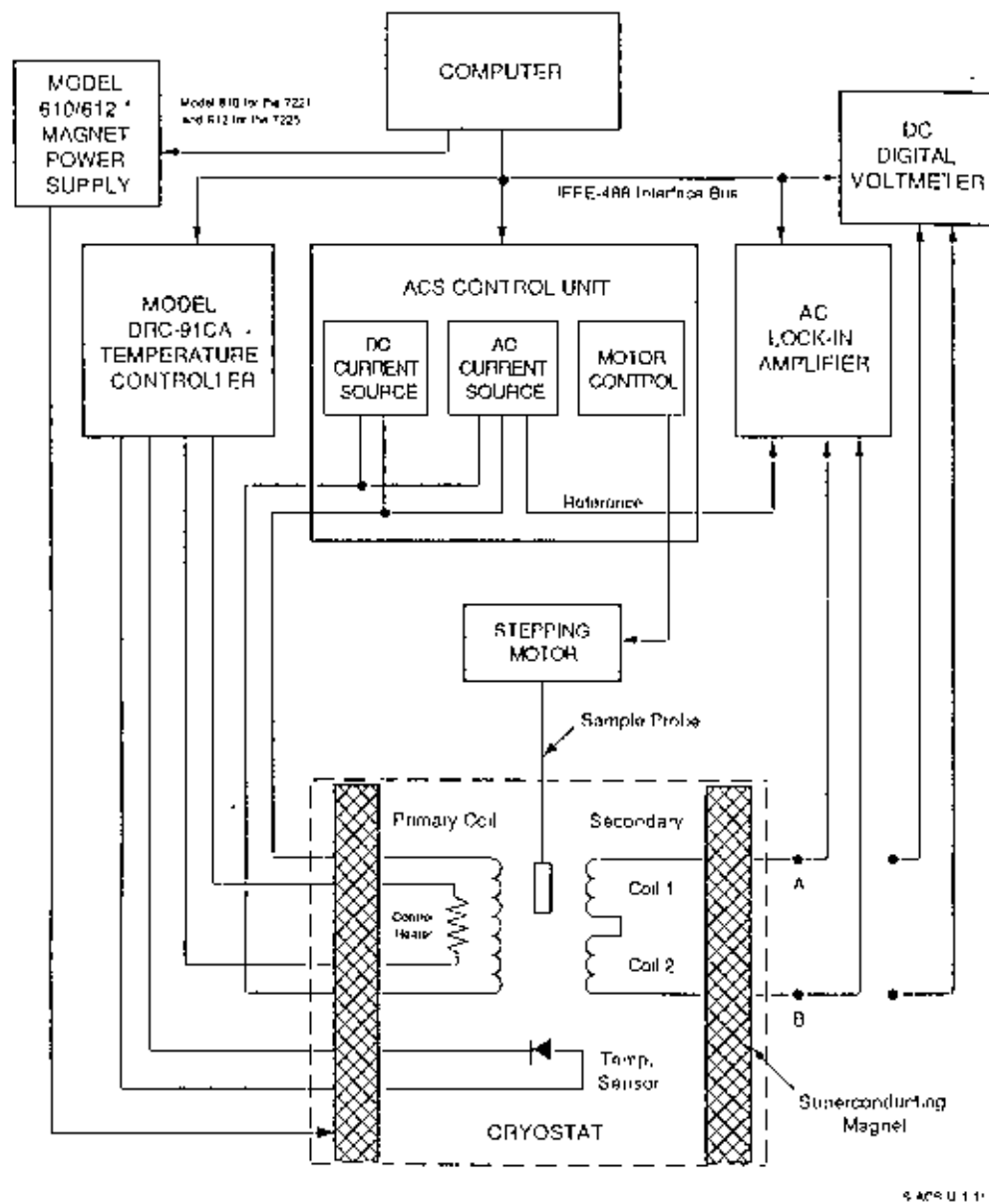


**Fig. 6.2 Model 7221 and 7225 AC Susceptometer/DC Magnetometer Block Diagram.**

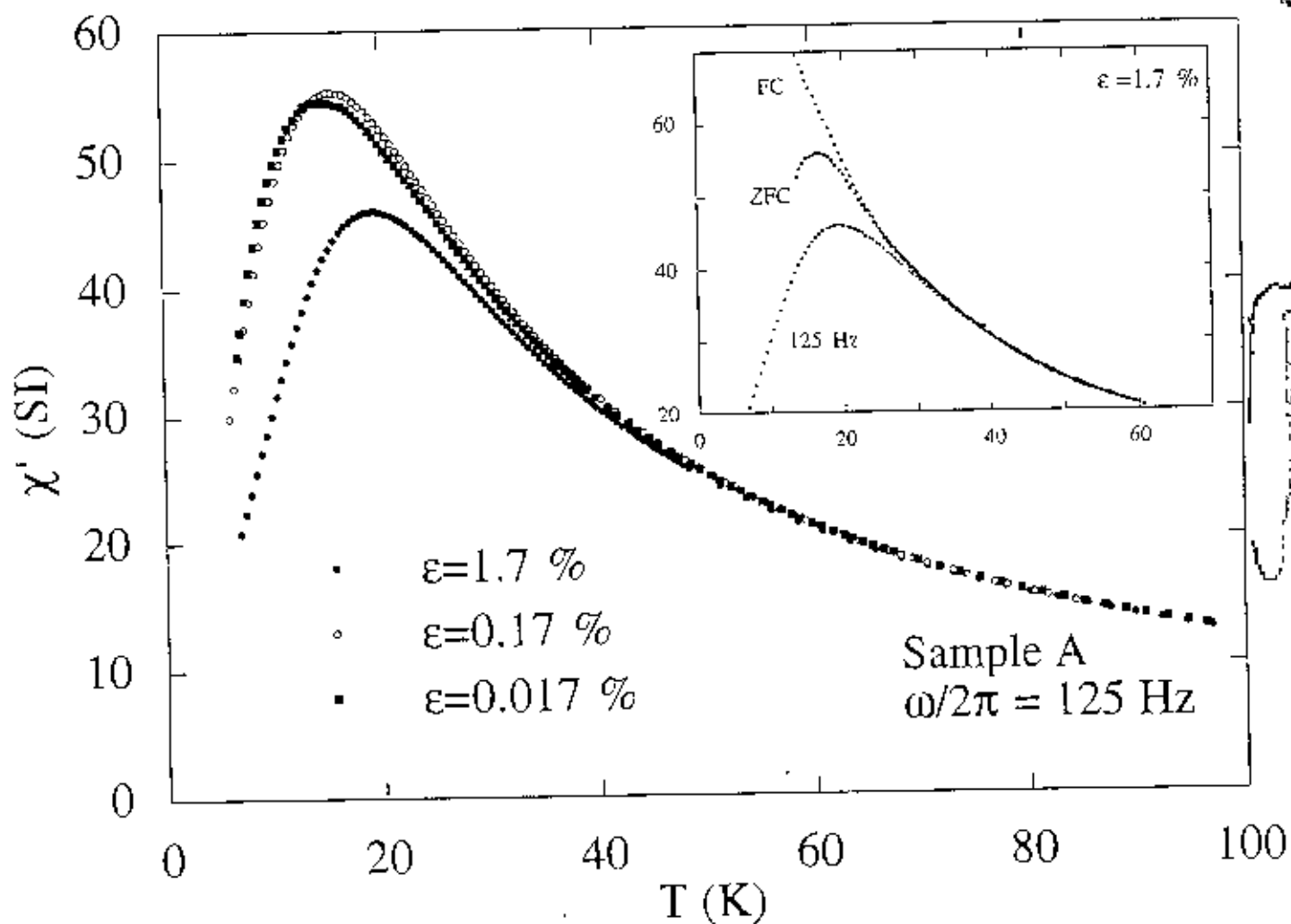


Fig. 6.3.a Real part of the complex a.c.susceptibility for sample A with different concentration at probing frequency 125 Hz



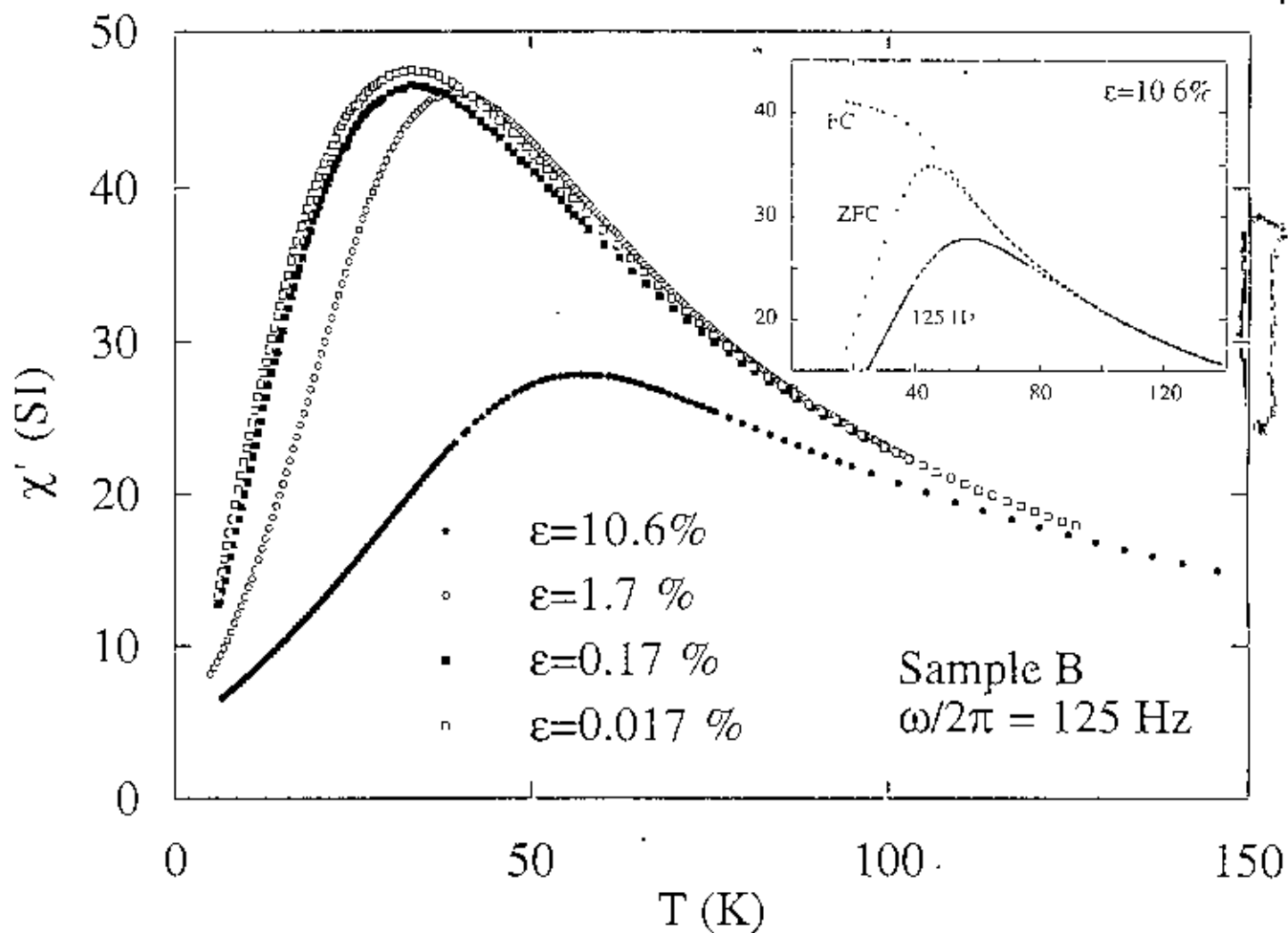


Fig. 6.3.b Real part of the complex a.c.susceptibility for sample B with different concentration at probing frequency 125 Hz

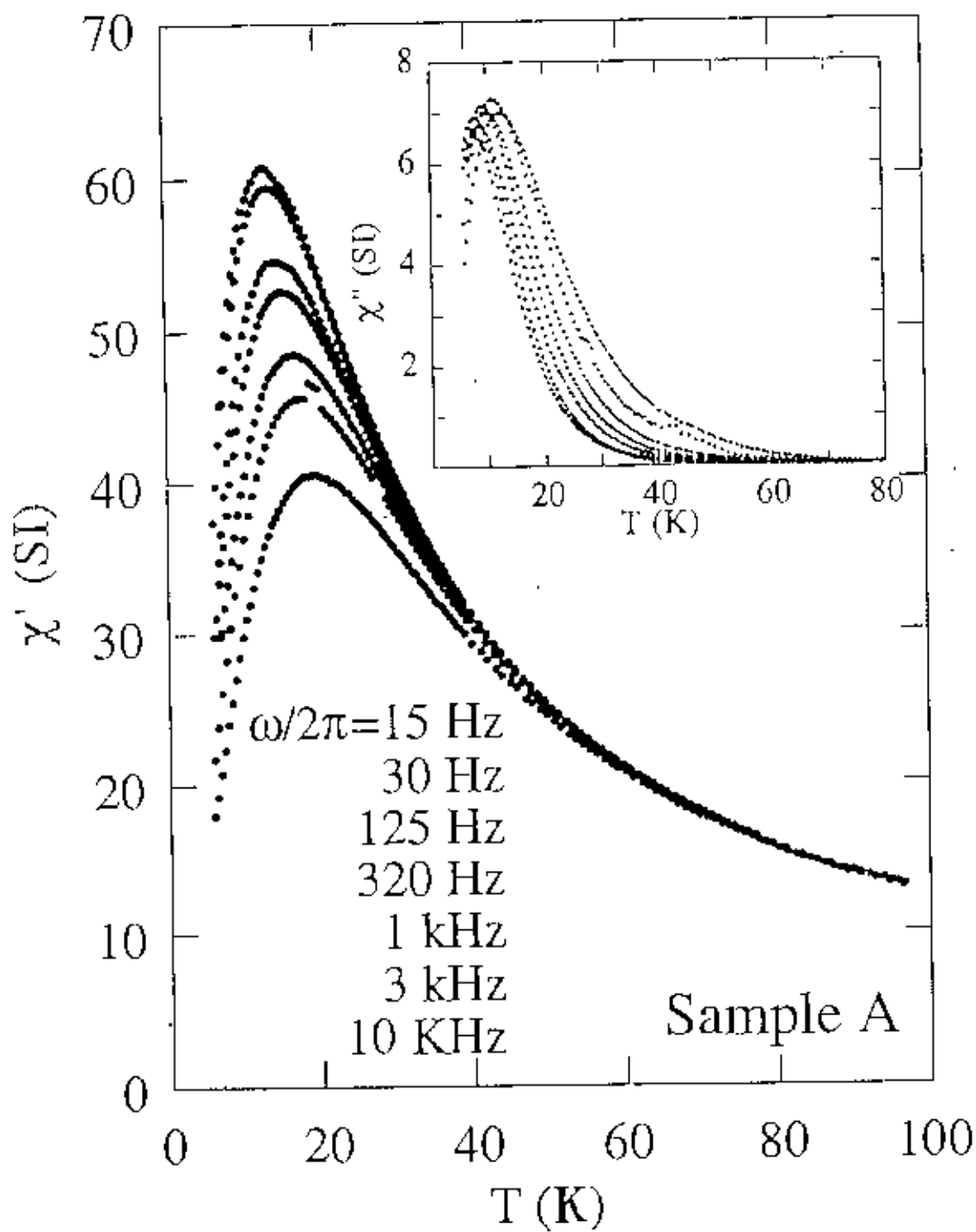


Fig. 6.4.a Real and Imaginary part of the complex a.c.susceptibility for sample A at different probing frequency.

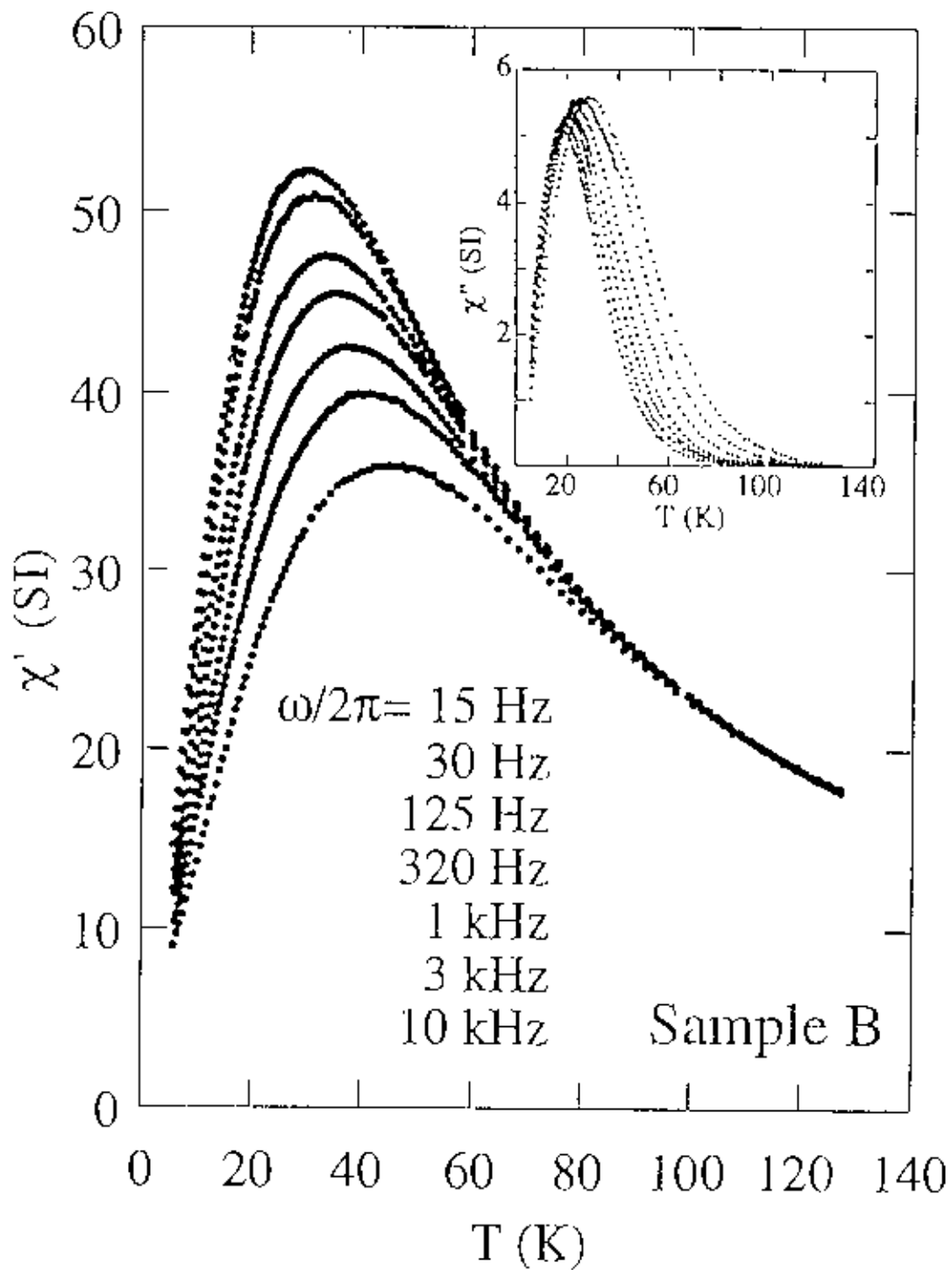


Fig. 6.4.b Real and Imaginary part of the complex a.c.susceptibility for sample B at different probing frequency.

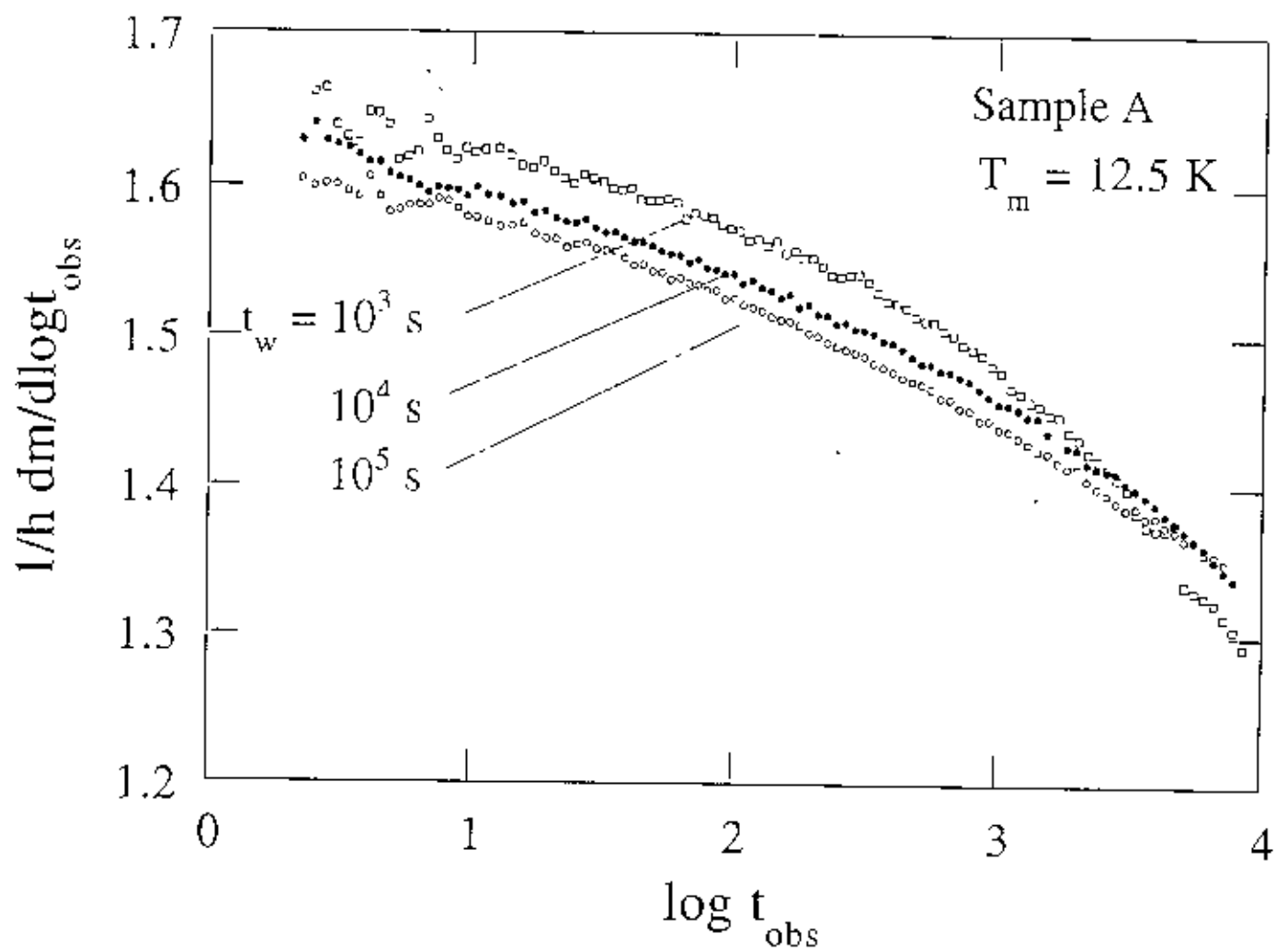


Fig. 6.5 Magnetic relaxation curve of sample A at 12.5K

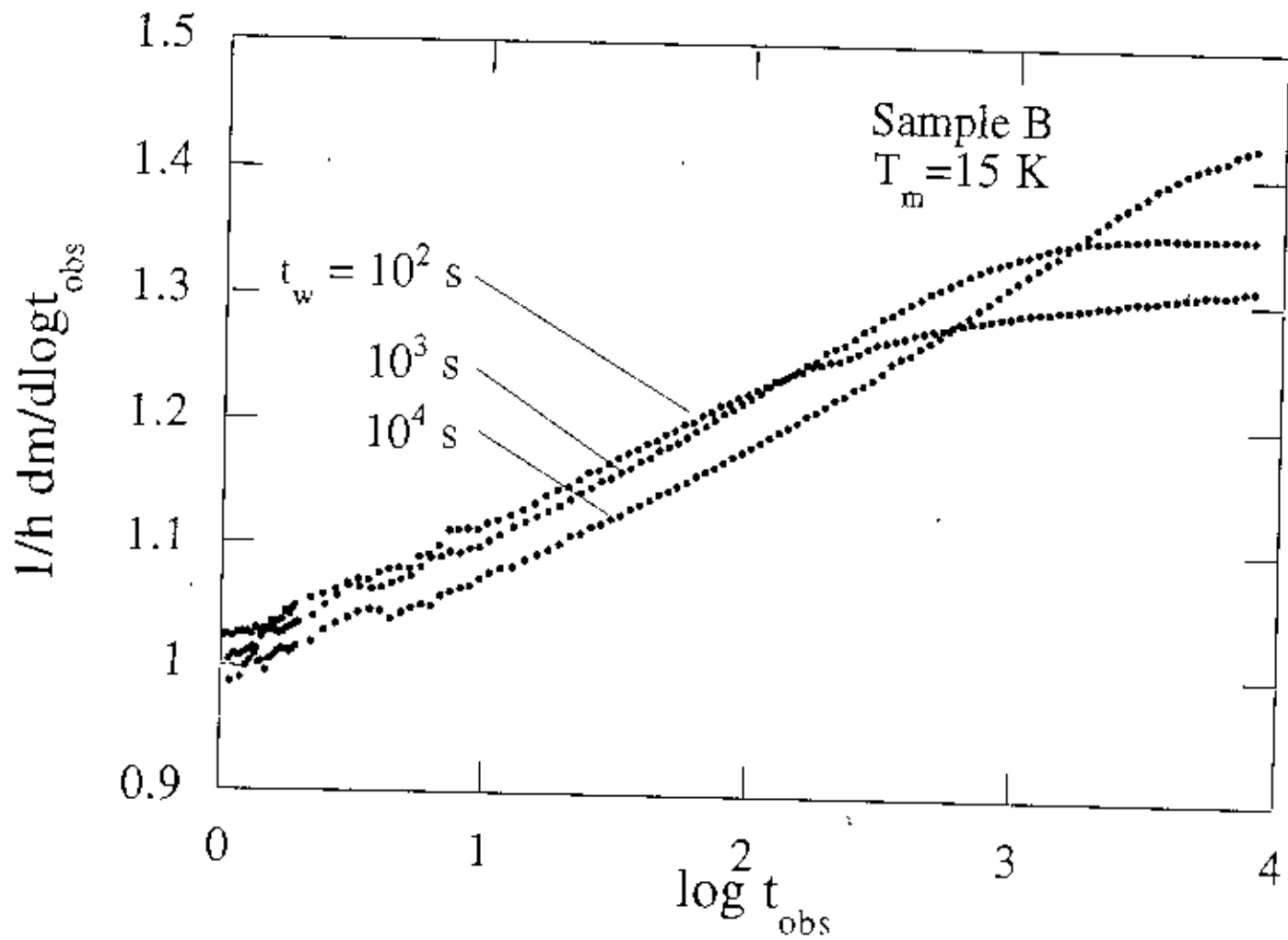


Fig. 6.6.a Magnetic relaxation curve of sample B at 15K

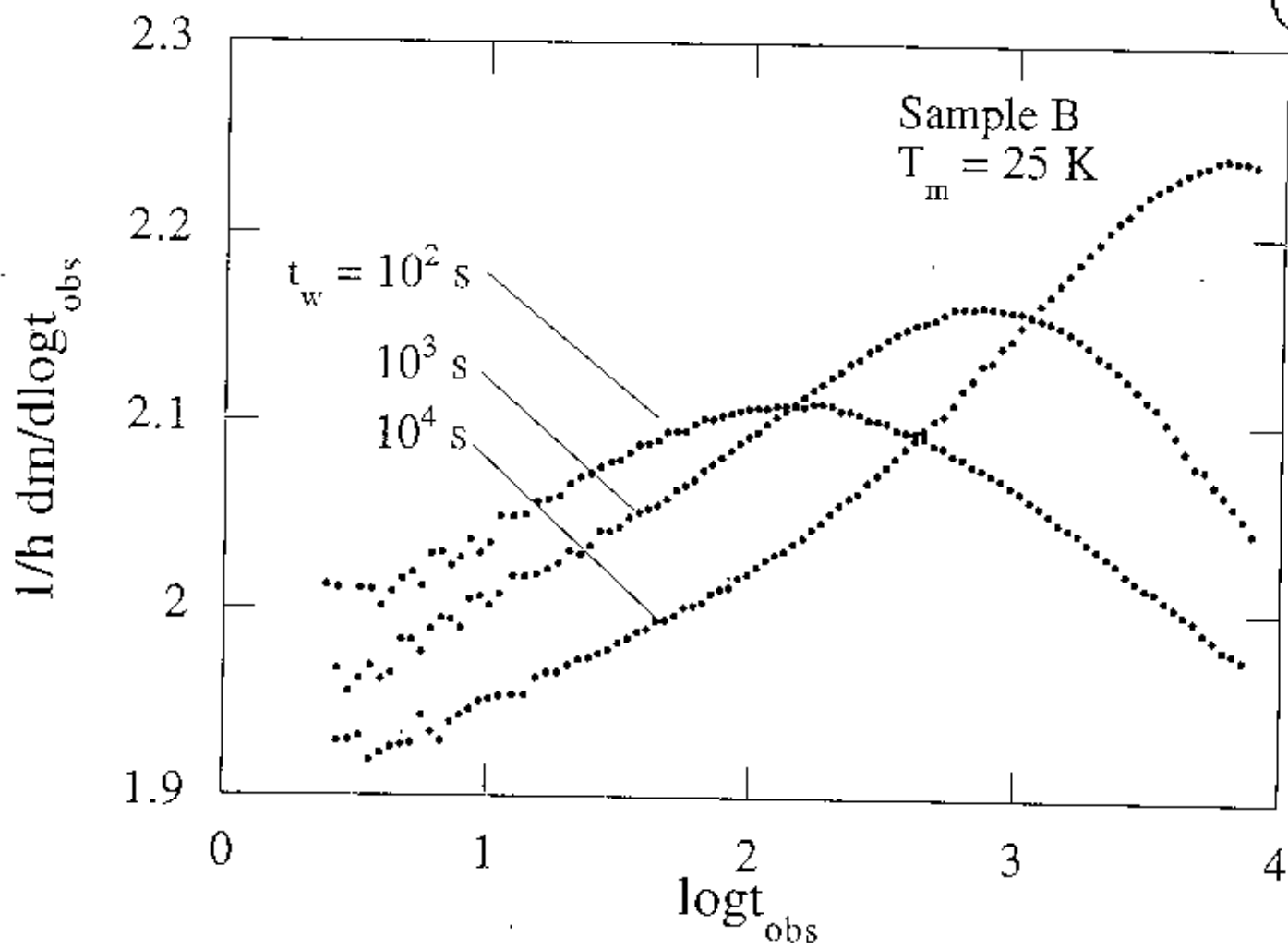


Fig. 6.6.b Magnetic relaxation curve of sample B at 25K

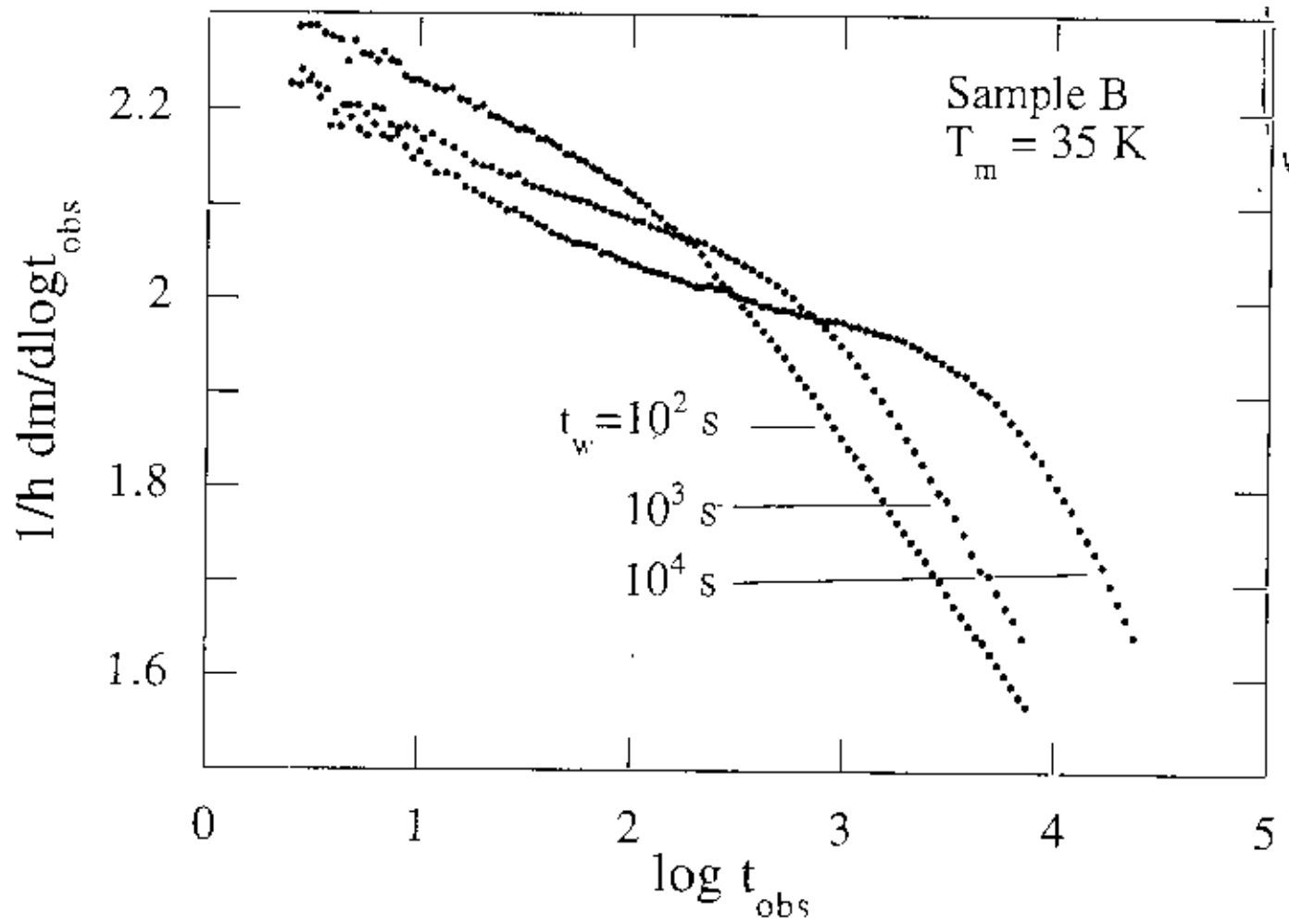


Fig. 6.6.c Magnetic relaxation curve of sample B at 35K

**Chapter 7**  
**Findings and Conclusion**



### 7.1 Findings of this research

In spite of the fact that excellent theories have been developed in magnetism, the magnetism of 3d transition metals is too complicated to provide as yet a unified theoretical understanding of this phenomenon. This is particularly so for Ni and its alloys due to the itinerant nature of their magnetic electrons.

The dependence of magnetisation on composition of Ni-Mo system shows that Mo atoms do not perturb the magnetic moments of Ni matrix but only dilute the magnetic atoms except at very low concentration of Mo, where a slight deviation from linearity is identified. The temperature dependence of anisotropy constants  $K_1$  of these alloys do not support the 10th power law as proposed by Zener but instead shows a 3rd power law dependence.

For  $Fe_2P$  system the investigation has been carried out from 4.2K to 216K, the Curie temperature of this alloy. The hexagonal anisotropy constant  $K_1$  of this alloy is found to obey  $\left[ \frac{M(T)}{M(0)} \right]^3$  law quite satisfactorily. Although, as a current research problem,

$Fe_2P$  system has been studied quite extensively, there is no data on the temperature dependence of the magnetocrystalline anisotropy constants on this system. The present work on the temperature dependence of the magnetocrystalline anisotropy constants  $K_1$  of  $Fe_2P$  from liquid helium temperature of 4.2K upto the transition temperature  $T_c$  (216K) is a new finding.

The spin glass is a system in which a non-magnetic element is doped with a small amount of ferromagnetic or antiferromagnetic element. In this system the spins do not know whether to order ferromagnetically or antiferromagnetically and as a result it behaves like a frustrated system. The characteristic property of this system is that the

magnetisation in this system decays with time, and the rate of decay of magnetisation depends on the waiting time  $T_w$ , which means that the system ages

In ferrofluid ( $\text{Fe}_3\text{O}_4$ ) the different magnetic properties of this anisotropic system have been studied, the origin of which is explained to be the dipole-dipole interaction. The superparamagnetism and the blocking characteristics of this particle system have been established through measurements of a.c.susceptibility and the d.c.relaxation. It has been observed for the first time through our experiment of magnetic relaxation (Fig.6.5- Fig.6.6) that the system ages and behaves like spin glass.

While it is so difficult to find a unified theory for even a single magnetic system, in the present thesis an operational view point is suggested to find a unified picture in the three diverse magnetic systems through the experimental determination of magnetic anisotropies in these systems

## 7.2 Conclusion:

Although the nickel based alloy systems are widely studied, the understanding of magnetism is quite complicated and still incomplete. It is more so for secondary effects like magnetic anisotropy and magnetostriction and their temperature dependence. In the present work single crystals of Ni-Mo and Fe<sub>2</sub>P alloys have been studied for the temperature and composition dependence of magnetization. The anisotropy constants of these alloys have been determined from magnetization versus field curves. This is an integral technique where the energy difference for magnetization between a chosen crystallographic direction and the direction of easy magnetization is measured from the complete field versus magnetization curves. Anisotropy energy is thus determined from the first principle. The success of this method depends entirely on the accuracy of the orientation of the specimen and the recording of magnetization and the magnetic field. Although anisotropy constants of the Ni-Mo single crystals have been measured by Janet using a Torque Magnetometer, it has not been published due to lack of confidence in the results ( As we came to know by private communication ). However it is very interesting to find that our results which are obtained by entirely different method nicely agree with Janet's results indicating that her measurements are more reliable than she herself presumed. We also checked some of the results by using our Torque Magnetometer, which is extremely sensitive. These results on Ni-Mo will provide new information on the existing experimental data on nickel based alloys and help in the development of the theoretical understanding of magnetism of 3d transition metals which is still incomplete.

The empirical relation 
$$\frac{K_1(c)}{K_1(0)} = \left[ \frac{M(c)}{M(0)} \right]^n$$

for the composition dependence of anisotropy constants on magnetization has been tested. The equation very nearly fits the third power law. This indicates that the composition dependence of the anisotropy constants on magnetization follows a third power law.

The composition dependence of anisotropy has to be understood in terms of the change in the magnitude of spin-orbit interaction through the change of both orbital angular momentum and spin angular momentum due to alloying. The mechanism is too complicated to be quantified theoretically. In fact there is no existing theory of the variation of magnetocrystalline anisotropy due to change of composition. Although there are excellent theories of temperature dependence of anisotropy constant but even these are not in complete agreement with the experimental results. It only shows that more experimental investigations are needed to comprehend this phenomena, especially with reference to nickel based alloys, nickel being the most difficult magnetic element for the itinerant nature of its magnetic electrons.

In a qualitative way we can explain the composition dependence of anisotropy constants of Ni-Mo system in the following way. The addition of non magnetic molybdenum to the nickel matrix changes the orbital magnetic moment as well as the spin magnetic moment. As a result the spin-orbit coupling becomes weaker. Since according to Nee'l, the spin orbit coupling changes the overlap of the wave functions between the neighbouring magnetic atoms and thereby make the exchange interaction direction dependent, the magnitude of this anisotropic exchange is likely to decrease with the decreasing strength of the spin-orbit coupling. The determination of the 'g' factor for these alloys are therefore needed to quantify our argument through the determination of the relative contributions of the spin and the orbital part of the total magnetisation.

Although magnetocrystalline anisotropy and the magnetostriction are both dependent on spin-orbit interaction (Lee and Asgar 1971), no unified explanation for the temperature dependence of these phenomenon has yet been developed. Future works, both theoretical and experimental are therefore needed for the satisfactory understanding of these phenomena. There has been experimental study of temperature dependence, pressure dependence, field dependence, and composition dependence of magnetic anisotropy (Veerman and Rathenau 1964). There should be some unifying theory to explain all these dependences. This can be another proposed field of future research.

Iron phosphide ( $\text{Fe}_2\text{P}$ ) is an interesting material for recent research. Its intricate magnetic behaviour to the change of composition and external parameters have completely dominated the mind of experimentalists to pursue further research on this system. In this work the magnetic anisotropy and its temperature dependence have been studied quite extensively. The experimental results have been compared with the theoretical formulations on temperature dependence of magnetic anisotropy. Although there is no experimental data on the temperature dependence of magnetic anisotropy constants of  $\text{Fe}_2\text{P}$  to be compared with our results, we have developed a suitable relationship of temperature dependence of magnetocrystalline anisotropy constant of this system. It has been found that the temperature dependence of magnetic anisotropy follows a third power law.

As mentioned earlier the anisotropic magnetic system ferrofluid ( $\text{Fe}_3\text{O}_4$ ) is a completely new material of current research. We have experimentally studied its different observable magnetic parameters at very low temperature regime. Particular emphasis was given on the behaviour of this anisotropic system around the transition region of blocking and superparamagnetism through experimental study of field cool

(FC) measurements, zero field cooled (ZFC) measurements, the a.c. susceptibility measurements and the magnetic relaxation measurements. It has been experimentally observed for the first time that the system ages and behaves like spin glass.

In the present work a unified operational meaning of magnetic anisotropy has been sought from experimental point of view for three very different magnetic systems. Since magnetism and especially magnetic anisotropy of various magnetic systems can not be explained by a single quantitative theory at present, it is only through the accumulation of detail experimental results of various systems that a comprehensive theory is expected to be developed in the future.

Aharoni, A., *Phys. Rev.* 177 (1969)793

Akulov, N., *Z. Phys.* 100, 197 (1936)

Andersson, Y., Rundqvist, S., Beckman, O., Lundgren, L., Nordblad, P., *Phys. Stat. Sol.(a)* 49, K 153, 1978

Asgar, M.A., Ph.D Thesis, University of Southampton 1970

Band, W., *Proc. Camb. Phil. Soc.* 42, 139(1946)

Bean, C.P., Rodbell, D.S , *Phys. Rev.* 126, (1962) 104

Bean, C.P., Livingston, J., *J.Appl.Phys.* 30 (1959) 120 S

Beckman, O., Lundgren, L., Nordblad, P., Svedlindh, P., Torne, A., Andersson, Y.,and Rundqvist, S., *Phys Scripta* 25, (1982) 679

Bell, G M , *Phil. Mag.* 43 127(1952)

Dellavance, D., Mikkelsen, J., and Wold, A., *J.Solid State Chem.* 2, (1970) 285-290

Benninger, G.N., Pavlovic, A.S., *JAppl Phys* 38, 1325 (1967)

Birss,R.R , Wellis,P.M., *J. Sci Instrum.* 40, 551 (1963)

Bloch, F., *Z Phys.* 57, 545 (1929)

Bozorth, R M.. *Ferromagnetism* ( Van Nostrand, New York, 1951 )

Brooks, H., *Phys. Rev.* 58, 909 (1941)

Brown, W.F.Jr., *Phys. Rev.* 130 (1963) 1677

Bryuchatov, N.L., Kitchensky, L.V., *J. Tech. Phys. (USSR)*5. 171(1938)

Callen, H.B., Callen, E R., *J. Phys. Chem. Solids* 27, 1271 (1966)

Callen, E.R., and Callen, H.B., *Phys. Rev.* 129,2,1963

Carlsson, B., Ohrlin, M., and Rundqvist, S , *J. Solid State Chem.* 8, (1973) 57

Carlsson, B., and Rundqvist, S., *J. Solid State Chem.* 13,(1975) 258

Carlsson, B., Golin, M., and Rundqvist, S., *J.Solid State Chem* 8, (1973) 57-67

Carr Jr., W.J., *Phys. Rev.* 108, 1158 (1957)

- Carr Jr., W.J., *Phys. Rev.* 109, 1971 (1958)
- Catalano, A., Amott, R.J., Wold, A., *J. Solid State Chem.* 7, 262, 1973
- Chandra, R., Bjarman, S., Ericsson, T., Haggstrom, L., Wilkinson, C., Wappling, R., *J. Solid State Chem.* 34, 389, 1980
- Chantrell, R.W., Popplewell, J., and Charles, S.W., *IEEE Trans. Magn.* 14, 975 (1978)
- Chantrell, R.W., Wohlfarth, E.P., *J. Magn. Magn. Mat.* 40 (1983) 1
- Chikazumi, S., *Physics of Magnetism*, John Wiley and Sons Inc., New York, 1964
- Comly, J.B., Holden, T.M., Low, G.G., *J. Appl. Phys.* 38, 1240 (1967)
- Cullity, B.D., *Introduction to Magnetic Materials*, Addison Wesley Publishing Company (1972)
- Dormann, J.L., Fiorani, D., Yamani, M.El., *Physics Letters A* 120, 2, (1987)
- El-Hilo, M., O'Grady, K., Chantrell, R.W., *J. Magn. Magn. Mat.* 114 (1992) 295-306
- El-Hilo, M., O'Grady, K., Chantrell, R.W., *J. Magn. Magn. Mat.* 117, 21, (1992)
- Enoch, R.D., Fudge, A.D., *Brit. J. Appl. Phys.* 17, 623 (1966)
- Eriksson, O., Sjostrom, J., Johansson, B., Haggstrom, L., Skriver, H.L., *J. Magn. Magn. Mat.* 74, 347-358 (1988)
- Fawcett, E., *Advan. Phys.* 13, 139 (1964)
- Fletcher, G.C., *Proc. Phys. Soc. (London)* A67, 505 (1954)
- Foner, S., *The Review of Scientific Instruments.* 30, 548 (1959)
- Friedel, J., Leman, G., Olzewski, S., *J. Appl. Phys.* 32, 3255 (1961)
- Friedel, J., Leman, G., Olzewski, S., *J. Appl. Phys.* 32, 3255 (1961)
- Fujii, H., Hokabe, T., Kamigaishi, T., Okamoto, T., *J. Phys. Soc. Japan* 43, 41, 1977
- Fujii, H., Komura, S., Takeda, T., Okamoto, T., Ito, Y., and Akimatsu, J., *J. Phys. Soc. Japan* 46, 1616 (1979)



- Fujii, H., Hokabe, T., Eguchi, K., Fujiwara, H., and Okamoto, T., *J. Phys. Soc. Japan* 51, 414 (1982)
- Fujii, H., Hokabe, T., Kamigaisbi, T., and Okamoto, T., *J. Phys. Soc. Japan* 43(1977)41
- Fujii, H., Hokabe, T., Fujiwara, H., and Okamoto, T., *J. Phys. Soc. Japan* 44,(1978) 96
- Fujii, H., Uwatoko, Y., Motoya, K., Ito, Y., and Okamoto, T., *J. Phys. Soc. Japan*, 57,6 (1988) 2143-2153
- Fujiwara, H., Kamatsu, H., Thoma, K., Fujii, H., and Okamoto, T., *J. Magn. Magn. Mat* 21, (1980) 262
- Fujiwara, H., Kadomatsu, H., Tohma, K., *J. Magn. Magn. Mat.* 21 (1980) 262-268
- Gupta, H.C., *Solid State Physics*, Vikas Publishing House Pvt. Ltd. New Delhi(1995)
- Hicks, T.J., Rainford, B., Kovel, J.S., Low, G.G., Comly, J.B., *Phys. Rev. Letters* 22, 531 (1969)
- Huq, M., Ph.D Thesis, University of Southampton 1975.
- Jannet, S., Ph.D thesis, University of Sheffield, 1969
- Jernberg, P., Yousif, A., Haggstrom, L., *J. Solid State Chem* 53, 313, 1984
- Johansson, C., Ph.D Thesis, University of Goteborg, 1993
- Kadomatsu, H., Isoda, M., Toma, K., Fujii, H., Okamoto, T., and Fujiwara, H., *J. Phys. Soc. Japan* 54,(1985) 2690
- Kanamori, J., *Magnetism, Vol. 1*, eds. Rado, G.T., Suhl, H., p. 127 (Academic Press, New York, 1963)
- Keffer, F., *Phys. Rev.* 100 1692 (1955)
- Kelly, P.E., O'Grady, K., Mayo, P.I., Chantrell, R.W., *IEEE Trans Magn.* 25, 3881,(1989)
- Kittel, C., Van Vleck, J.H., *Phys. Rev.* 118, 1231 (1960)
- Kneller, E., *Magnetism and Metallurgy Vol. 1*, eds. Berkowitz, A.E., and Kneller, E., Academic Press New York (1969) 365

- Komura, S., Tajima, K., Fujii, H., Ishikawa, Y., and Okamoto, T., *J. Magn. Magn. Mat.* 15-18. (1980) 351-352
- Komura, S., Tajima, K., Fujii, H., Ishikawa, Y., and Okamoto, T., *J. Magn. Magn. Mat.* 31-34 (1983) 615-616
- Lee, E.W., and Birss, R.R., *Proc. Phys. Soc.* 78, 391 (1961)
- Lee, E.W., Asgar, M.A., *Proc. R. Soc. Lond. A.* 326, 73-85 (1971)
- Lundgren, L., Tarmohamed, G., Beckman, O., Carlsson, B., Rundqvist, S., *Physica Scripta* 17, 39, 1978
- Luo, W., Nagel, S.R., Rosenbaum, T.F., Rosenweig, R.E., *Phys. Rev. Lett.* 67, 19 (1991)
- Martin, D.H., *Magnetism of Solids*, London ILIFFE Books Ltd.
- Moriya, T., Usami, K., *Solid State Commun.* 23 (1977) 935
- Morup, S., Tronc, E., *Phys. Rev. Lett.* 72, 20 (1994)
- Née'l, L., Pauthenet, R., Rimet, G., Giron, V.S., *J. Appl. Phys.* 31, 5, 1960
- Née'l, L., *Compt. Rend.* 224 (1947) 1488
- Nordblad, P., Ph.D thesis, University of Uppsala, 1980
- Pearson, W.B., *Handbook of Lattice Spacings and Structure of Metals and Alloys*, Vol. 2, Pergamon Press, Oxford, 1967
- Pugh, E.W., Argyle, B.E., *J. Appl. Phys.* 33, 1178 (1962)
- Puzci, I.M., *J. Tech. Phys. (USSR)* 19, 653 (1949)
- Roger, A., 1970, Thesis (Orsay 1970)
- Rundqvist, S., Jellinek, F., *Acta, Chem. Scand.* 13 (1959) 425
- Rundqvist, S., and Jellinek, F., *Acta. Chem. Scand.* 13 (1959) 3
- Sato, M., Tino, Y., *J. Phys. Radium* 17, 5 (1956)
- Scott, J., Ph.D Thesis, University of Sheffield, 1970

- Shtrikman, S., Wohlfarth, E.P., Phys. Lett. 85A(1981) 467
- Slater, J.C., Phys. Rev. 49, 537 (1936)
- Slater, J.C., Phys. Rev. 49, 931 (1936)
- Stoner, E.C., Phil Mag. 15, 1018 (1933)
- Stoner, E.C., Proc. Roy. Soc. (London) A 165, 372 (1938)
- Stoner, E.C., Proc. Roy. Soc. (London) A 169, 339 (1939)
- Stuart, R.N., Marshall, W., Phys. Rev. 120, 353 (1960)
- Thompson, E.D., Wohlfarth, E.P., Bryan, A.C., Proc. Phys. Soc. (London) 83, 59 (1964)
- Turov, E.A., Mitsek, A.I., Zh.ETF 37, 1127, (1959) (Trans. Soviet Phys.-JETP 10, 801)
- Van Vleck, J.H., Rev. Mod. Phys., 25, 220 (1953)
- Van Vleck, J.H., Phys. Rev. 52, 1178 (1937)
- Van Vleck, J.H., J. Phys. Radium, 20, 124 (1956)
- Veerman, J., and Rathenau, G.W., Proceedings of the International Conference on Magnetism, Nottingham, 1964
- Veerman, J., and Rathenau, G.W., Proc. Int. Conf. on Magnetism, Nottingham, 1964
- Vonsovsky, S.V., J. Phys. (USSR) 10, 468 (1946)
- Vonsovsky, S.V., Turov, E.A., Zh.ETF (USSR) 24, 419 (1953)
- Wappling, R., Haggstrom, L., Eriksson, T., Devanarayanan, S., J. Solid State Chem. 13, (1975) 258
- Wappling, R., Hartmann, O., Wackelgard, E., Sundqvist, T., J. Magn. Magn. Mat. 50 (1985) 347-353
- Wenger, L.E., and Mydosh, J.A., Phys. Rev. B 29 (1984) 4156
- Westerstrandh, B., Gafvert, U., Lundgren, L., Physica Scripta. 14 5-10 (1976)
- Wohlfarth, E.P., Phil. Mag. 40, 1095 (1945)

- Wohlfarth, E.P., Proc. Roy. Soc. (London), A195, 434(1949)
- Wohlfarth, E.P., Phil. Mag.,42, 374(1951)
- Wohlfarth, E.P., J.Appl.Phys 50, (1979) 7542
- Yosida. K., J.Appl. Phys., 39, 511 (1968)
- Zaluska-Kotur, M.A., Cieplak, M., Europhys. Lett, 23(2), pp. 85-90 (1993)
- Zener, C., Phys. Rev. 81, 440(1951)
- Zener, C., Phys. Rev. 83, 299(1953)
- Zener, C., Phys. Rev 96, 1335 (1954)
- Zvada, S.S., Medvedeva, L.I., Sivachenko, A.P., Khartsev, S.I., J.Magn.Magn.Mat. 72 (1988) 349-356

## List of symbols

|           |   |
|-----------|---|
| $B$       | Magnetic flux density                         |
| $H$       | Magnetic field                                |
| $H_m$     | Molecular field                               |
| $C$       | Curie constant                                |
| $T$       | Temperature                                   |
| $\lambda$ | Weiss constant                                |
| $g$       | Lande 'g' factor                              |
| $\mu_0$   | Permeability constant                         |
| $\mu_B$   | Bohr magneton                                 |
| $J$       | Total angular momentum                        |
| $k_B$     | Boltzmann constant                            |
| $T_C$     | Curie temperature                             |
| $B_J$     | Brillouin function                            |
| $M$       | Magnetisation                                 |
| $M_s(0)$  | Saturation magnetisation at 0°K               |
| $M_s(T)$  | Saturation magnetisation at T°K               |
| $M_s(c)$  | Saturation magnetisation at concentration $c$ |
| $m$       | Magnetic moment                               |
| $N$       | Number of atoms per unit volume               |
| $K_0$     | Zero order anisotropy constant                |
| $K_1$     | First anisotropy constant                     |
| $K_2$     | Second anisotropy constant                    |
| $K_{u1}$  | First uniaxial anisotropy constant            |
| $K_{u2}$  | Second uniaxial anisotropy constant           |
| $K_1(T)$  | Anisotropy constant at temperature T°K        |

|                  |  |
|------------------|--|
| $K_1(0)$         | Anisotropy constant at 0°K                         |
| $\alpha$         | Direction cosine                                   |
| $Y_n^m$          | Spherical harmonics                                |
| $r$              | Distance between two neighbouring magnetic moments |
| $\gamma$         | Gyromagnetic ratio                                 |
| $L$              | Inductance   |
| $\phi_a$         | Flux due to applied field                          |
| $I_c$            | Critical current                                   |
| $I_s$            | Super current                                      |
| $T_B$            | Blocking temperature                               |
| $\tau$           | Relaxation time                                    |
| $\psi$           | Phase lag  |
| $E_B$            | Energy barrier                                     |
| $F$              | Free energy  |
| $\chi_i$         | Initial magnetic susceptibility                    |
| $\chi_{ferro}^m$ | Ferromagnetic susceptibility                       |
| $\chi'$          | Real part of the a.c. susceptibility               |
| $\chi''$         | Imaginary part of the a.c. susceptibility          |
| $\chi_0$         | Static initial susceptibility                      |
| $T_m$            | Measuring temperature                              |
| $T_W$            | Waiting time                                       |
| $t_m$            | Characteristic measuring time                      |
| $t_{obs}$        | Observation time                                   |

